AN ABSTRACT OF THE THESIS OF

Paul Steven Walczak for the degree of Master of Science in Oceanography presented on May 30, 2006.

Title: Submarine Plateau Volcanism and Cretaceous Ocean Anoxic Event 1a: Geochemical Evidence from Aptian Sedimentary Sections.

Abstract approved:

_____

Robert A. Duncan

Marine sediments exceptionally rich in organic carbon, known as black shales, occur globally but intermittently in well correlated Cretaceous successions. The presence of black shales indicates that sporadic, ocean-wide interruption of normal respiration of marine organic matter during oxygen-deficient conditions has occurred. Submarine volcanism on a massive scale, related to the construction of ocean plateaus, could be responsible for the abrupt onset and conclusion of these Ocean Anoxic Events (OAEs), via the oxidation of magmatic effluent, the stimulation of increased primary productivity, and the resultant respiration of sinking organic matter. These discrete periods of global ocean anoxia are accompanied by trace metal enrichments that are coincident with magmatic activity and hydrothermal exchange during plateau construction.

The link between submarine volcanism associated with the emplacement of the Ontong Java - Manihiki plateau (~122 Ma) and Cretaceous Ocean Anoxic Event 1a is explored in this study. Two marine sedimentary sections, recovered in cores from Deep Sea Drilling Program (DSDP) Site 167 (Magellan Rise) and Site 463 (Mid-Pacific Mountains), were analyzed for a suite of major, minor, and trace elements. Trace element abundance patterns for these locations were compared to similar data from the CISMON core (Belluno Basin, Northern Italy) to determine if a relationship existed between the timing of trace metal anomalies and global biogeochemical events.

To account for the variable effects of terrestrial input, trace element data were normalized to Zr and major element data were normalized to Al. Distinct, stratigraphically correlatable peaks could be seen deviating from background levels in the trace element data from the three sites. These anomalous trace metal intervals are related to melt-gas partitioning associated with magmatic degassing and hydrothermal activity resulting from chemical exchange of seawater with cooling plateau rocks. The stratigraphic coincidence of trace metals with other biogeochemical events is consistent with the idea that submarine plateau volcanism, on a massive scale, pushed the global deep ocean into anoxic conditions at discrete intervals of the Cretaceous period.

Submarine Plateau Volcanism and Cretaceous Ocean Anoxic Event 1a: Geochemical Evidence from Aptian Sedimentary Sections

by

Paul Steven Walczak

A THESIS

submitted to

Oregon State University

in partial fulfillment of
the requirements for the
degree of

Master of Science

Presented May 30, 2006

Commencement June 2007

Master of Science thesis of Paul Steven Walczak presented on May 30, 2006.

APPROVED:

_____

Major Professor, representing Oceanography

_____

Dean of the College of Oceanic and Atmospheric Sciences

_____

Dean of the Graduate School

I understand that my thesis will become part of the permanent collection of Oregon State University libraries. My signature below authorizes release of my thesis to any reader upon request.

_____

Paul Steven Walczak, Author

ACKNOWLEDGEMENTS

I would like to thank the many people that have made the last several years possible. Foremost, I would like to thank Bob Duncan, my advisor. His support and encouragement have been unwavering, and he has always been on the lookout for opportunities that would interest me and further expand my experiences in the field of oceanography. Another thank you to Randy Keller and Nick Pisias, I don't feel like my education in oceanography would have been complete without the seagoing experiences that I have had. Thanks also to Gary Klinkhammer and Fred Prahl for serving on my committee, providing great feedback, and teaching enjoyable courses. Without to teachings of Andy Ungerer, Bobbi Conard, and John Huard I would have been very lost in the lab. Additionally, the assistance of Moya and Coreen made my life not only easier, but also more entertaining. Thanks to Dr. Leon Clarke at the University of Wales, Bangor for providing me with samples and data.

Further, I would like to thank everyone else who has been a part of my life during the last couple of years. Thanks to my classmates for all of the help, encouragement, and good times. Thanks to Chris for helping me keep my priorities in order. Thanks to Mike, Kurt, Ken, Scott, Garrett, Barney, Aaron, Faron, Wilo, and all of my other friends for keeping me aware of the big picture. Thanks to my parents, well, for everything.

I also shouldn't forget to mention boys up north, for being a constant in my changing world and for giving me a wave or two. Finally, I would like to thank Alison for always being there.

Support for this project was provided by the American Chemical Society's Petroleum Research Fund. Without it, none of this would have been possible.

TABLE OF CONTENTS

TABLE OF CONTENTS (CONTINUED)

PAGE

LIST OF FIGURES

FIGURE PAGE

LIST OF TABLES

LIST OF APPENDIX FIGURES

Submarine Plateau Volcanism and Cretaceous Ocean Anoxic Event 1a: Geochemical Evidence from Aptian Sedimentary Sections

Chapter 1: Ocean Plateau Emplacement and Black Shales

Introduction

The early Aptian stage of the Cretaceous period is recognized for its extreme environmental conditions. The Cretaceous, lasting from 144 to 65 Ma (Harland et al. 1990) time scale, was markedly different from the world we know today. During this time, CO_2 levels were between 3 and 12 times greater than pre-industrial levels, resulting in temperatures on land and in the ocean that were up to 10-12 ˚C warmer than today (Berner, 1994). This period was also characterized by a lack of polar ice caps, a reduced temperature gradient between the equator and the poles, and higher sea levels due the combination of a lack of glacial ice and shallower (younger) seafloor (Schlanger et al., 1981). The Cretaceous was a period of exceptional volcanism: the dramatic increase in seafloor spreading rates and a number of rapidly-erupted large igneous provinces (LIPs) on land and in all the ocean basins were remarkable. Eruption of a mantle "superplume" in the Pacific basin increased oceanic crustal production by approximately 50-100% at this time (Larson 1991 a,b; Duncan and Richards 1991; Coffin and Eldholm 1994).

For oceanographers, one of the most intriguing features of this period was discovered during the early years of the Deep Sea Drilling Program (DSDP). At this time sediments exceptionally rich in organic carbon, known as black shales, and accompanied by distinct positive $\delta^{13}C$ isotopic excursions were recovered from

Cretaceous successions in the Atlantic, Indian and Pacific Oceans (Erba, 2004). These events were soon discovered to be one of the most fascinating features of the Cretaceous period because intervals of finely laminated, organic-rich sediments indicated that sporadic, ocean-wide interruption of normal sedimentary respiration during oxygen-deficient conditions had occurred (Schlanger and Jenkyns, 1976). These periods, termed Oceanic Anoxic Events (OAEs), and the geological and climatic processes responsible for their occurrence, have received much attention during the last three decades but satisfactory explanation has remained elusive.

Recent advances in isotopic measurements as well as plankton speciation and extinction suggest that other major events seem to be correlated with the OAEs. Leckie et al. (2002) produced an overview of Cretaceous OAEs in which he correlated their occurrence with sea level changes, biostratigraphy, seawater $^{87}Sr/^{86}Sr$ ratios, $\delta^{13}C$ curves, and major volcanic events evident in the formation of large igneous provinces (Figure 1, Leckie et al., 2002).

It can be seen that both global anoxic events (OAE1a and OAE2) are accompanied by distinct positive $\delta^{13}C$ excursions in carbonate or organic carbon preserved in marine sediments. Such departures from the long-term compositions are attributed to the accelerated burial of marine (^{12}C-enriched) organic matter during episodes of enhanced productivity (Erba, 2004). These OAEs are also marked by a major decrease in the $^{87}Sr/^{86}Sr$ record found in carbonates. Volcanism is known to be a source of unradiogenic Sr, and given the long residence time of Sr in the ocean, abrupt inputs of Sr will be broadened to intervals of at least 3 Ma in duration. Erba (2004)

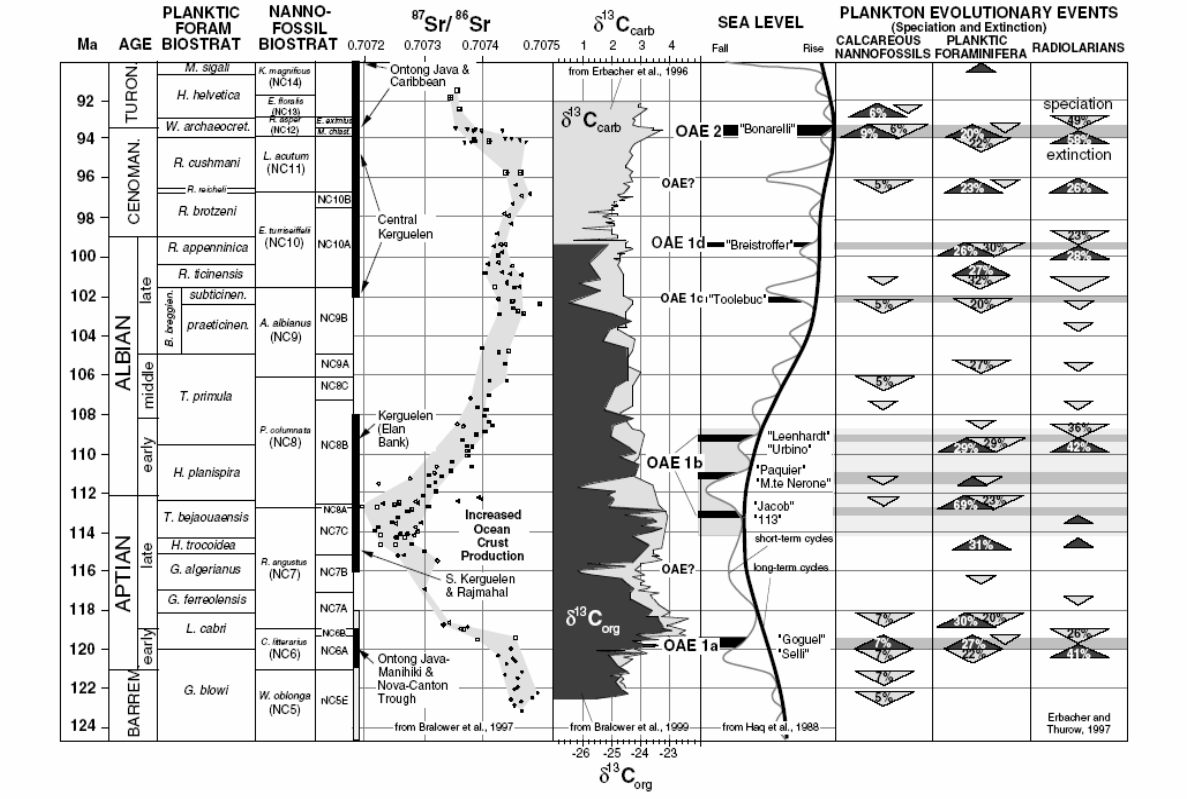

Figure 1. The timing of ocean plateau volcanic activity correlates with Cretaceous biostratigraphic boundaries and plankton evolutionary events, timing of oceanic plateaus (LIPs), seawater $^{87}Sr/^{86}Sr$ and $\delta\ ^{13}C$ variations, and changes in sea level (from Leckie et al., 2002). Note the sudden decrease in the $^{87}Sr/^{86}Sr$ ratio found just after the Ontong Java-Manihiki plateau formation (~122 Ma) and Caribbean plateau formation (~93 Ma).

attribute this decrease to the input of hydrothermal Sr from submarine volcanism during the emplacement of the Ontong-Java and Manihiki plateaus (OAE1a).

However, the fundamental relationship between ocean plateau volcanism, species extinction, and global ocean anoxia remains unclear and the temporal coincidence of these factors does not necessarily imply that the phenomena are related. Many theories have been offered to explain the relationship between trends seen and the deposition of black shales. Perhaps the most intriguing of these hypotheses is that of Sinton and Duncan (1997) who first proposed that metal rich eruptive "event plumes" resulting from the emplacement of individual, massive lava flows during the construction of ocean plateaus may have stimulated black shale deposition.

Snow (2003) and Snow et al. (2005) have expanded upon Sinton and Duncan's (1997) hypothesis to better understand the specific links between event plumes and global ocean anoxia that occurred at the Cenomanian-Turonain boundary (~93 Ma), which is correlated with Ocean Anoxic Event 2 (OAE2). Snow et al. (2005) measured the distribution of major, minor, and trace element abundances from pelagic carbonate and black shale sequences from Pueblo, Colorado, along with four other marine sedimentary sections from around the world. Anomalies in the metal abundances were then compared to the types of metal signatures expected from both normal (chronic) hydrothermal activity and eruptive "event plume" activity for evidence of either. Finally the stratigraphic position of these metal anomalies was used to determine the timing of the plateau emplacement with respect to the onset of anoxia, as determined

by the $\delta^{13}C$ profiles. Snow's research suggests that the presence and stratigraphic location of metal anomalies associated with the formation of the Caribbean ocean plateau could be directly related to OAE2.

The purpose of this study is to determine if the same relationships seen by Snow et al. (2005) exist in other Cretaceous black shale sequences. In order to realize this goal a selection of samples from marine sedimentary sections that include Ocean Anoxic Event 1a (early Aptian) was collected and analyzed for a wide range of major, minor and trace elements. Elemental abundance anomalies in these sediment records were then subjected to the same comparisons used by Snow et al. (2005) that seemed to support the hypothesis of Sinton and Duncan's (1997).

Background:

Large Igneous Provinces

Large igneous provinces (LIPs) are massive emplacements of basaltic lava flows, dikes, and sills that formed during very brief eruptive periods (a few million years) (Coffin and Eldholm, 1994). Continental flood basalts, oceanic plateaus, and volcanically rifted margins all can form through LIP activity. LIPs apparently originate by processes unrelated to steady-state plate tectonics (volcanic arcs, mid-ocean ridges), but are instead thought to be erupted at the beginning stages of hotspot activity (Richards et al., 1989; Campbell and Griffiths, 1989). As such, LIPs are thought to begin as mantle plumes ascending by thermal buoyancy through the overlying mantle (Kerr, 2003). Numerical modeling and tank experiments suggest that when the plume approaches the base of the lithosphere, it broadens out in a roughly

flattened disk shape and undergoes adiabatic decompression producing melt in the area covered by the mushroomed-out plume head (Kerr, 2003). The temperature of the plume and thickness of the overlying lithosphere dictate the amount of melt produced; that is, the extent to which upwelling mantle may rise and decompress. For this reason oceanic plumes, which rise to shallower depths beneath thinner lithosphere, produce greater amounts of melt than their continental counterparts (Kerr, 2003). A schematic of LIP formation from Leckie et al., 2002 is shown as Figure 2.

The Cretaceous period includes a number of oceanic plateau LIP events, several of which appear to be correlated with a distinct decrease in the $^{87}Sr/^{86}Sr$ record (Wilson et al., 1998). Seawater $^{87}Sr/^{86}Sr$ values record the balance between strontium received in seawater via fluxes of hydrothermal activity ($^{87}Sr/^{86}Sr$ ~0.704), weathering of old sialic continental rocks ($^{87}Sr/^{86}Sr$ ~0.720), and the weathering of marine carbonate rocks ($^{87}Sr/^{86}Sr$ ~0.708) (Faure, 1986). As volcanism is a significant source of unradiogenic strontium it seems that the distinct decrease in seawater $^{87}Sr/^{86}Sr$ is due to an increase in submarine volcanic activity of some sort. Moreover, the presence of dramatically (up to 100 times background) increased concentration of trace metals found in sediments deposited at this time has been attributed to the enhanced seafloor

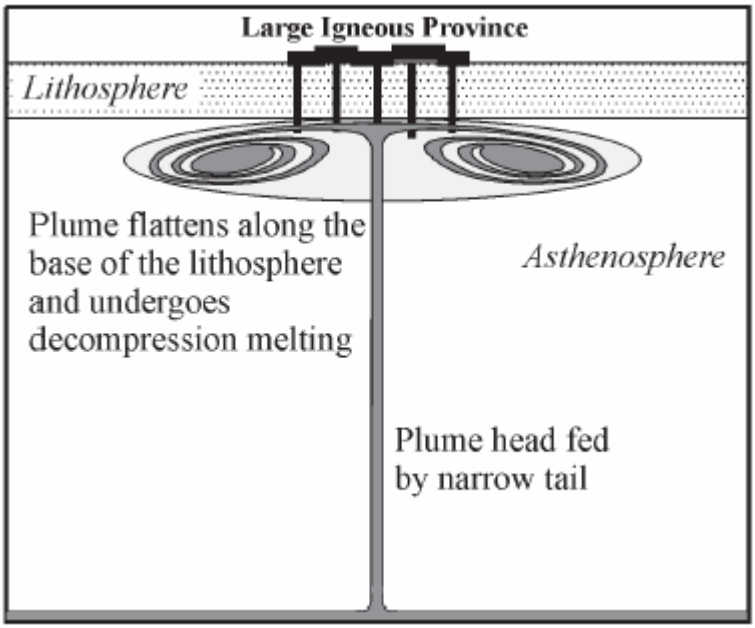

Figure 2. A thermally buoyant plume head approaches the base of the lithosphere, broadens out in a roughly flatttened disk shape, and undergoes adiabatic decompression producing melt in the area covered by the mushroomed-out plume head. The temperature of the plume and the thickness of the overlying lithosphere dictate the amount of melt produced, for this reason oceanic plumes produce greater amounts of melt than their continental counterparts. (After Coffin and Eldholm, 1994).

spreading rates (Orth et al., 1993). These metal anomalies have also been shown to coincide with species extinctions in ammonites and forams as well as ocean-wide anoxic events (OAEs) (Erba, 2004). Due to the close stratigraphic relationships between these events, considerable effort has been devoted to determining what the global responses to increased volcanism would be, as well as what the timing of the oceanographic, atmospheric, and biotic reactions would be.

Studies of continental flood basalts show that they were formed by the rapid eruption of massive lava flows, with individual flows amounting to thousands of cubic kilometers in volume. Each separate flow may have erupted over a period of weeks (Ho and Cashman, 1997). In addition, Swanson et al. (1975) demonstrated that a single flow could be as large as 1,500 cubic kilometers. As lavas that formed oceanic plateaus erupted through relatively thin lithosphere compared to continental flood basalts, their melt proportions could have been greater due to upwelling of mantle to shallower depths and greater decompression. Thus, over time scales of 100,000 to 1,000,000 years, the magmatic production of crust at oceanic LIPs is thought to exceed that of mid-ocean ridge spreading centers (divergent boundaries) (Duncan and Richards, 1991, Larson, 1991a, b).

Ocean Anoxic Events

While the concept that global anoxia in the deep ocean is responsible for the exceptional preservation of organic carbon during the Cretaceous is widely accepted (Schlanger and Jenkyns, 1976), there is still considerable debate as to the process forcing the ocean into such a condition. Two broad processes have been proposed for

the formation of black shales during the Cretaceous time period: markedly increased productivity and enhanced preservation (Schlanger and Jenkyns, 1976). In an effort to better understand the Cretaceous events, it is helpful to look for modern analogs. Anoxic events in the Cretaceous ocean are notable for their excellent preservation of organic material in the sediment record, this is generally attributed to a complete lack of oxygen in the seawater - clearly this is not the case in today's ocean. In fact, modern-day Earth has few areas of anoxia, and these are located in regions that exhibit either restricted circulation (like the Black Sea) or extremely high primary productivity (like the Santa Barbara Basin) (Brumsack, 1989).

Formation of anoxic water occurs in the Black Sea because the circulation of oxygen supplying waters is restricted due to the presence of a sill at less than 50 meters water depth at the outlet to the Mediterranean Sea. Oxygen initially becomes depleted in the deep waters due to the settling and decomposition of organic matter. Next, hydrogen sulfide diffusing from the sediments consumes the remaining oxygen, thus an anoxic water column is formed (Brumsack, 1989). The Santa Barbara Basin becomes anoxic in a slightly different manner. Here a basin with somewhat restricted circulation receives input water from the oceanic oxygen minimum zone (OMZ) in addition to a high organic flux from the coastal system; decomposition of the organic matter then depletes the available oxygen (Cannariato et al., 1999).

Cretaceous ocean anoxic events differ from these modern cases due to their incredible scale. Black shale sequences are found on oceanic plateaus, in ocean basins, on continental margins, and in shallow and shelf seas. The global extent of these

conditions during this time period suggests that they were not formed by means of restricted circulation and/or decomposition, as these are the result of the local environment. Instead, it seems indisputable that some fundamental change in ocean circulation and/or the production and preservation of organic material occurred (Sarmiento et al., 1988).

Hypotheses for Cretaceous Oceanic Anoxia

As mentioned above, two general methods have been proposed to explain the formation of these organic-rich shale sequences. Schlanger and Jenkyns (1976) suggested that the increased sea level during this time increased the area of shallow banks and inland seas, thus increasing the area receiving large terrestrial nutrient influxes. This "organic overloading", in turn, spurred primary productivity which would have then generated an increase in the depth range and perhaps intensity of the oxygen minimum zone (OMZ). The "enhanced preservation" model is based on the principle that diminishing oxygen contents have less capacity to oxidize organic detrital material, in order for this concept to be realistic a process must be shown to exist that will deplete the bottom water of oxygen (Schlanger and Jenkyns, 1976). Two possible environmental conditions have been suggested as possible stimuli for Cretaceous ocean stagnation. Schlanger and Jenkyns (1976) suggested that increased global temperatures and the reduction of the poleward temperature gradient during this time may have reduced the supply of oxygenated bottom water to the oceans. Saltzman and Barron (1982) suggest that bottom waters of the time reached as high as 15° C, more than 10° C warmer than today. The solubility of oxygen decreases

considerably as temperatures increase, so Cretaceous deep ocean waters probably contained significantly lower dissolved oxygen concentrations than the present.

The scenarios of "organic overloading" and "enhanced preservation" do not, however, satisfactorily explain all of the facets surrounding global anoxic periods. Most glaringly, the necessary variables for organic overloading and enhanced preservation were present throughout much of the Cretaceous era, but black shale sequences are present only in discrete, short intervals (Herbin et al., 1986). The very abrupt onset and conclusion of these events suggests that some other intermittent means of forcing existed, and that it perhaps pressed an already dysoxic ocean towards abrupt periods of anoxia.

Sinton and Duncan (1997) examined the impacts of catastrophic submarine volcanism and postulated that the creation of oceanic plateaus (like the Caribbean plateau whose first pulse of formation occurred ~93 Ma), directly contributed to the drawdown in seawater O_2. They hypothesized that this decrease was due to the oxidation of reduced metals in hydrothermal effluent "event plumes" and the stimulation of primary productivity in the surface waters. The most compelling evidence for this connection is the dramatically (up to 100 times background) increased concentration of trace metals found in sediments of this time (Orth et al., 1993; Snow et al., 2005). These metal anomalies coincide with species extinctions in ammonites and forams (Erba, 2004). In addition, this time frame also shows a distinct decrease in the $^{87}Sr/^{86}Sr$ marine carbonate record (Wilson et al., 1998). As ocean floor volcanism is a significant source of unradiogenic strontium it has been proposed that

this distinct decrease is due to an increase in hydrothermal inputs. Sinton and Duncan (1997) suggest that the short interval of this drop can be explained only by the emplacement of oceanic plateaus via large igneous provinces. A similar drop could possibly develop due to increased spreading rates, but in this scenario Sr levels would then remain at a decreased value.

As oceanic plateaus today are very large, thick, buried under sediments, and located mostly in submarine environments they are difficult to study. Current studies are subject to analytical uncertainties ($\geq$ 1 Ma) for the existing radiometric ages of the plateau rocks and the difficulty of directly observing the volcanic stratigraphy. Consequently, researchers have not yet resolved a precise eruptive history regarding flow volumes, rates, and duration (Sinton and Duncan, 1997). Instead, Sinton and Duncan (1997) relied on studies of continental flood basalt provinces as analogies, as oceanic plateaus are generally regarded as the submarine equivalent of the continental provinces due to their similar sizes, eruptive time frames, basaltic compositions, and a shared relation to hotspots. Sinton and Duncan (1997) used a hypothetical maximum lava flow volume of 10,000 cubic kilometers. Using this volume and modern hydrothermal compositions Sinton and Duncan (1997) showed that 7.92×10^{15} moles of O_2 would be consumed if all of the material in the vent effluent were completely oxidized. This is approximately six percent of the total dissolved oxygen in the modern ocean beneath the mixed layer. Due to its elevated water temperatures (and resultant lower dissolved oxygen content), the Cretaceous ocean would be even more affected than the modern ocean. Further calculations illustrated that if five percent of

the hydrothermal Fe reached the surface (warm hydrothermal fluids move upwards) of a high-nitrate, low-chlorophyll zone the amount of organic carbon produced would be enough to consume all of the seawater O_2 and deposit organic-rich sediments on the seafloor (Sinton and Duncan, 1997).

Erba (2004) suggests that global warming induced by volcanically elevated CO_2 levels would also trigger the melting of gas hydrates. The methane released in this scenario would further consume oxygen as it converted to carbon dioxide. Increased carbon dioxide levels in the atmosphere lower the pH of precipitation and contribute to increased continental weathering and nutrient flux through rivers, and increased coastal productivity. This scenario, while exhibiting that a small fraction of some limiting nutrient could produce a significant increase in organic carbon, is an extreme case and it is quite likely that phytoplankton production would be limited by some other biologically necessary nutrient before blooming to this extent (Coale et al., 1996). A schematic diagram illustrating an overview of the above processes is shown below, in Figure 3.

Sedimentary Signatures

Metal signatures found in sediments are the result of a complex series of events. Metals enter the seawater either carried by rivers in terrestrial runoff, as dust blown from continental weathering or volcanic events, and from submarine processes such as hydrothermal vents and submarine volcanic events (Segar, 1998). These

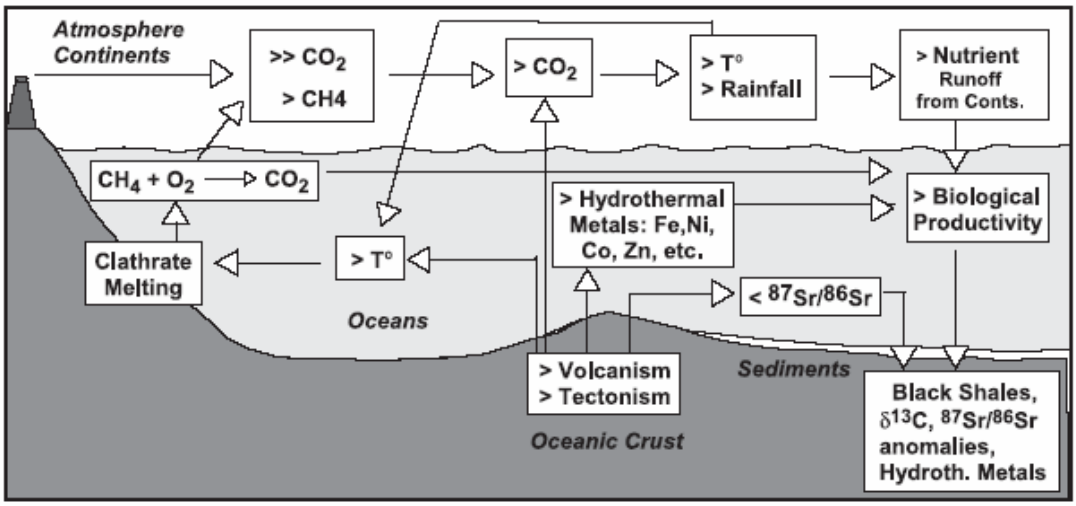

Figure 3. A proposed cycling system developed by Erba (2004) to explain Cretaceous sedimentary biological and geological processes. As volcanism increased CO_2 levels, global warming would be induced. Additionally, increased atmospheric CO_2 would lower the pH of rainwater, increasing continental weathering. This, in turn, would have elevated nutrient flux through rivers and resulted in increased coastal productivity.

metals can be transported either in particles or as dissolved ions. Particles are deposited on the ocean floor as sediments while dissolved ions eventually are precipitated and reach the sediments as organic detritus (having been used in biological process), or through a scavenging reaction (where the ions have an affinity for some other particle or substance and form a larger particle which then settles) (Pilson, 1998). It has been known for some time that hydrothermal fluxes of chemical elements to and from the oceans occur as cold seawater circulates through the highly permeable parts of the crust all along the mid-ocean ridge system and its flanks (Segar, 1998). As the water passes through the crust in these high temperature areas a series of reactions occurs, depleting this fluid of some elements while enriching it with others. The composition of these fluids is thus dominated by solubility-driven exchange between hot water and solidified rock (Rubin, 1997). This fluid then leaves the crust as a high temperature hydrothermal effluent, taking with it heat and a range of elements dissolved from high temperature rock. The hot, buoyant vent water rises up above the ridge, entraining surrounding seawater as it rises to a level of neutral buoyancy. Currents move this warm plume of water away from the ridge and it mixes with and finally becomes indistinguishable from the surrounding water. However, a sedimentary signature is left behind consisting of oxides of the more insoluble elements (e.g., Fe, Mn) which have short residence times.

Rubin (1997) has described the effects of the mass transfer of chemical elements to seawater occurring during underwater volcanic eruptions taking place both along the mid-ocean ridge system and at volcanically active seamounts. The magmatic

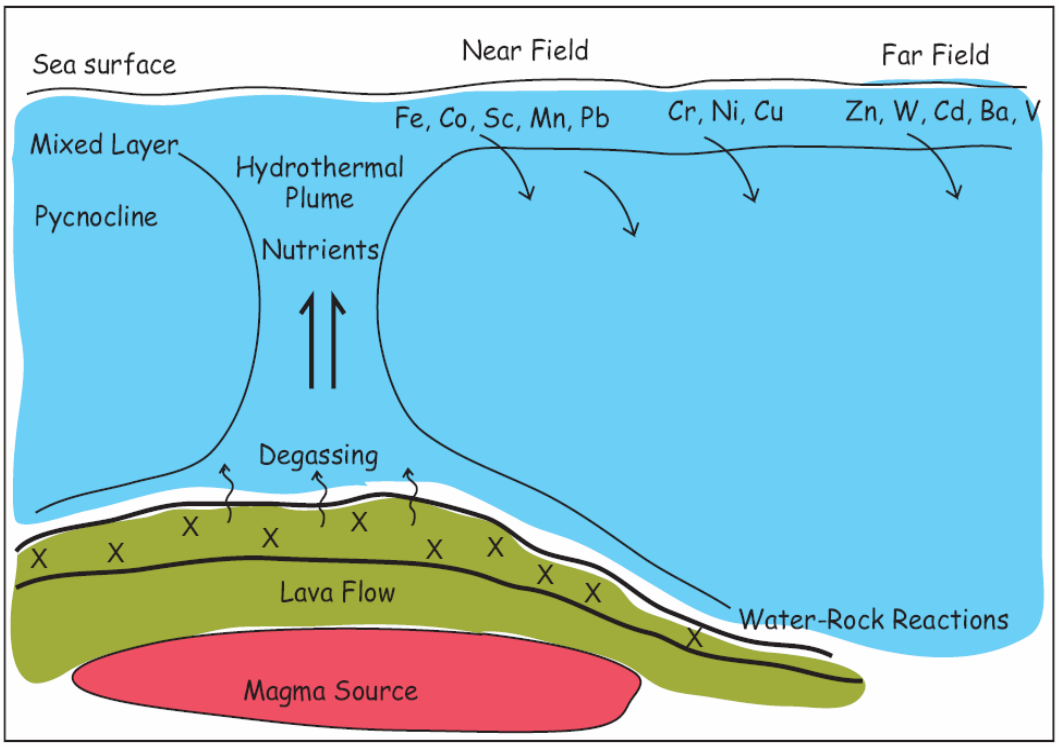

Figure 4. Schematic from Snow et al. (2005), demonstrates the relationship between near and far-field elements found in the sedimentary record and the location of the LIP eruption. The thermally buoyant megaplume rises to the surface caring a load of trace metals derived from both magmatic degassing and hydrothermal activity, these trace metals are subsequently fractionated out of the water column depending on their reactivity. More reactive elements (with shorter residence times) are termed “near field” elements, while elements more reactive elements are termed “far field” elements.

fluids that are associated with these underwater eruptions, derived from outgassing, are different in composition from their hydrothermal counterparts, in this case composition is dominated by volatility (Rubin, 1997). Due the estimated size of individual eruptive episodes during ocean plateau formation, these magmatic degassing events can have a much more pronounced thermal impact on the ocean than that of typical spreading ridge generated hydrothermal vent fluids. In the modern ocean, hydrothermal megaplumes rising 1000 meters above spreading ridges are known (Vogt, 1989). Vogt (1989) calculated that eruptions of 15 km^3 or more of magma onto the ocean floor would release enough heat to overcome the oceans stratification and drive a buoyant plume to the surface. Estimated volumes for single flows are one to two orders of magnitude larger. Considering also that ocean plateaus build up well above the ocean floor to shallow depths, it is certain that degassed magmatic fluids from these events had enough buoyancy to rise to the surface. Plumes would ultimately bring large amounts of metal-rich magmatic fluid to the surface, these substances would then undergo biological and chemical reactions, eventually ending up in the sediment record spread out in a manner dictated by their individual reactivities. A schematic diagram illustrating this process is shown in Figure 4.

As mentioned above, the abundance patterns of elements released to seawater hydrothermal fluids is different from that of degassed magmatic fluids. Rubin (1997) has estimated the general enrichment patterns associated with each group. He

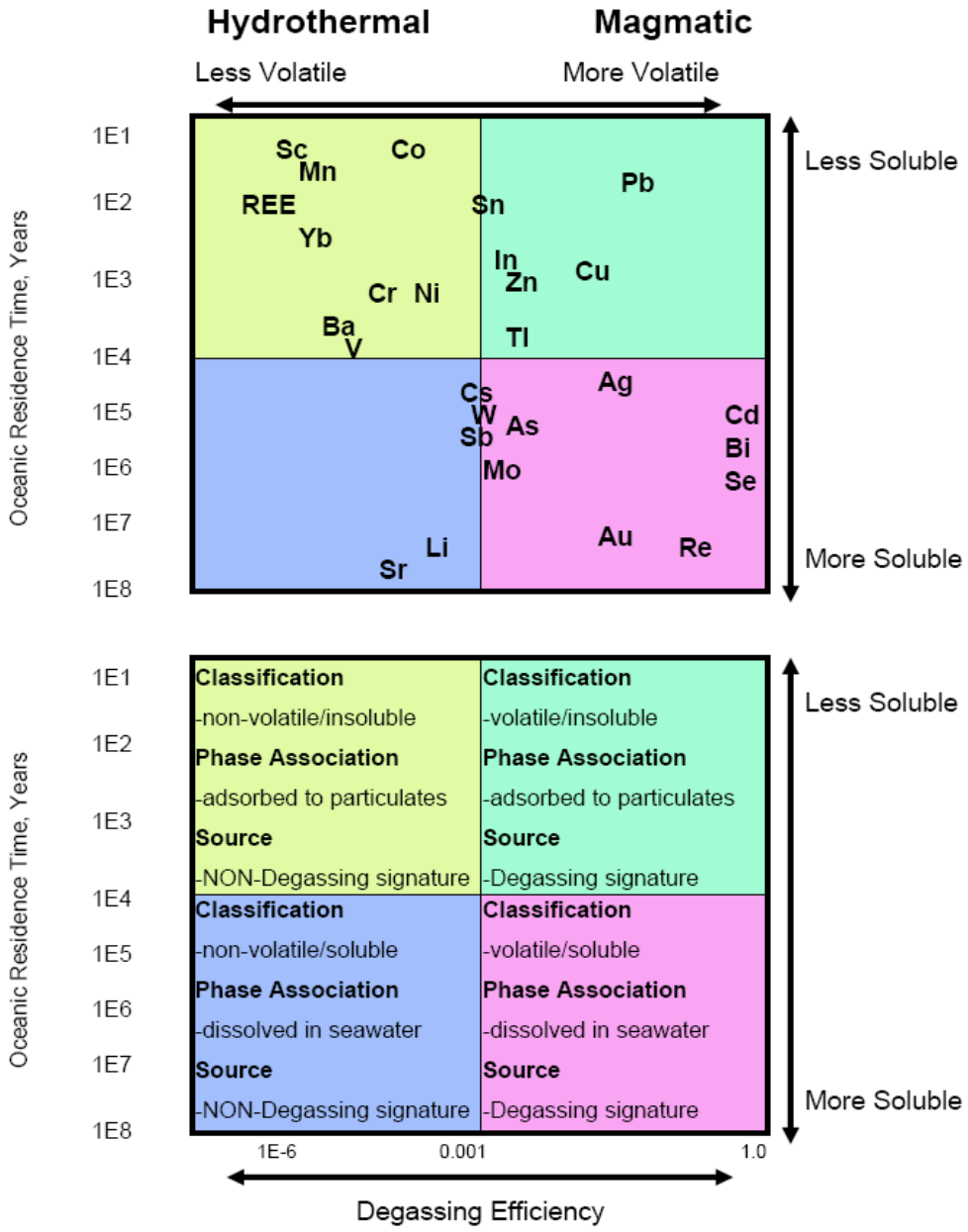

Figure 5. A chart developed to analyze the effects of volatility and mean ocean residence time of an element in seawater (after Rubin, 1997). This diagram is useful in determining the sources of elements found in pelagic sedimentary signatures. Hydrothermal waters would be enriched in Sc, Mn, Co, Yb, Cr, Ni, Ba, V, Li, and Sr while magmatic fluids would have enhanced levels of Pb, In, Zn, Cu, Tl, Ag, Au, Cd, Bi, Se, Au, and Re.

propose that the general enrichment pattern for steady-state hydrothermal events would be:

alkaline earths & alkali metals → transition metals → rare earths and actinides → main group elements

Degassed magmatic fluids are nearly the reverse of this; their enrichment pattern would be:

main group elements → transition metals → alkaline earths and alkali metals → rare earths and actinides

Hydrothermal (water-rock reactions) waters would be enriched in Al, Zn, Fe, Mn, Au, and Ir while thermally buoyant plumes rich in magmatic fluids would have enhanced levels of Mo, W, Hg, Bi, Se, Cd, and As (Rubin, 1997). A diagrammatic representation of this is shown in Figure 5.

The different chemical signatures could thus be used to discriminate sedimentary metal enrichments generated by the two processes. However, in the case of ocean plateau eruptive events, one would expect to see a mixture of the two: the initial magmatic degassing signature, followed by the hydrothermal signature as new lava flows and subsurface intrusions are infiltrated by seawater. This information could be used to help infer if the emplacement of the Ontong Java-Manihiki Plateau had effects that were global in nature.

Scavenging

The low dissolved trace metal content in the modern ocean cannot be attributed to lack of supply through geologic time, therefore researchers have suggested that these metals are subject to a rapid and efficient removal process, dubbed scavenging

(Balistrieri et al., 1981). Scavenging, or the absorption of chemical elements onto solid surfaces, has been recognized in recent decades as an important control on the distribution of these elements in seawater and sediments (Balistrieri et al., 1981, Bruland, 1983). An analysis of sinking particulate matter in the deep ocean suggests that the adsorptive properties are controlled by organic coatings on detrital material. As biological particles fall through the water column, the adsorption of metal ions or ionic complexes on their surfaces is a very effective means of removing trace elements from the seawater solution (Brown et al., 1994). Adsorption occurs because charges on the metal ions or ionic complexes are attracted to suitable bonding sites on particle surfaces. Scavenging occurs as particles (with their absorbed trace metal loads) coalesce into larger conglomerates and fall out of the water column and to the seafloor sediment (Brown et al., 1994). Scavenging is a remarkably efficient means of transferring elements from the seawater to the sediment, and will collect metals that are not biologically active as well. In the open ocean this detrital material is primarily generated by phytoplankton, or as waste products of the zooplankton that prey upon them (Bruland, 1983). Balistrieri et al. (1981) found that the residence times, with respect to scavenging, depend on three factors: the competing complexing abilities of the marine particle groups and the solution ligands, in addition to the flux of particulate matter in the water column. We therefore assume that scavenging was an important factor in removing trace metals from the Cretaceous ocean.

Diagenesis

Diagenesis is the physical, chemical, or biological alteration of sediments into sedimentary rock at low temperatures at the ocean floor which can result in changes to the original mineralogy and texture (Pirie, 2006). The oxidation of organic material during sedimentary diagenesis has been demonstrated to change the distribution of certain metals in sedimentary pore waters (Froelich et al., 1979). Some of these metals can become concentrated as a peak within the sediments, while others can diffuse across the sediment-water interface and back into the water column (Froelich et al. 1979; Nameroff et al., 2002). Different metals have different sensitivities to redox changes, meaning that different enrichment patterns will occur depending on the oxygen content of their depositional environments (Nameroff et al., 2002). Calvert and Pedersen (1993) demonstrated that some minor and trace elements (Cr, Mo, Re, U, V) become enriched in ocean bottom sediments during periods of bottom water anoxia, while other elements (I, Mn) indicate that the sediments accumulated during an oxygenated stage (Calvert and Pedersen, 1993).

While these elements are shown to accumulate in the upper sediment during anoxic periods, one can only wonder if the anoxic diagenetic processes can generate trace element rich bands. However, Algeo and Maynard (2004) state that there is "little evidence for translocation of trace elements under continuously anoxic conditions" like those that prevail during the deposition of black shales. As a caveat they add that remobilization of certain trace elements is possible, but only at a relatively fine scale (<1cm).

Cretaceous Metal Anomalies

Metal abundance peaks immediately below the C/T boundary were described by Orth et al. (1993). This study reported finding two metal excursions immediately preceding this boundary in a number of sites from around the world, these anomalies seem to correlate well with the nannofossil, foraminifera, and radiolaria speciation events of this time period in addition to excursions in the Sr isotope and ^{13}C records (Figure 1).

Specifically, the Orth et al. (1993) study discovered enhanced levels of Au, Co, Cr, Mn, Ni, Pt, Sc, Ti, and V in the same stratigraphic interval as the "Bonarelli Level" of Italy (Arthur and Premoli-Silva, 1982) and "Black Band" of England (Leary et al., 1989). This layer has been attributed to Ocean Anoxic Event 2.

Orth et al. (1993) concluded that the metal anomalies discovered in their study were the result of elevated mid-ocean ridge or hotspot activity. As stated earlier, this conclusion does not satisfactorily explain the short, discrete nature of these excursions but the hypothesis of Sinton and Duncan (1997) does. In this particular instance, metals released during the emplacement of the Caribbean plateau formed in discrete intervals in the sediment column due to the isolated yet substantial metal loading associated with event plumes. This combined evidence led Snow (2003) to choose Cretaceous Ocean Anoxic Event 2, at the Cenomanian-Turonian Boundary, as an appropriate interval to study in order to evaluate Sinton and Duncan's (1997) proposed link between ocean plateau emplacement and ocean anoxic events. Snow determined the distribution of trace, minor, and major element abundances for a sedimentary section (Rock Canyon, Colorado) spanning Cretaceous OAE2. By demonstrating that

the stratigraphic position of an interval of metal anomalies matched with other events assocated with OAE2, this studies findings indicated that metal anomalies did exist in the sedimentary record at the time of OAE2, indicating that similar anomalies should exist at other OAE events.

This Study

Snow's (2003) work provided evidence supporting the hypothesis that metal-enriched magmatic "event plumes" generated during the emplacement of the Caribbean plateau pushed the ocean into anoxia, a principal component leading to the formation of Ocean Anoxic Event 2 and ultimately the creation of black shales that are seen around the world today. This study's intention is to provide additional testing of Sinton and Duncan's (1997) hypothesis via an examination of the Ocean Anoxic Event 1a (OAE1a), thus providing evidence that this process was also the causative agent behind global ocean anoxia at other times during the Cretaceous. The following chapters will discuss major, minor, and trace elemental abundances found during the Aptian interval of sediment cores collected from the western mid-Pacific mountains. These cores, from the Deep Sea Drilling Project's sites 167 and 463 will provide two points of comparison for timing and near and far field effects of Ontong-Java plateau emplacement on local oceanic biogeochemistry. Additionally, data from the Cismon core (Belluno Basin, northern Italy) will be included in order to see the far field effects of Ontong Java - Manihiki plateau formation.

Chapter 2: Trace Element Abundances in Deep Sea Drilling Project Sites 167 and 463: Their Relationship to the Ontong Java-Manihiki Plateau Emplacement and Ocean Anoxic Event 1a.

Methods

In recent years it has become increasingly clear that the emplacement of several oceanic large igneous provinces is, at the very least, coincident with environmental effects on a global scale (Kerr, 2003). Snow (2003) studied the pattern and distribution of trace metal abundances in marine sediments deposited around the Cenomanian-Turonian boundary to establish whether the emplacement of the Caribbean plateau was related to the creation of Ocean Anoxic Event 2, as proposed by Sinton and Duncan (1997). This study strongly indicated that metal-rich effluents from submarine volcanism promoted anoxia. However, supporting evidence from another Ocean Anoxic Event would further strengthen the validity of this connection. In order to provide this evidence, this chapter reports the results of a study of Cretaceous Ocean Anoxic Event 1a, an event that is associated with the largest of the Cretaceous plateaus.

The Ontong Java Plateau

The Ontong Java Plateau is the largest of the oceanic plateaus formed during the Cretaceous, covering an area of approximately 1.9×10^6 km^2 and having an

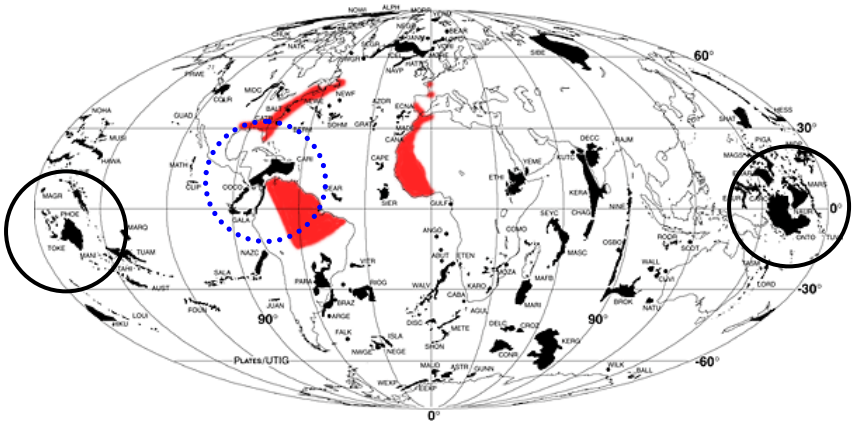

Figure 6. Location of global large igneous provinces in their modern day locations**.** After Coffin and Eldholm (1994), who listed the full names for the abbreviations. Note the Ontong Java and Manihiki plateaus circled in black (solid) and Caribbean plateau circled in blue (dashed).

estimated total volume of 4.4 x 10^7 km^3, with an average thickness of 32 km (Kerr, 2003). When it formed, the Ontong Java region was located at approximately 43°S (Fitton et al., 2004). Its current location spans the equator in the western part of the Pacific basin (see Figure 7). As the Ontong Java Plateau (OJP) collided with the Solomon arc, the southern margin of the plateau was uplifted, creating on land exposures of basaltic basement in the Solomon Islands (Fitton et al., 2004). Studies of these islands reveal a repetitive succession of Early Cretaceous tholeiitic pillow basalt, sheet flows, and sills (Petterson, 2004; Fitton et al., 2004). Additionally, rare and thin interbeds of laminated pelagic chert or limestone suggest high eruption frequency and emplacement into water deeper than 1000 meters.

A precise timing and duration of Ontong Java Plateau magmatism has not been established due to the difficulty of performing $^{40}Ar/^{39}Ar$ dating on the low potassium plateau basalts (Fitton et al., 2004). Studies by Mahoney et al. (1993) and Tejada et al. (1996, 2002) using $^{40}Ar/^{39}Ar$ data agree that there was a major episode of plateau magmatism ~122 Ma and another, smaller episode ~90 Ma. Ages determined using biostratigraphic data based on forams and nannofossils interbedded in the lava flows suggest that magmatism occurred from the early to late Aptain, a period corresponding to ~122-112 Ma on the Harland et al. (1990) time scale.

Alteration of Ontong Java Plateau basalts has occurred. Evidence exists for the low temperature alteration of these rocks through contact with seawater, and alteration ranges from slight to complete (Fitton et al., 2004). The replacement of olivine by clays is the most common, and initial type of alteration seen in the basalts. Later stages

of alteration occurred as cold, oxidizing seawater caused limited replacement of primary phases and mesostasis by smectite and iron oxyhydroxides (Fitton et al., 2004). These types of alteration have been shown to occur in the same manner as that of ridge basalts (Fitton et al., 2004). No evidence was recovered to indicate that high-temperature alteration occurred in any of the recovered basalts.

The Manihiki Plateau

Basalts cored at the Manihiki Plateau have been compared to those recovered from the Ontong Java Plateau. They share many common characteristics including their vesicular nature, the fact that they contain phyric plagioclase, and that they share probable oceanic tholeiitic composition (Schlanger et al., 1973). Ontong Java basalts contain somewhat more altered olivine phenocrysts, but appear identical in texture, in the presence of small plagioclase phenocrysts, and in the suspected presence of two pyroxenes in the groundmass (Schlanger et al., 1973). Additionally, based on radiometric, magnetostratigraphic, and biostratigraphic dating of sediment and basement, Tarduno et al. (1991) placed the age of the Manihiki Plateau at ~122 Ma. Finally, radiometric dating and isotopic geochemistry done by Mahoney et al (1993) identified two common lava series (the Singgalo and Kwaimbaita). This combined evidence suggests that the Manihinki Plateau may be an additional manifestation of the Ontong Java large igneous province, if this were the case this LIP would have affected ~1% of the surface of the Earth (Coffin and Eldholm, 1994).

The Magellan Rise

Paleontological evidence has indicated that the oldest sediments found on the crest of the Magellan Rise are about 135 million years old, making them some of the oldest material cored in the Pacific. As a consequence this location includes a sedimentary record that predates the formation of the Ontong Java Plateau (Winterer et al., 1973). Additionally, the summit of the Rise is above the present calcium carbonate compensation depth (CCD) allowing for preservation of calcareous nannofossils; the continued presence of these fossils down-core suggests that the summit of the rise has always been above the CCD (Winterer et al., 1973). Models indicate that the initial water depth of the plateau could have ranged anywhere from approximately 3750 meters (calculated based on a static model accounting for isostatic subsidence under the load of sediments) to only 400 meters (calculated based on plateau subsiding apace with typical seafloor in addition to sediment isostatic loading), depending on model parameters (Winterer et al., 1973). Regardless of depth, no evidence of resedimented shallow water material was detected in the core (or at this site), demonstrating that this area remained stable and above the CCD since Cretaceous times (Winterer et al., 1973).

The Magellan Rise has shared a pattern of movement with the Ontong Java Plateau, as both ride upon the Pacific Plate. Prior to the Cretaceous period, the Magellan Rise was located at approximately the same latitude as the Ontong Java Plateau (~40° S, see above). Based on the shape of the sediment accumulation curve during the Cretaceous, the Rise moved northward on the Pacific Plate, bringing it to an equatorial position by the end of this period. Since this time, it has been moving

northward at approximately 1° every 4 million years to its present location (Winterer et al., 1973).

Sample Acquisition, Site 167

One set of samples used in this study is from the Deep Sea Drilling Project (Winterer et al., 1973) Site 167 Hole recovered from the Magellan Rise at 07°04.1'N , 176°49.5'W in 3166 meters of water (Winterer et al., 1973). Figure 8 illustrates the location of this and other drill sites in the Central Pacific Basin. This core was selected due to its relative completeness (owing to its elevation above the present CCD) in addition to biostratigraphic and magnetostratigraphic studies that provide an age model and demonstrate reasonably continuous sedimentation during the Aptian period. In addition, the core was sampled in a location reasonably close to the Ontong Java plateau, where trace metal abundances are expected to be very high, especially for those elements having short residence times (see Figure 5). Cretaceous chalk, limestone, and chert were cored from about 680 meters to 1165 meters, an interval covering ~110 Ma to ~125 Ma (Winterer et al., 1973). Sediment accumulation rates were relatively slow during the Early Cretaceous (~4-10 m/m.y.) but increased during the Late Cretaceous (~20 m/m.y.) (Winterer et al., 1973). Samples (in 20 cm intervals), covering the period spanned by cores 63 to 70, from Hole 167 were obtained from the Ocean Drilling Program core repository. This provided a sedimentary record from 870 meters below sea floor (mbsf) (core 63) to 935 mbsf (core 70) during a time interval

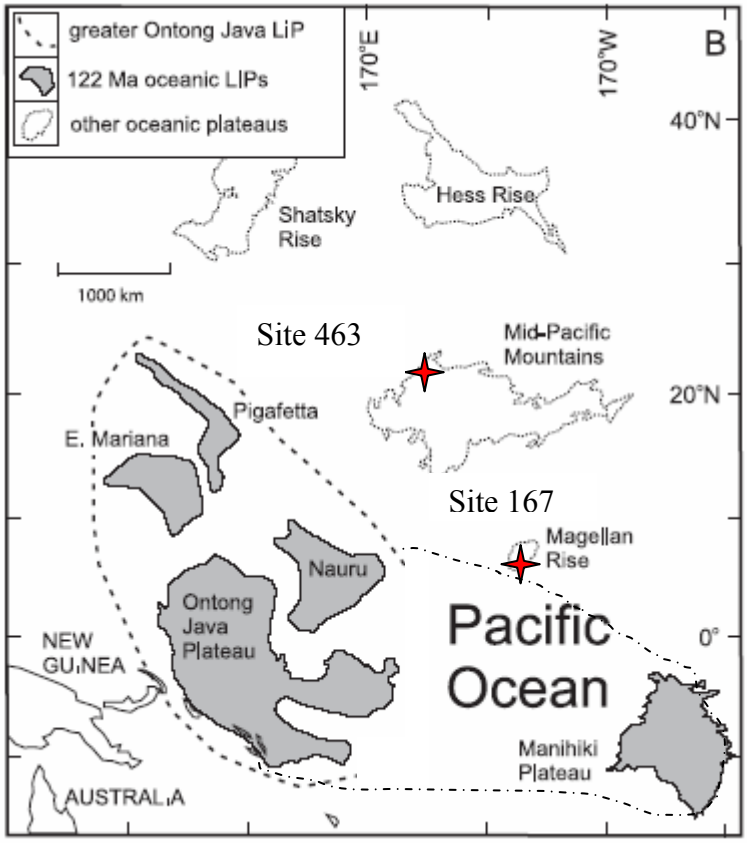

Figure 7. Locations of DSDP Sites 167 and 463 (red stars) in the modern day.

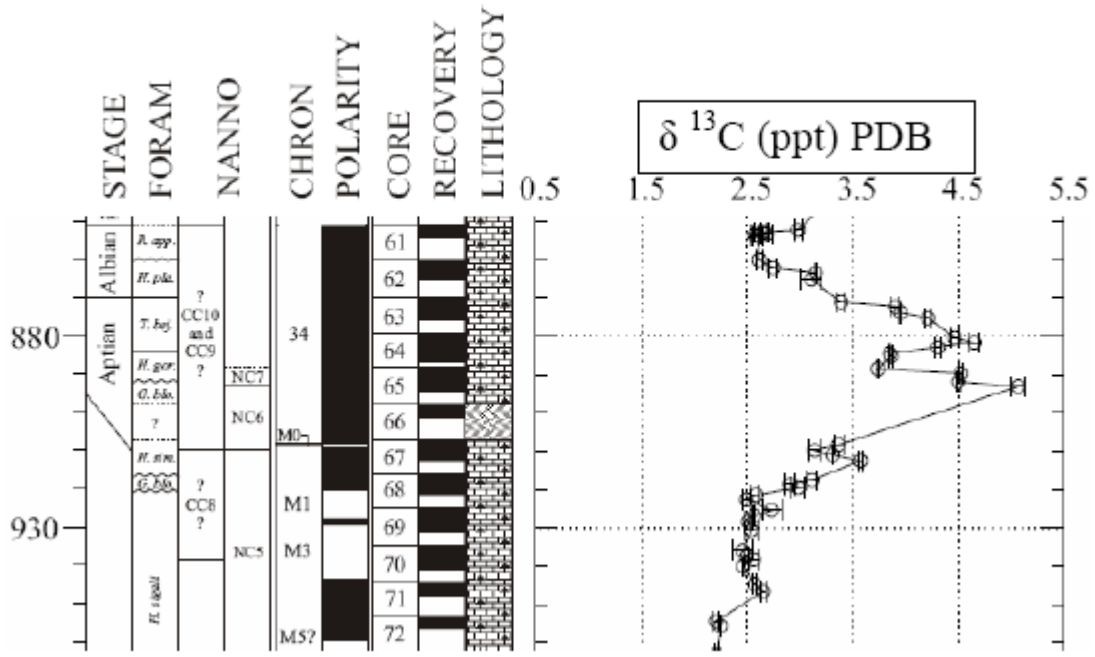

Figure 8. $\delta^{13}C$ for Site 167. Notice the dramatic positive excursion, beginning at ~920 mbsf. Data from L. Clarke (unpublished data).

exhibiting a dramatic positive $\delta^{13}C$ excursion (L. Clarke, unpublished data), see Figures 1 and 9.

Core 63 consists of limestone and chert, the upper part of which is generally marly and owes its reddish-brown color to hematite and has a total carbon content (%) ranging from 8.8 (top) to 11.0 (bottom) (Winterer et al., 1973, Bode, 1973). Cores 64-67 sampled a layer of dark green material containing volcanic glass and zeolites and have total organic carbon contents ranging from 10.4 % (top) to 7.6 % (bottom) (Winterer et al., 1973, Bode, 1973). In the cores 68-70, the limestone is commonly light in color with clay minerals concentrated into thin shale layers ; some zeolites and Fe/Mn oxide layers are intermixed as well (Winterer et al., 1973). These cores range from a low value of 2.9 % total organic carbon in core 68 to a high of 11.1 % in core 70, with an average of about 7.5 % total organic carbon (Bode, 1973).

The basaltic basement reached at this site was highly altered, containing many small calcite specks, some calcite amygdules, and rare thin calcite veinlets (Thiede et al., 1981). It was also highly brecciated. The nature of the amygdules, the thickness of the volcanic glass formed, the fine-grained nature of the basalt, and the brecciation all support the conclusion that Hole 167 ended in extrusive basalt (Thiede et al., 1981).

The Mid-Pacific Mountains

The Mid-Pacific Mountains are presently located in the central subtropical north Pacific (Thiede et al., 1981). They represent an ancient (Late Jurassic to Early Cretaceous) structural high rising between 2 and 3 km above the surrounding abyssal plain (Thiede et al., 1981). As a result of their position, the Mid-Pacific mountains are

a favorable location to collect ancient sedimentary sections, similar to that of the summit of the Magellan Plateau (see above). Also similar to the Magellan Plateau, the Mid-Pacific mountains have moved to the northwest, starting at approximately 20°S x 145°E, according to the rotation model of the Pacific plate developed by Lancelot and Larson (1975). Pringle and Duncan (1995) demonstrated that MIT Guyot, in the same area was ~123 Ma. All evidence indicates that this region is of early to mid-Cretaceous in age (Thiede et al., 1981).

Sample Acquisition, Site 463

A second set of samples used in this study was collected from the Western Mid-Pacific Mountains at 21°21.01'N ,174°40.07'E in 2525m water depth (Thiede et al., 1981). See Figure 8 for a map of this area. The selection criteria for this core are the same basic ones as those discussed above; e.g. a relatively complete and continuous sedimentary record existed for the Aptian interval. This core, however, was collected in an area that was (is) significantly farther (~2700km vs. 1500km to nearest point, see Figure 8) from the eruptive events forming the Ontong Java - Manihiki Plateau and, thus, should see some of the effects of dilution displayed in the trace element ratios of its sediments.

Multicolored, silicified, tuffaceous, calcareous, pelagic, and clastic limestones were cored between the Late Albian to Late Barremian stages (Thiede et al., 1981). The Early Aptian period, between these two stages, demonstrates a predominately tuffaceous and calcareous lithology (Thiede et al., 1981). Paleo-water depth at this

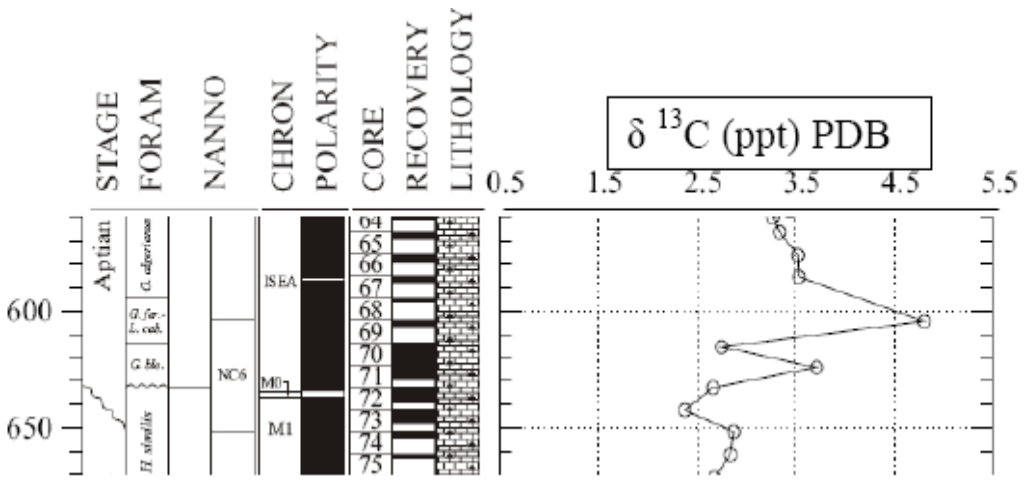

Figure 9. $\delta^{13}C$ for Site 463. Notice the dramatic positive excursion, beginning at ~630 mbsf. Data from L. Clarke (unpublished data).

time was several hundred meters. Samples were obtained for the section spanning the sub-bottom depth form approximately 585 mbsf to approximately 660 mbsf (~115 to ~125 Ma respectively), starting with core 67 and ending with core 75. Accumulation rates on average were ~12 m/m.y. during the Albian and ~27 m/m.y. during the Aptian. Total organic carbon content is 0.1 (%) in cores 67 and 68, jumps to 1.5-1.6 in core 69, falls off in Core 70 which has a high value of 0.7 (%) and a low of 0.0 (Thiede et al., 1981). Core 71 has a low of 0.1(%) and a high of 0.4 (%), while core 72 spikes form 0.1(%) to 1.4 (%) and then drops off (Thiede et al., 1981). Cores 73-75 have very similar values, with a dominant value of 0.1% (Thiede et al., 1981). These samples were processed in 20 to 40 cm intevals, allowing for a higher resolution picture of particular areas shown by L. Clarke (unpublished data) to have high $\delta^{13}C$ excursions (see Figure 10).The basaltic basement was not reached at this site.

Sample Processing

Crushing

The samples were prepared for microwave dissolution, first with a rigorous cleaning (using laboratory wipes and analytical grade acetone) of the alumina plates of a mini jaw-crusher. Once the plates were satisfactorily cleaned, the jaw crusher was reassembled and a sample was run through the crusher. The crushed material landed in a plastic weighing dish and was immediately placed into a plastic bag awaiting further preparation. The jaw crusher was then brushed off prior to the careful cleaning of the machine in preparation for the next sample. Throughout the entire process, every effort was made to prevent any outside metal contamination.

Powdering

Next, a quarter of all jaw-crushed material was selected for powdering. This strategy was selected to avoid the possible biases that sieving to a certain size fraction may have instilled into the sample composition. The selected portion of crushed material was placed into a previously acetone-cleaned diamonite mortar, and a pestle of the same material was used to mill the material into a homogenous powder. The resultant powder was then poured into a vial that had been blown out with canned air. All parts of this step were designed to provide a sample with the lowest possible contamination between samples and from ambient dust.

Microwave Dissolution

Finally, the samples were dissolved using a Microwave Accelerated Reaction System 5 (MARS5). This process begins with 0.0600 g (+/-0.0005g) of sample being weighed and placed into a Teflon tube (vessel). Twelve tubes are used, tubes one and two consisting of repeats of the same sample, as tube one is used in the temperature and pressure monitor vessel and does not provide accurate results. Reagent blanks were included on nearly every run. Standard reference materials were also prepared in this manner. After the samples were weighed and placed into the vessels 5 mL of reagent grade hydrofluoric acid (HF), 3 mL of omni-trace 16 normal nitric acid (16N HNO_3), and 1 mL of omni-trace 6 normal hydrochloric (6N HCl) were added to the samples to assist in the dissolution process. These vessels were then assembled into their frames in the following manner: vessels were placed into pressure sleeves and lids with safety membranes (new each time) were added. This assembly was placed into the frame and screwed down with 5 ft-lb provided by a torque wrench. A

temperature monitor was added and the entire carousel was placed into the MARS microwave. Digestion was completed using the program SHALE where the microwave operated at 1200 Watts for a 15 minute ramp to a temperature of 200° C and a pressure of 250 pounds per square inch. The samples were held at this level for 45 minutes, then allowed to cool to less than 60°C before evaporation.

Microwave Evaporation

Evaporation involved moving the vessels from the dissolution frames into an evaporation carousel. For the initial evaporation lids were rinsed with 1 mL of double distilled water which was then added to the digestion mixture. The evaporation carousel was assembled with a temperature probe and vacuum exhaust and placed into the microwave for evaporation. A vacuum was generated in the exhaust by a pump, this vacuum exhaust was directed, via its tube, to a system of three scrubbers. These scrubbers contained 4% boric acid, 5% sodium hydroxide, and water, samples ran through each of these scrubbers respectively to neutralize the evacuated gases. In this case, the program used was EVAP MIXED ACIDS, microwaving the samples at 600 Watts for 4 minutes to a temperature of 105°C, holding the sample at this temperature until a rapid temperature drop was noticed. Normally the machine was manually stopped at this time to reduce the risk of damage to the temperature probe. Samples were allowed to cool to less than 60°C before secondary and tertiary evaporations, these followed similar methodology to the initial evaporation with some slight variations. Instead of water, 4 mL of HNO_3 was added to the vessels, and the evaporation program used was EVAP HNO3 featuring a 2 minute ramp to 110°C.

Upon completion of the third evaporation sequence, 9 mL of 2N omni-trace HNO_3 was used to rinse the sample into weighed 15 mL Nalgene bottles. Upon completion of this step, samples were ready to run through the mass spectrometer.

Microwave Cleaning

A cleaning run concluded the digestion process. Vessels were filled with 12 mL of 8 N HNO_3 and reassembled into the frames as described in the *dissolution* step. The CLEAN program used 1200 Watts and ramped the samples for 8 minutes to 200°C. All parts were then washed in double distilled water and placed in the clean hood to dry before the next run.

Sample Analyses

Trace and Minor Elements

Microwave dissolved samples were analyzed for trace and minor elements using Oregon State Universities VG PQ-Excell Inductively Coupled Plasma Mass Spectrometer (ICP-MS). This instrument is located in the College of Oceanic and Atmospheric Sciences' W.M. Keck Collaboratory. Analysis starts with pipetting a 25-fold dilution into test tubes; 0.2 mL of sample solution is diluted with 5.0 mL of 1% triple-quartz distilled HNO_3. Additionally, 0.1 mL of a In-115/Re-187 internal

Table 1. Means and standard deviations for Minor and Trace element data. Units are ppm.

Element	MAG-1 Accepted Values	MAG-1 Mean	MAG-1 Standard Deviation	63 R1 29-31 Mean	63 R1 29-31 Standard Deviation	69 R1 30-33 Mean	69 R1 30-33 Standard Deviation	63 R3 120-123 Mean	63 R3 120-123 Standard Deviation
45Sc	17.00	17.97	2.14	0.36	0.00	0.15	0.00	0.31	0.01
51V	140.00	129.12	17.67	0.64	0.01	0.25	0.00	0.34	0.01
52Cr	?	99.13	7.30	0.35	0.00	0.26	0.01	0.24	0.01
59Co	20.00	19.98	0.33	0.79	0.13	0.28	0.06	1.16	0.60
60Ni	53.00	49.92	6.87	1.67	0.04	0.75	0.01	0.62	0.08
65Cu	30.00	27.37	1.50	1.96	0.03	0.37	0.02	0.32	0.02
66Zn	130.00	132.65	7.97	2.38	0.05	1.05	0.02	0.72	0.04
74Se	?	5.10	0.28	9.72	0.19	3.10	0.26	4.07	0.48
75As	9.20	9.99	1.10	44.00	1.42	0.11	0.00	28.83	2.88
85Rb	150.00	182.04	23.71	73.75	0.40	0.61	0.01	68.59	0.82
86Sr	150.00	172.82	5.59	38.01	0.18	10.86	0.11	17.27	0.25
89Y	28.00	34.97	5.49	658.28	3.54	0.67	0.01	184.76	2.42
90Zr	130.00	125.40	11.05	0.16	0.00	0.48	0.01	0.13	0.02
95Mo	1.60	1.46	0.28	463.29	7.46	0.00	0.01	13.86	7.97
107Ag	0.08	0.50	0.09	2.85	0.90	1.86	0.23	3.89	1.03
111Cd	0.20	0.26	0.03	14.59	0.32	11.16	0.36	5.42	0.74
118Sn	3.60	3.51	0.30	21.55	2.66	8.86	10.51	6.96	0.48
121Sb	0.96	1.13	0.15	8.80	0.18	2.01	0.13	2.04	0.14
133Cs	8.60	11.92	2.57	6.22	0.07	0.02	0.00	4.37	0.06
182W	1.40	1.34	0.25	103.52	0.56	29.71	0.39	16.74	0.29
197Au	0.00	0.14	0.02	1.01	0.16	0.66	0.14	0.52	0.22
205Tl	?	0.83	0.25	54.30	1.58	13.64	0.18	13.77	0.47
208Pb	24.00	17.08	0.63	5.60	0.20	4.19	0.01	5.21	0.04
209Bi	0.34	0.24	0.06	17.60	0.73	3.26	0.26	11.05	0.68
232Th	12.00	10.93	5.99	2026.04	152.84	978.67	31.10	423.42	12.40
238U	2.70	2.29	0.15	45.25	26.65	403.49	10.10	235.19	6.57

standard solution was added to correct for instrument drift, loss of sensitivity, and matrix effects. All ICP-MS runs for this study followed a similar sample layout. The first tube of the set is always an analytical blank, this is followed by several standard reference materials, next a blank, and finally samples were placed in racks, with a repeat every 10^{th} sample to account for sensitivity effects. Each run contained between 80 and 100 samples. The samples were followed by another blank, and then re-runs of the standard materials.

Upon completion of the ICP-MS run, calibration curves (developed from the standard reference materials) are checked for accuracy. Once this step is completed, two forms of data are available for comparison. Raw ICP-MS results are reported in "analyte integrated counts per second" (counts), these are converted by the instrument software using the standard curves to "analyte dilution concentration" (ppm, ppb, or ppt in solution). Finally, the elemental concentration in liquid is converted manually to elemental concentration in the solid sample. Analysis of the United States Geological Survey (USGS) MAG-1 marine sediment and blind duplicates indicates that the percentage error for most elements is less than 10% (Table 1). Some elements, however, do have higher errors. These include Bi, Th, and U with percentage errors averaging between 10 and 20%. The elements Ag, Au, Cd, Co, and Mo have errors greater than 20%. Due to this larger instrumental uncertainty, inferences made using data from these elements should be treated with more caution. Analytical errors may also be introduced because only two internal standards were used during this analysis, as opposed to the normal three to four.

Table 2. Means and standard deviations for Major element data. Units are ppm.

Element	MAG-1	MAG-1	MAG-1	167 63R1 0-3 (1)	167 63R1 0-3 (1)	63R 01W 29-31 (1)	63R 01W 29-31 (1)
	Accepted	Mean	St. Dev.	Mean	St. Dev.	Mean	St. Dev
Al 167.079	86810.80	89691.41	2584.67	17.00	0.42	29.11	17.26
Ba 455.403	480.00	470.09	123.27	9.70	0.04	9.58	0.14
Ca 317.933	9792.20	10049.03	767.53	293.46	2.11	301.88	5.38
Fe 259.940	47566.20	48651.72	4987.48	17.55	0.12	16.48	0.45
K 766.491	29471.90	29806.55	2491.47	2.23	0.43	3.65	0.50
Mg 279.078	18093.50	17898.09	731.97	6.47	0.05	6.72	0.12
Mn 257.610	759.00	783.77	68.44	3.06	0.02	3.06	0.04
Na 589.592	28415.30	27590.31	1369.75	2.92	0.37	3.72	0.19
P 178.283	698.40	666.82	479.63	1.77	0.19	2.32	0.60
Ti 336.122	4496.10	4682.24	389.50	1.32	0.02	1.24	0.04

Major Elements

Major element concentrations were determined using two different instruments. The majority of Site 463 major element data was collected using inductively coupled plasma-atomic emission spectrometry (ICP-AES). This instrument was subsequently replaced with a new inductively coupled plasma-optical emission spectrometer (Varian Liberty 150) that was used to collect all of the major element data for Site 167. Additional samples from Site 463 were also processed on this instrument. All samples were processed in the same manner, regardless of instrument. Microwave dissolved standard reference materials, sample solutions, and procedure blanks were all diluted 100 times; 0.1 mL of sample solution 10 mL of 1% triple-quartz distilled HNO_3. All ICP-AES runs for this study followed a similar layout. The first tube of the set is always an analytical blank, this is followed by a group of external standard reference materials.

Next, an acid memory check is run (for extra wash time) followed by the samples themselves. Throughout the runs, one sample was used as a unknown repeat between every 10 samples. Results for ICP-AES are reported as intensities which are proportional to the concentration of that element in the sample. Using calibration curves developed with the standard reference materials element compositions of a given sample are quantified. Finally, a correction is applied to account for the dilution of the sample. Based on the analyses of blind duplicates and standards, the percentage error for the ICP-AES data used in this study is between 2-8% (Table 2), depending on the element analyzed and the sample. The elements Ba, Na, and P have

errors larger than this in some of the samples, so data concerning these elements should be treated with more caution.

Results

This study reports abundance measurements for twenty-eight trace and minor elements using an ICP-MS, and ten elements using ICP-AES instruments. All measurements for DSDP Sites 167 and 463 were made in Oregon State University's Keck Lab for Plasma Mass Spectrometry. Results for these experiments can be seen in Appendix 2. All minor element concentrations were normalized to zirconium (Zr), while major element concentrations were normalized to aluminum (Al). The only significant source of both of these elements to pelagic sediments is from terrigenous input, therefore this normalization accounts for the variable effects of terrestrial input into the composition of these sediments (Milnes and Fitzpatrick, 1989). One caveat must be made, however, about normalizing to Zr. Much of the zirconium found in pelagic sediments arrives in the form of zircons, which are very difficult to fully dissolve. However, the dissolution method developed by Snow (2003) proved to be very effective at fully dissolving the Zr present in shales. The same method was used for this study, and a comparison to a similar external standard reference material shows good Zr dissolution (see Table 1).

Site 167

The DSDP Site 167 core data collected during this study show two distinct Zr-normalized trace metal anomalies (Figure 10 and Appendix 2). The first (earliest) and smaller anomaly occurs in the interval between ~920 and ~910 mbsf. This anomaly

can be seen in all elements except Cd, W, Au, Hg, and Bi. A second, larger, anomaly occurs in the interval between ~890 and ~880 mbsf. This anomaly can be seen in all elements except W, Cd, and Hg. Major element data appear to remain at background levels throughout most of this sampling interval (Figure 10 and Appendix 2). However, the elements P and Ti contain slight positive excursions in the interval between ~890 and ~880 mbsf.

Site 463

The DSDP Site 463 core data collected during this study show two distinct Zr-normalized trace metal anomalies (Figure 11 and Appendix 2). The first (earliest) and smaller anomaly occurs in the interval from ~622 mbsf to ~617 mbsf. This anomaly can be seen in the minor elements V, Zn, Se, As, Y, Mo, In, Sb, Cs, Ba, W and Re. A second, larger, anomaly begins at ~610 mbsf and extends to ~580 mbsf. A very coarse sampling interval (due to incomplete core recovery) makes it difficult to determine if the peak seen in the Figures 11 is a separate occurrence or merely a continuation of the excursion starting at ~610 mbsf. As the same elements show anomalies in both areas, it was assumed that the latter is the case. This anomaly can be see in all of the minor elements with the exception of Y and Hg. Throughout this interval all major elements except Ti demonstrate a distribution indicative of background levels, no trends are easily distinguished (Appendix 2).

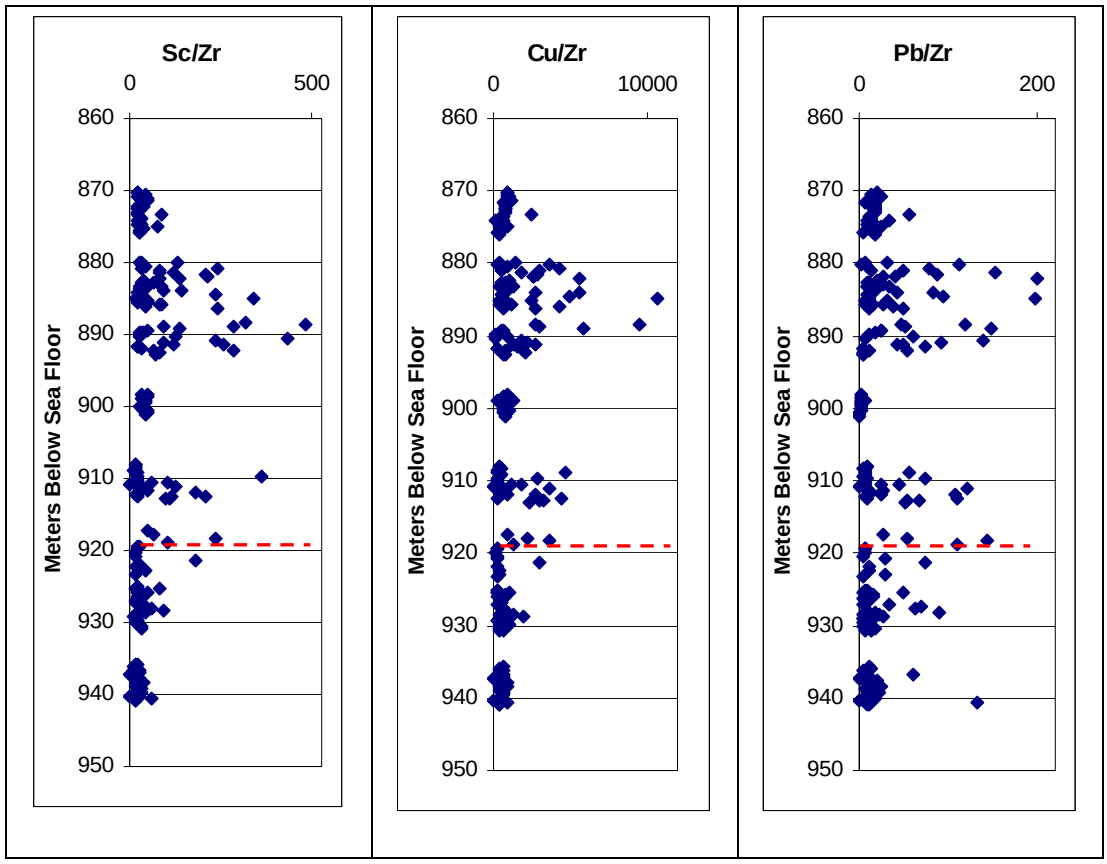

Figure 10. Minor (Sc, Cu and Pb) element data from DSDP Site 167**.** Two intervals of high metal abundance can be seen. The H. sigali/G. blowi. foraminiferal boundary (which marks the Aptian/Barremian boundary) is shown as a red line for reference.

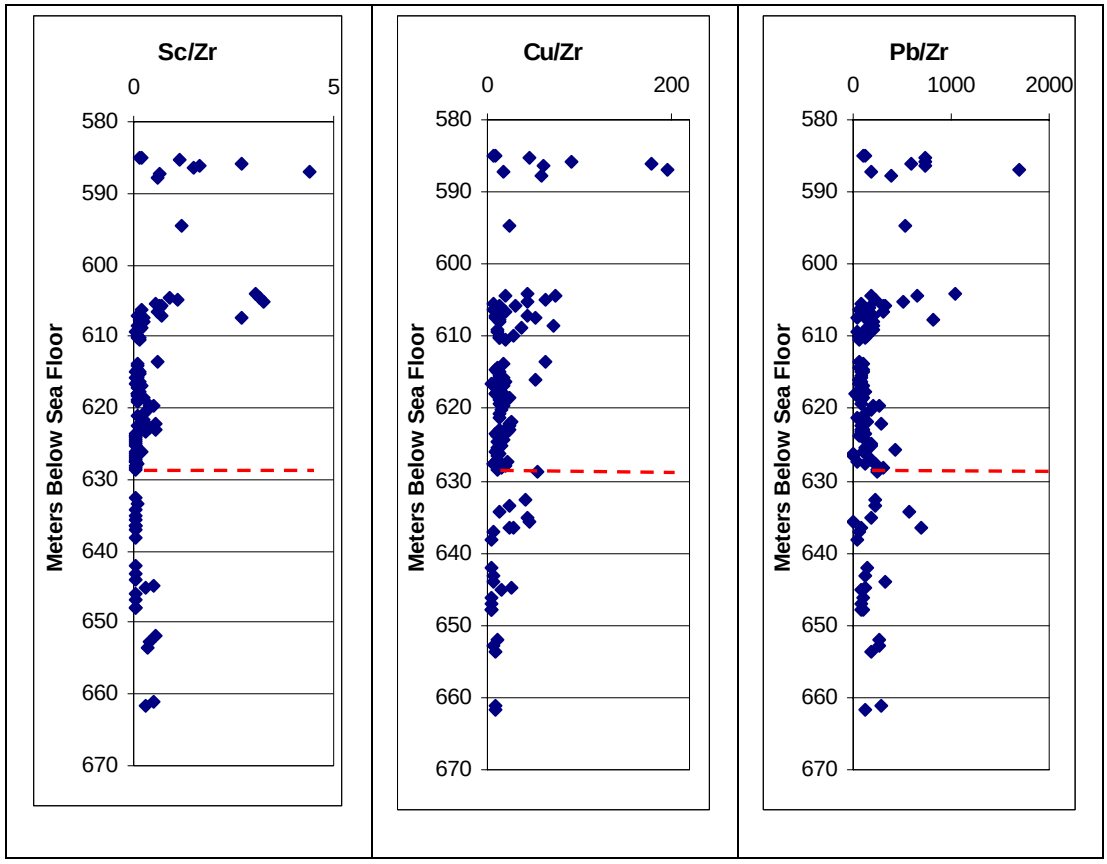

Figure 11. Minor (Sc, Cu, and Pb) element data from DSDP Site 463. Two intervals of high metal abundance can be seen. The H. sigali/G. blowi. foraminiferal boundary (which marks the Aptian/Barremian boundary)is shown as a red line for reference.

Discussion

The goal of this study was to assess the geochemistry of early Aptian (~122 Ma) sediments, deposited at the time of Ocean Anoxic Event 1a (OAE1a) from several locations, with respect to the hypothesis of Sinton and Duncan (1997). Specifically, if ocean anoxic events were promoted by plateau volcanism, there should be an identifiable signature of anomalously high trace metal abundances in the sediment record. Snow (2003) and Snow et al. (2005) found that trace metal anomalies in marine sediments that include the Cenomanian/Turonian boundary (~93.5 Ma) correlate closely with excursions in the $\delta^{13}C$ record, extinctions of benthic species, and turnover in plankton communities – all of which constitute Ocean Anoxic Event 2 (OAE2). This study is an extension of the previous work by Snow (2003), to evaluate the proposed link between OAE1a and submarine volcanic construction of the Ontong Java - Manihiki Plateau (~122 Ma).

Upon entering the ocean trace metals are ultimately removed from the seawater reservoir to marine sediments (Bruland, 1983). However, trace elements undergo varying degrees of recycling prior to their final removal to oceanic sediments. This recycling can involve particle interactions, benthic fluxes, scavenging reactions, diagenesis, or a combination of these processes (Bruland, 1983). Figure 12 is a schematic diagram demonstrating trace element sources to seawater. As discussed in the Introduction, there are several means by which trace metals can become enriched in sediments. Plankton themselves carry a suite of trace elements into the sediment

record, however the composition of planktonic organisms cannot explain the trace element peaks seen in this study. For a more detailed discussion of how the composition of plankton affects the sediment record, see Appendix 1. Additionally, as particles from decomposing plankton and other sources sink through the water column, they perform a crucial role in the scavenging of trace elements from seawater by providing suitable binding sites for the absorption of metal ions or ionic complexes. Scavenging was unquestionably an important factor in the trace metal enrichment of black shales. Water column oxygen and sediment diagenesis also can mobilize metals and create concentrations in the sediment record. However, the scope of these processes is not great enough to explain the anomalies seen in this study. For a more detailed discussion of these processes, see Appendix 1. Figures in Appendix 1 demonstrate the relationship found between metal fluxes in modern chemistry and marine planktonic composition, degassing and hydrothermal events, and metal abundance anomalies found in this study. These figures demonstrate that the element fluxes generated via degassing and hydrothermal means most closely resemble the trace metal abundance anomalies seen in the marine sediment record.

It is clear that undersea magmatic and hydrothermal activity due to the emplacement of the Ontong Java - Manihiki plateaus greatly altered the seawater chemistry intermittently, over a geologically brief interval in the early Cretaceous, and that this is what we see reflected in the sediment record containing OAE1a. If hydrothermal activity and degassing associated with the formation of the plateau were

responsible for the metal peaks seen in OAE1a, one would expect these peaks to have a close stratigraphic relationship to these events at globally distributed sites. Enrichment in trace metals, seen throughout the global ocean, would certainly be expected to influence marine life. Experiments done by Coale et al. (1996) demonstrated that iron fertilization in modern oceanic high-nitrate, low chlorophyll (HNLC) regions could greatly stimulate primary productivity. Using this experiment as a guide Sinton and Duncan (1997) calculated that the iron injected into the water column by ocean plateau formation could have triggered greatly enhanced primary productivity. Enhanced primary productivity would have had several effects: (1) increased organic particles falling through the water column depleted seawater oxygen through respiration; (2) organic particles scavenged trace metals and accumulated as black shales; (3) eutrophic conditions (and perhaps metal toxicity) would have favored the most opportunistic nannoplankton taxa, leading to crises of less successful competitors (Erba, 2004).

As major episodes of organic carbon removal occur, the lighter of the two carbon isotopes found in seawater (^{12}C and ^{13}C) is preferentially removed from the oceanic reservoir (Faure, 1986). This relationship leads to a shift to more positive carbon isotope compositions in marine sediments. Looking at integrated biostratigraphic and magnetostratigraphic data, together with carbon isotope data and the trace metal results of this study will help us determine if there was a biological response (i.e., removal of carbon) at the time of the hydrothermal plumes. Figure 13 shows selected trace metal data for each of the three sites compared with their

corresponding $\delta^{13}C$ record, aligned with bio- and magnetostratigraphic information for this period. All three sites (DSDP Sites 167 and 463, as well as the CISMON Apticore) reveal remarkably similar profiles. All profiles show a small positive $\delta^{13}C$ peak followed by an abrupt negative carbon isotope excursion during or just after the "M0" period. This is then followed by a dramatic increase in the $\delta^{13}C$ composition of carbonate.

Further comparison of Figures 1 and 13 demonstrate that the $\delta^{13}C$ anomaly is preceded by a documented worldwide change in nannofloral assemblages (Erba, 2004 and references therein). The nannoplankton response described above was suggested by Erba (2004) to be a result of a paleoenvironmental crisis. Erba (2004) proposed that this type of response is likely the result of eutrophication on a global scale. The trace metal peaks seen in Figure 13 are stratigraphically coincident (occurring both before and during the events) with the biotic changes reported at this same time (see Leckie, 2002 and Erba, 2004 for an overview of biologic events during this time).

As the trace metal peaks seen in this study have been demonstrated to be of hydrothermal and magmatic degassing origin, it seems evident that submarine volcanism had two drastic influences on marine phytoplankton. The "nannoconid crisis" was a global decrease in the abundance of rock-forming nannoconids marking the Early Aptian OAE1a (Erba, 2004). Erba (2004) suggested in the same work that this crisis was the result of selective metal toxicity because the nannoconid decline and crisis, correlates with metal peaks. The peaks she noted correlate with the larger (upper) metal peak seen in this study at Sites 167 and 463. Second, submarine

Figure 12. Trace elements cycle into and out of seawater in various ways. Sources include rivers, dust, hydrothermal activity, and magmatic “event plumes”. The main sink is sediment, although it can be a source under certain circumstances.

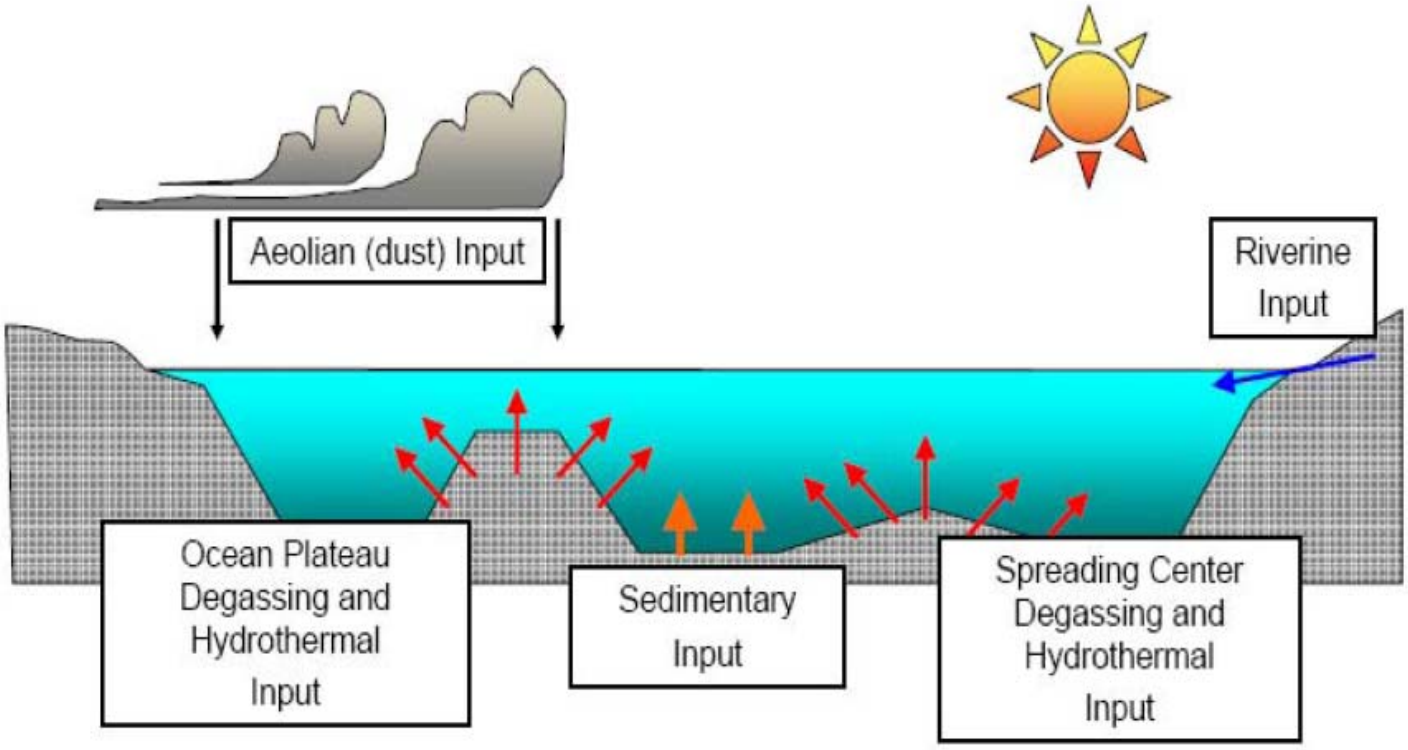
Aeolian (dust) Input
Riverine Input
Ocean Plateau Degassing and Hydrothermal Input
Sedimentary Input
Spreading Center Degassing and Hydrothermal Input

volcanic input of biolimiting metals could have triggered eutrophic conditions. This study suggests that the influence of the Ontong Java - Manihiki plateau emplacement affected marine organisms around the world. The eutrophic conditions stimulated by this event may have spurred primary productivity to the extent that respiration of organic matter would have depleted global ocean oxygen and promoted preservation of organic-rich sediments, resulting in OAE1a.

The submarine volcanic activity that formed the Ontong Java - Manihiki plateau should have left a combination of two patterns of trace metal chemical signatures in the marine sediment record. The first is from the release of a high temperature magmatic fluid degassed directly into the submarine environment as a direct result of eruptive activity (shown as "degassing" in Figure 12). A second signature is from hydrothermal fluids produced by exchange of heat and elements between seawater and porous lava flows as spreading centers cooled on the seafloor (shown as "hydrothermal" in Figure 12). Each of these processes delivers a distinct suite of elements into seawater (Rubin, 1997). If hydrothermal activity and degassing associated with the formation of the Plateau was responsible for the metal peaks seen in the black shales, one would expect these peaks to have a close stratigraphic relationship to these events.

The positions of representative trace metal anomalies found by this study in DSDP Sites 167 and 463 were plotted with respect to the $\delta\ ^{13}C$ curves for the same sites in Figure 13. Figure 13 also includes data obtained from the CISMON Apticore, northern Italy (Duncan and Erba, pers. comm.). The $\delta\ ^{13}C$ curve is a global signal, so

Figure 13. Figure is a plot comparing representative elements from the three sites used in this study, DSDP Sites 167 and 463 as well as CISMON (data from Duncan and Erba, unpublished). These sites have been correlated to each other using mageneto- and nannofossil- stratigraphy in addition to $\delta^{13}C$ excursions. Blue bar indicates the M0 period of magnetic anomaly. Organic carbon rich intervals are indicated with light green boxes. The $\delta^{13}C$ profile is represented by the light blue line with blue stars (L. Clarke, per. comm.). The dark blue line with circles represents the Zr normalized Sc data, the pink line with squares represents Zr normalized Zn data, and the green line with triangles represents the Zr normalized Pb data. In order to fit on the same scale, data from each site has been adjusted in the following manner: Site 167 (Sc/Zr/125; Zn/Zr*18; and Pb/Zr/50), Site 463 (Sc/Zr*2; Zn/Zr*2; and Pb/Zr/100), and CISMON (Zn/Zr/10).

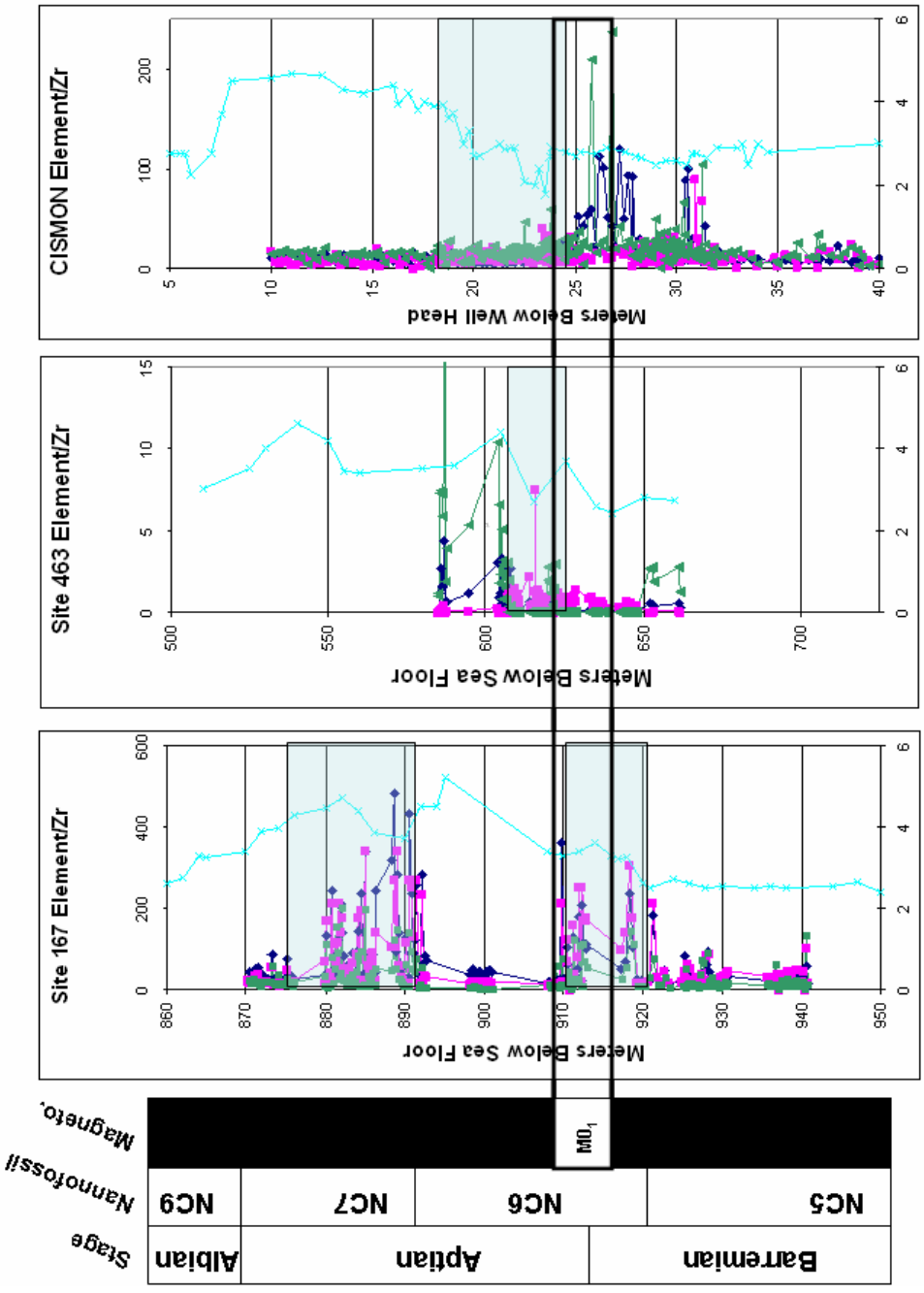
CISMON Element/Zr
Meters Below Well Head
Site 463 Element/Zr
Meters Below Sea Floor
Site 167 Element/Zr
Meters Below Sea Floor
Magneto.
Nannofossil
Stage
NC9
NC7
NC6
NC5
Albian
Aptian
Barremian
M0$_1$

the plots were aligned to each other using the common features of these profiles. Additionally, the plots were aligned using nannofossil and magnetostratigraphy. This provided tie points necessary to match the records and correct for differences in accumulation rates. Upon inspection of Figure 13, a small trace metal peak can be seen immediately preceding the first, smaller positive excursion in the carbon isotopic profile at Site 167. Site 463 demonstrates a small increase in trace metals shortly after this excursion as well. A trace metal peak is seen in the CISMON core at this same time. In Site 167 a second, larger trace metal peak can be seen following the larger positive carbon isotope excursion. Trace metal data for the same interval from the Site 463 and CISMON cores are not yet available for comparison. Comparing Figures 1 and 13 clearly demonstrates that the trace metal peaks seen in DSDP Sites 167 and 463 are stratigraphically coincident with the $^{87}Sr/^{86}Sr$ isotopic drop, planktonic evolutionary events, and the timing of the Ontong-Java and Manihiki plateau emplacement. This indicates that the trace metals released during the emplacement of oceanic plateaus are coincident the onset of ocean anoxia.

Degassing, Hydrothermalism, and Trace Metals

Hydrothermal activity related to the steady-state volcanic processes at mid-ocean ridges production emits trace metals, but it is unlikely that the effects of this activity would be confused with the volcanic activity on a massive scale associated with plateau formation. As noted earlier, the intermittent nature of these metal peaks is one indication that they are not directly related to the continual process of ridge formation. Additionally, Vogt (1989) has argued that hydrothermal plumes from

spreading ridges do not have enough thermal energy to reach the oceans surface and therefore cannot contribute metals to OAEs through the surface ocean. Rubin (1997) has shown that the two processes (hydrothermal and degassing) contribute a broad suite of metals to the water column.

Figure 5, adapted from Rubin (1997) provides a guide in understanding what elements are released by these two processes, and what their ultimate fate in seawater is. This figure shows volatility versus residence time for a number of elements. Volatility in this context is described as "the concentration difference of an element between pre-erupted magma and post-erupted lava" (Rubin, 1997). In other words, those elements that have higher volatilities more easily escape the magma as a fluid (gas) phase that mixes with seawater. A mean oceanic residence time is determined from the total mass of a substance dissolved in the oceans divided by the rate of supply (or removal) of the substance (Brown et al., 1994). Those elements with short residence times do not remain in the water column for long period of time, while elements with long residence times do. Hence, we expect to see a shift in the pattern of trace element abundances with distance from source, as a result of preferential removal, and an overall decrease in abundance of all such elements as a result of dilution.

Using the Rubin diagram to classify elemental abundance anomalies, a selection of elements seen in the ~920 mbsf peak at DSDP Site 167 are plotted (Figure 14). The less volatile, short residence time elements are quite enriched at this

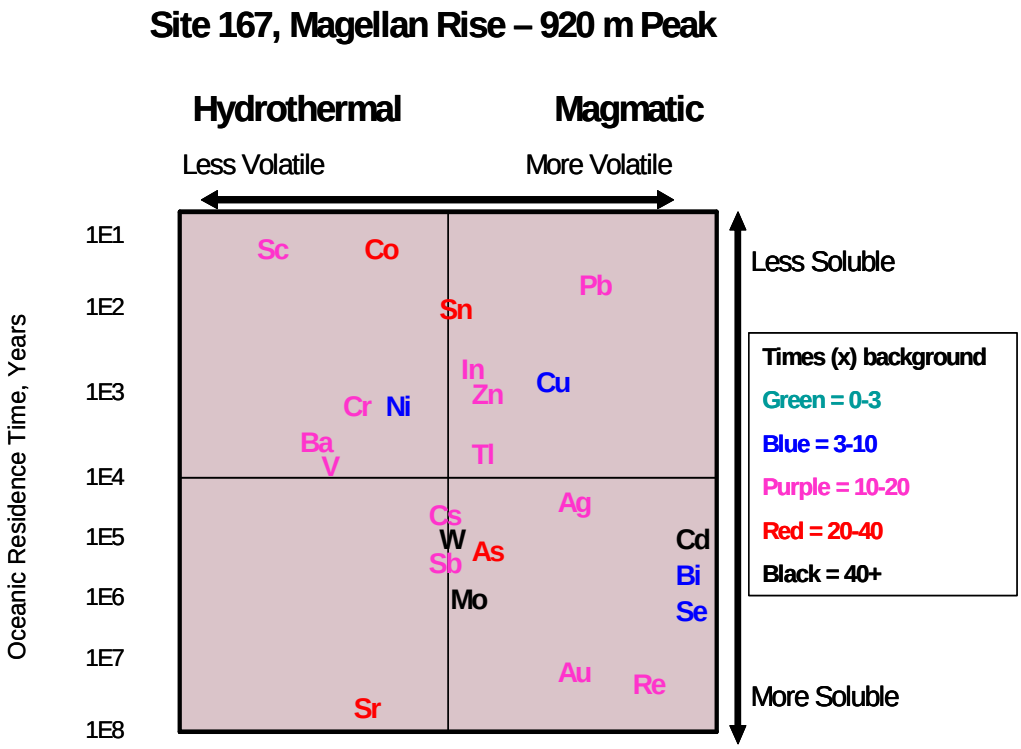

Figure 14. Volatility versus residence time for DSDP Site 167's lower (920 mbsf) peak. The less volatile, shorter residence time elements are quite enriched at this interval.

interval indicating that sediments in this area reflect significant hydrothermal input. This is not surprising considering the close proximity of this site to the Ontong Java - Manihiki plateaus. Elements having higher volatility and correspondingly short residence times are also quite enriched, demonstrating that this interval also had chemical input from magmatic degassing. This same interval also contains a number of quite enriched, long residence time, hydrothermal elements, and is very enriched in magmatically degassed elements of long residence time. The most reasonable interpretation is that magmatic degassing and hydrothermal effluent emanating from the Ontong Java - Manihiki plateaus are responsible for the metal peaks seen in the DSDP Site 167 at 920 meters below sea floor.

Plotting elemental abundances for the 890 mbsf peak at DSDP Site 167 (Figure 15) shows a very similar pattern, albeit with even more elevated anomalies. This upper peak probably had a very similar type of supply of elements as that of the lower, but larger due to greater eruptivity. This pattern of elements suggests that the residence time effects and ocean circulation patterns must have remained relatively constant. This would imply a second period of intense eruptive activity occurring at the Ontong Java - Manihiki plateaus, following an interval in which ocean chemistry returned to normal, steady-state composition.

As data from one site may not be sufficient to draw solid conclusions additional data from other locations were collected. Not only can we examine the stratigraphic position of these events, but we can also see if significant residence time effects occur. Figure 16 plots elemental abundance anomalies for the ~620 mbsf peak

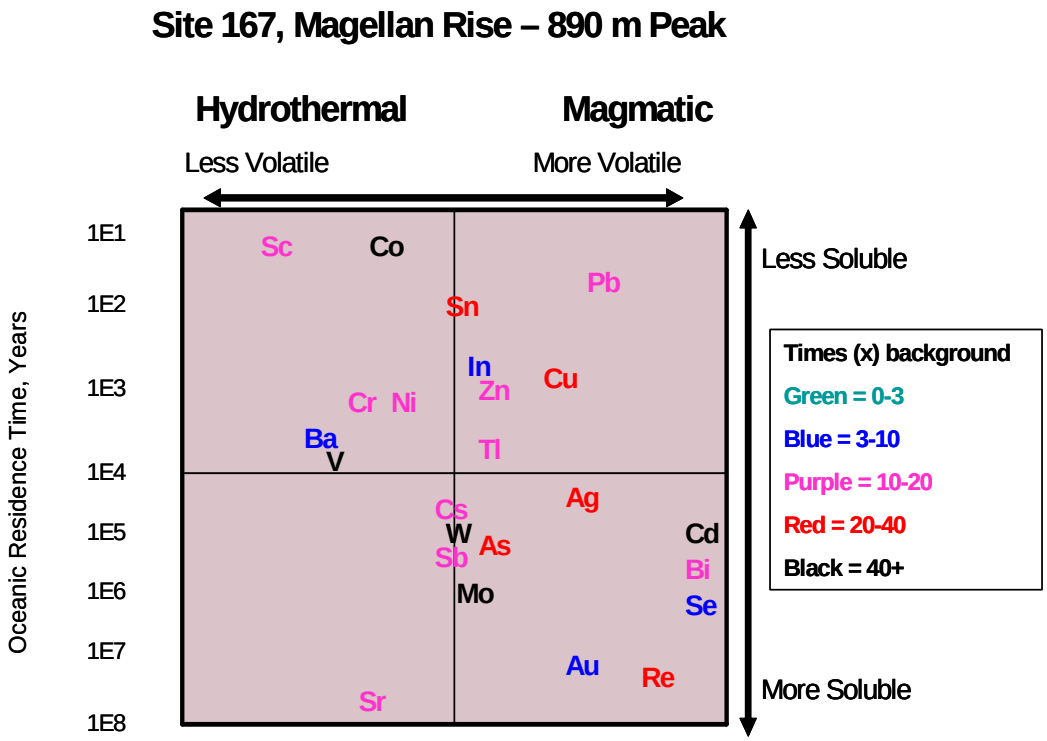

Figure 15. Volatility versus residence time for DSDP Site 167's upper (890 mbsf) peak. The less volatile, shorter residence time elements are very enriched at this interval.

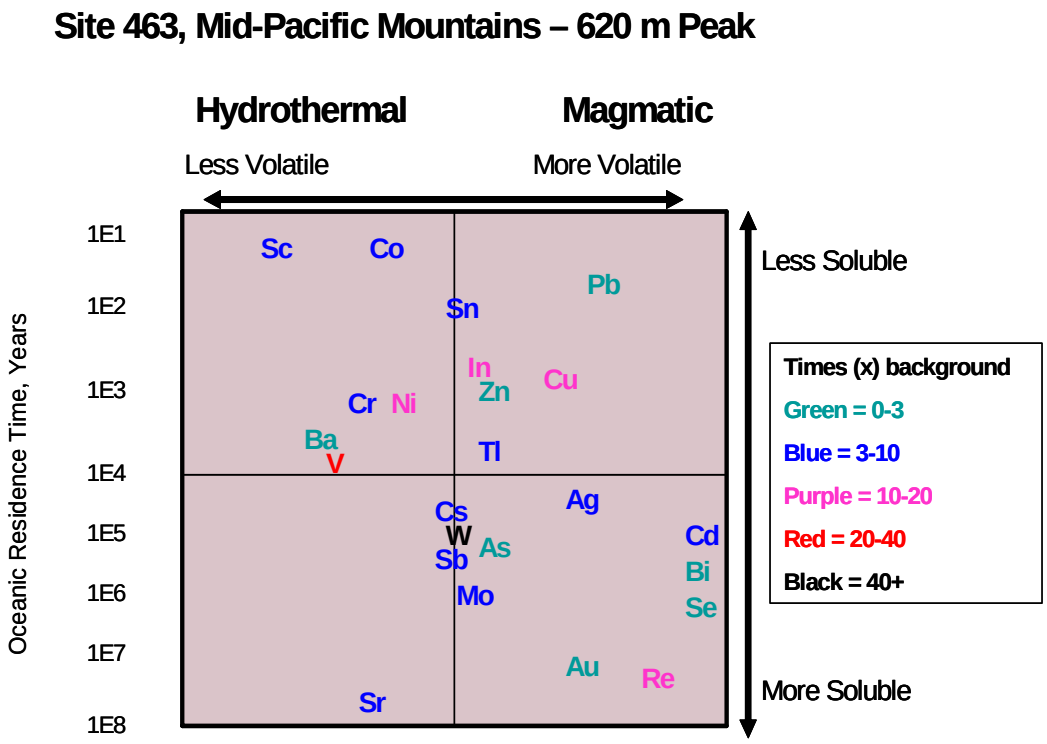

Figure 16. Volatility versus residence time for DSDP Site 463's lower (620 mbsf) peak. The less volatile, shorter residence time elements are enriched at this interval.

at DSDP Site 463. This corresponds to the lower peak seen in Site 167 (see Figure 14). It is clear that Site 463 is less enriched in all elements when compared to Site 167. The upper peak (at 610 mbsf) in Site 463 (Figure 17) seems to follow this same general pattern, having slightly lower values than Site 167's upper peak (Figure 15). However, Sc and Cu are exceptions, having higher enrichments in this area; perhaps due to regeneration effects close to the plateau these heavily recycled elements would tend to travel somewhat farther in the surface waters before reaching the seafloor. One would expect to see overall different enrichments in different sites, due to residence time effects and the variable contributions of degassing and hydrothermal inputs to effluent plumes. As a general rule, lower concentrations of hydrothermal or degassed elements in seawater occur with distance as the plume effluent mixes with the surrounding seawater. Those elements having shorter residence times would not remain in the water column as long and would be most strongly expressed in near-field sediments, while they may have lower abundances in more distant areas.

Residence Time, Cretaceous Circulation, and Location

The consequences of dilution and varying residence times are discernable between DSDP Sites 167 and 463. Figure 18 shows a general upper ocean circulation model for Early Cretaceous time. This model reconstruction (Poulsen et al., 2001) was developed for the Albian (~100 Ma) epoch using atmospheric CO_2 content of four times the present day level (1380 vs. 340 ppm). Similar to modern circulation, the mid-Cretaceous upper ocean was dominated by subtropical and subarctic gyres in

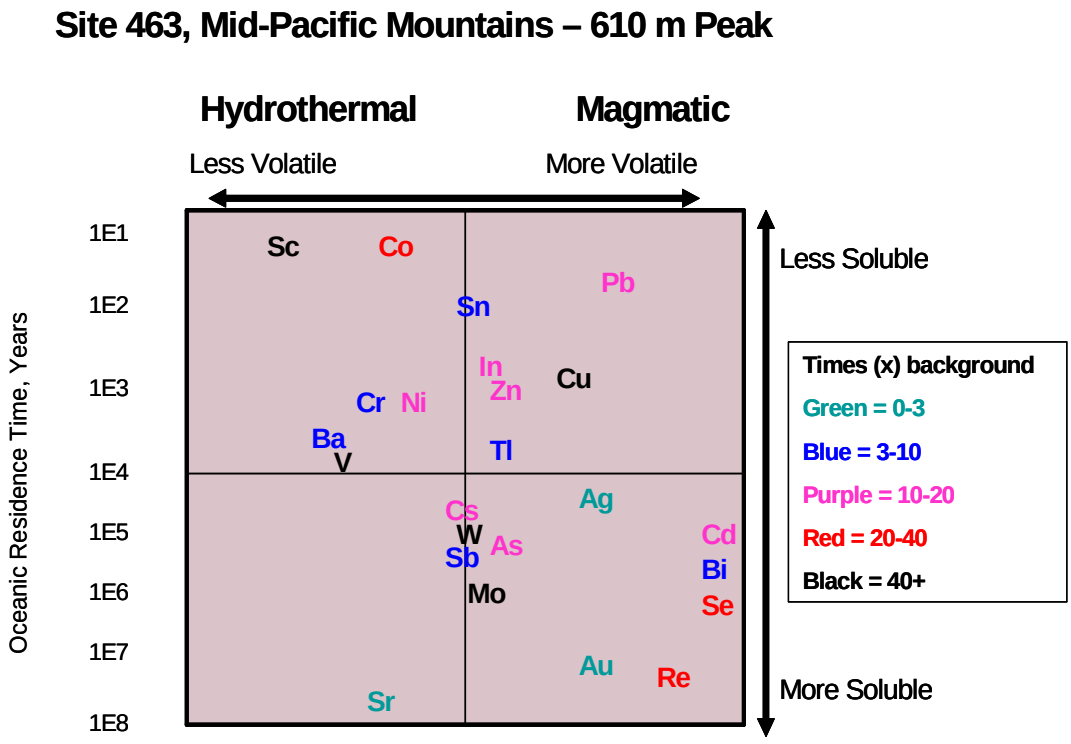

Figure 17. Volatility versus residence time for DSDP Site 463's upper (610 mbsf) peak. The less volatile, shorter residence time elements are enriched at this interval.

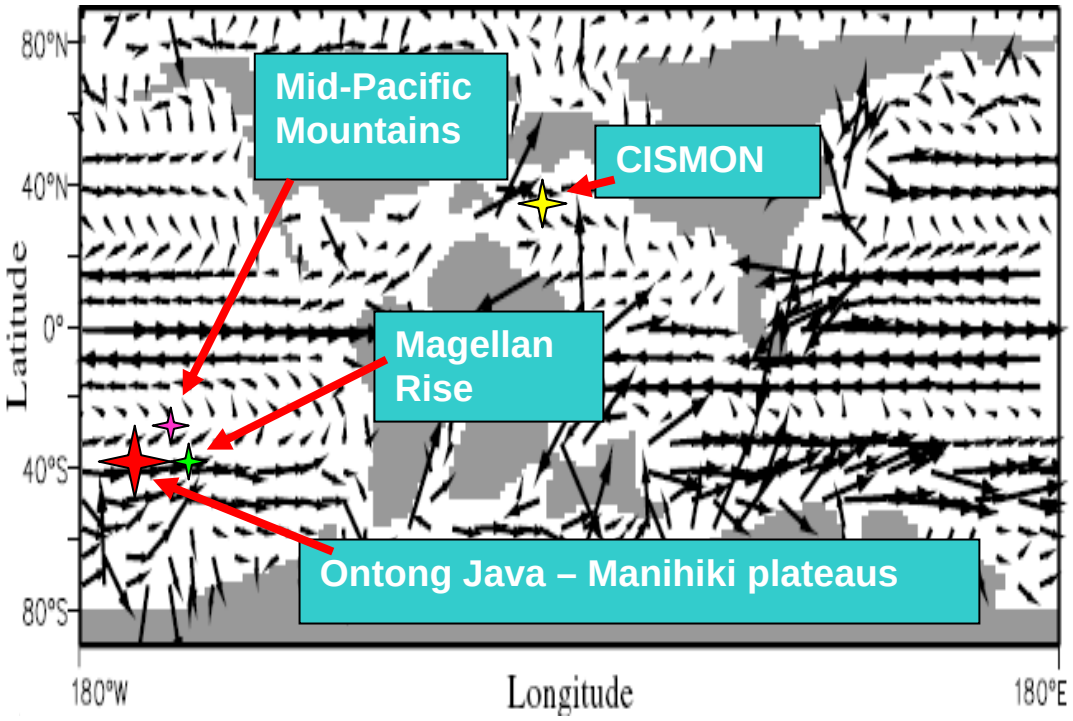

Figure 18. The Ontong Java-Manihiki plateaus, Mid-Pacific Mountains, Magellan Rise, and CISMON (in modern-day Italy) shown in their paleo-locations on a schematic diagram of Cretaceous (~100 Ma) ocean circulation (modified after Poulsen et al., 2001). Length and orientation of black arrows correspond to surface current velocity and direction.

addition to strong equatorial currents. Poulsen et al. (2001) propose that deep ocean water originated in two locations of the southern ocean and spread north to fill the Pacific and Indian basins. Marked on the figure are the paleo-positions of several sites: Deep Sea Drilling Project Sites 167 and 463 used in this study, as well as the CISMON Apticore, Tethys ocean.

In the present day ocean the slower eastern boundary currents move at a rate of approximately 50 kilometers per day (Segar, 1998). The entire ocean can be expected to mix in 1000 to 2000 years (Berner and Berner, 1996). Cretaceous circulation was probably slower than this because of reduced temperature gradients between the equator and the poles. From Figure 18 one can get a general idea of transit times from the Ontong Java – Manihiki plateau to the sites used in this study. Hydrothermal plumes would have reached the Magellan Rise (Site 167) in approximately 30 days, and between 50 (closest point to closest point) and 300 (traveling around the gyre) days to reach the Mid-Pacific mountains (Site 463). While the above times are gross estimates, they nonetheless indicate that Cretaceous surface circulation would have brought seawater with hydrothermal and magmatic signatures to both of these sites in periods less than the shortest residence time for the metals that they carried. This lends credence to Figures 14-17, and also clearly demonstrates why Site 167 contains higher metal abundance anomalies.

To determine if these hydrothermally-dispersed elements created a truly global seawater signature additional data from the CISMON Apticore were obtained (Duncan, Erba, unpublished results). These drill cores were collected from a site in the

Belluno Basin, Northern Italy. During the emplacement of the Ontong Java - Manihiki plateau, however, this site was located in the northern Tethys ocean – very far away from the eruptive area (see Figure 19). Using the same Cretaceous ocean circulation model, surface waters could take several years to travel to this location. Figure 19 indicates that a metal peak did indeed reach this area during the "M0" interval. Interestingly, the stronger, upper peak seen in Sites 167 and 463 does not appear as distinctly at this location. As the upper peak occurred during the stronger positive $\delta^{13}C$ excursion, it is possible that this period also experienced higher surface productivity and more complete seawater anoxia, thus more effectively removing metals from the seawater closer to the source. The water reaching to the most distal extent may have been very metal barren for this reason, or perhaps dilution effects were sufficient to explain the smaller abundance anomalies.

Figure 19 shows that overall elemental abundances are lower for the CISMON "M0" interval than for Sites 167 and 463. This is expected, as element concentrations in the seawater would have dropped substantially with biogenic uptake, particle scavenging, and dilution as surface ocean water circulated from the source to the northern Tethys ocean (northern Italy). From this evidence, it seems clear that the emplacement of the Ontong Java - Manihiki plateaus had seawater trace element effects that were truly global.

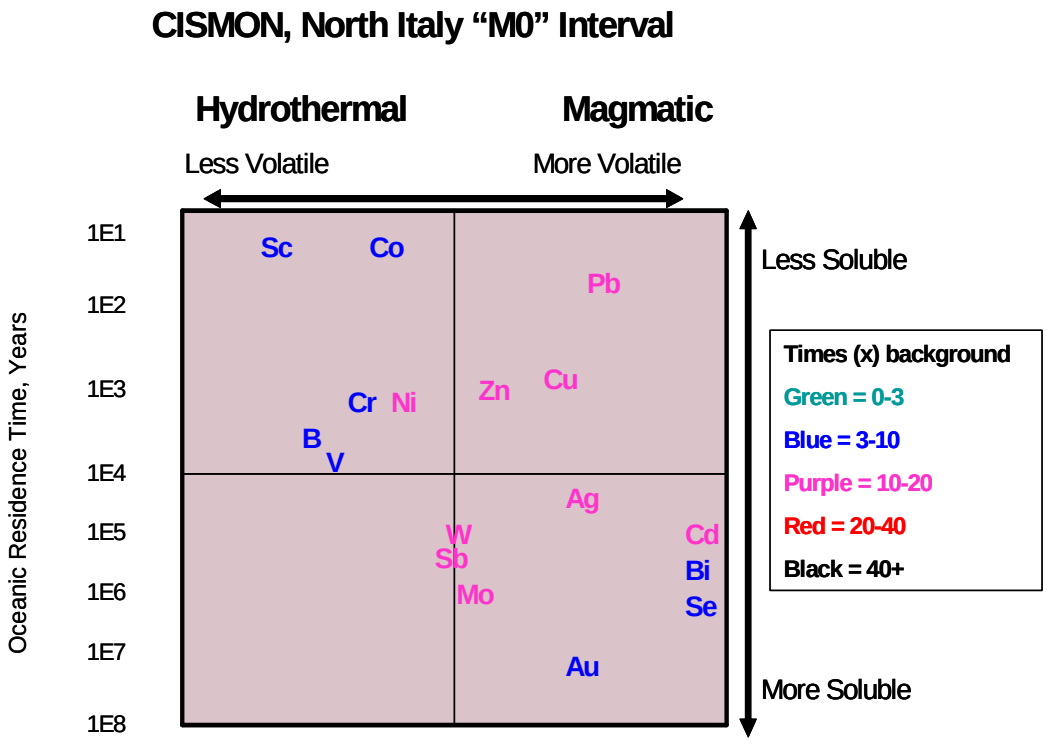

Figure 19. Volatility versus residence time for the CISMON, North Italy "M0" Interval. The less volatile, shorter residence time elements are enriched at this location as well, but not nearly to the extent that they were at Sites 167 and 463.

Chapter 3. Summary, Conclusions, and Future Studies

This study examined three Early Cretaceous marine sedimentary sections, two of which were located in close proximity (near-field) to the emplacement of the Ontong Java - Manihiki plateau, and one which was quite distant (far-field) from the event. Major, minor, and trace element abundance data were obtained in an effort to determine if a connection exists between the emplacement of submarine large igneous provinces (the Ontong Java - Manihiki plateau in this instance), the associated magmatic degassing and hydrothermal activity, and ocean anoxia. The results indicate that trace metal abundance anomalies are stratigraphically correlated with other biogeochemical events during this time period, supporting the hypothesis that trace metals released during magmatic event plumes may trigger the onset of ocean anoxia.

Further, using trace element abundance patterns based on volatility versus residence time, this study demonstrated that the less volatile and more reactive (magmatic) elements were somewhat more enriched in the locations closer to the Ontong Java - Manihiki plateaus and less enriched farther from the source. The patterns of abundance in DSDP Sites 167 and 463 are similar, with Site 463 showing some effects of dilution. This is expected as these sites are relatively close to each other, however some elements would have been more subject to residence time effects. At the CISMON Apticore site (northern Italy) there is also an elevation in trace metals in the same interval (M0), however the extent of enrichment is not as great. This is also logical, owing to its great distance from the eruptive event and the

ensuing dilution effect. The pattern of trace elements seen is consistent with the location of the Ontong Java - Manihiki plateau during this time, and their distribution is also consistent with a model of Early Cretaceous ocean circulation.

While this study has demonstrated that a connection between Ocean Anoxic Event 1a and the emplacement of the Ontong Java - Manihiki plateau exists, further work is needed to reinforce this link. In an effort to demonstrate near- and far-field effects this study used data from three different locations. This work would benefit greatly from the inclusion of trace, minor, and major element data from several more sites of varying distances from the source of volcanic ativity. Possible drilling legs from which to study additional samples from include Ocean Drilling Program legs 103 (the Galicia Margin) and 143-44 (Northwest Pacific Atolls and Guyots). Leg 103 would provide samples from the (then) proto-Atlantic ocean. These locations would unquestionably provide useful intermediate submembers, helpful in determining additional near and far-field effects.

Another exciting area of future work lies in determining if the element anomalies found in Cretaceous sediments reflect those elements lost by degassing and hydrothermal fluxes during the same time period. This mass balance could be calculated by determining the composition of unaltered basalt, and subtracting the composition of altered basalt from this. The difference between these two compositions should reflect what is found in the element abundance anomalies seen in the sediment record. In order to carry out this experiment, the composition of the parental melts could be determined from melt inclusions trapped in phenocrysts in

erupted lava flows. Second, the compositions of altered basalts from Ontong-Java and Manihiki Plateaus are easily determined from previously recovered cores.

Literature:

Algeo, T., and Maynard, J. Trace-element Behavior and Redox Facies in Core Shales of Upper Pennsylvanian Kansas-type Cyclothems. Chemical Geology, 206. Pg. 289-318. 2004.

Arthur, M., and Premoli-Silva, I. Development of widespread organic carbon-rich strata in the Mediterranean Tethys. Nature and Origin of Cretaceous carbon-rich facies. Eds: Schlanger, S., and Cita, M. Academic Press, London. Pg. 7-54. 1982.

Bach, W., and Edwards, K. Iron and sulfide oxidation within the basaltic ocean crust: Implications for chemolithoautrophic microbial biomass production. Geochimica et Cosmochimica Acta, 67. Pg. 3871-3887. 2003.

Balistrieri, L., Brewer, P., and Murray, J. Scavenging residence times of trace metals and surface chemistry of sinking particles in the deep ocean. Deep-Sea Research, 28A. Pg. 101-121. 1981.

Berner, E., and Berner, R. Global Environment: Water, Air, and Geochemical Cycles. Prentice Hall. Pg. 1-24, 312-359. 1996.

Berner, R. Geocard II: A revised model of atmospheric CO_2 over Phanerozoic time. American Journal of Science, 294. Pg. 56-91. 1994.

Bertine, K., and Turekian, K. Molybdenum in marine deposits. Geochimica et Cosmochimica Acta, 37. Pg. 1415-1434. 1973.

Bice, K., Bralower, T., Duncan, R., Huber, T., Leckie, R., Sageman, B. Cretaceous climate-ocean dynamics: future directions for IODP. Executive Summary, Workshop on Cretaceous Climate and Ocean Dynamics. 2002. Web available at: http://www.whoi.edu/ccod/CCOD_report.html

Bode, G. Carbon and Carbonate Analyses, Leg 17. In, Initial Reports of the Deep Sea Drilling Project XVII. Pg. 927-930. 1971.

Bralower, T., Fullager, P., Paull, C., Dwyer, G., Leckie, R. Mid-Cretaceous strontium-isotope stratigraphy of deep-sea sections. GSA Bulletin, 109. Pg. 1421-1442. 1997.

Bralower, T., CoBabe, E., Bradford Clement, B., Sliter, W., Osburne, C., and Longoria, J. The record of global change in mid-Cretaceous (Barremian-Albian) sections from the Sierra Madre, northeastern Mexico. In Huber, B., Bralower, T., and Leckie, R, A memorial volume to William V. Sliter, Journal of Foraminiferal Research, 29. Pg. 418-437. 1999.

Brown, J., Colling, A., Park, D., Phillips, J., Rothery, D., and Wright, J. Ocean Chemistry and Deep-Sea Sediments. Ed. Bearman, G. Pergamon, in association with the Open University. Pg. 20-58. 1994.

Bruland, K. Trace Elements in Sea-water. Chemical Oceanography. Volume 8, Chapter 45. Pg 157-220. 1983.

Brumsack, H.J. Geochemistry of recent TOC-rich sediments from the Gulf of California and the Black Sea. Geologische Rundschau, 78. Pg. 851-882. 1989.

Brumsack, H. and Thurow, J. The Geochemical facies of black shales from the Cenomanian-Turonian Boundary Event (CTBE). Biogeochemistry of Black Shales; Case Studies from a Workshop, 60. Pg. 247-265. 1986.

Campbell, I., and Griffiths, R. Implications of mantle plume structure for the evolution of flood basalts. Earth and Planetary Science Leters, 99. Pg. 79-93. 1990.

Calvert, S., and Pederson, T. Geochemistry of recent oxic and anoxic marine sediments: Implications for the geological record. Marine Geology, 113. Pg. 67-88. 1993.

Cannariato, K., Kennett, J., and Behl, R. Biotic response to late Quaternary rapid climate switches in Santa Barbara Basin: Ecological and evolutionary implications. Geology, 27. Pg. 63-66. 1999.

Coale, K., and 18 others. A massive phytoplankton bloom induced by an ecosystem-scale iron fertilization experiment in the equatorial Pacific Ocean. Nature, 383. Pg. 495-501. 1996.

Coffin, M., and Eldholm, O. Large igneous provinces: crustal structure, dimensions, and external consequences. Reviews of geophysics, 32. Pg. 1-36. 1994.

Colodner, D., Sachs, J., Ravizza, G., Turekian, K., Edmond, J., and Boyle, E. The geochemical cycle of rhenium: A reconnaissance. Earth and Planetary Science Letters, 117. Pg. 205-221. 1993.

Crusius, J., Clavert, S., Pedersen, T., and Sage, D. Rhenium and molybdenum enrichments in sediments as indicators of oxic, suboxic, and sulfidic conditions of deposition. Earth and Planetary Science Letters, 145. Pg. 65-78. 1996.

Duncan, R., and Richards, M. Hotspots, mantle plumes, flood basalts, and true polar wander. Reviews of geophysics, 29. Pg. 31-50. 1991.

Erba, E. Calcareous nannofossils and Mesozoic oceanic anoxic events. Marine Micropaleontology, 52. Pg. 85-106. 2004.

Erbacher, J., Huber, B., Norris, R., and Markey, M. Increased thermohaline stratification as a possible cause for an ocean anoxic event in the Cretaceous period. Nature, 409. Pg. 325-327. 2001.

Erbacher, J., and Thurow, J. Influence of oceanic anoxic events on the evolution of mid-Cretaceous radiolarian in the North Atlantic and western Tethys. Marine Micropaleontology, 30. Pg. 139-158. 1997.

Faure, G. Principles of Isotope Geology. Second Edition, John Wiley and Sons, Inc. Pg. 154-199, 491-507. 1986.

Fitton, J., Mahoney, J., Wallace, P., and Saunders, A. Leg 192 Synthesis: Origin and Evolution of the Ontong Java Plateau. Proceedings of the Ocean Drilling Program, Scientific Results, 192. Pg 3-17. 2004.

Froelich, P., Klinkhammer, G., Bender, M., Luedtke, N., Heath, G., Cullen, D., Dauphin, P., Hartman, B., and Maynard, V. Early oxidation of organic matter in pelagic sediments of the Eastern Equatorial Atlantic: suboxic diagenesis. Geochemica et Cosmochimica Acta, 43. Pg. 1075-1091. 1979.

Harland, W., Armstrong, R., Cox, A., Craig, L., Smith, A., and Smith, D. A geologic time scale. Cambridge University Press, Cambridge, England. Pg. 263. 1990.

Haq, B., Hardenbol, J., and Vail, P. Mesozoic and Cenozoic chronostratigraphy and eustatic cycles. In Wilgus, C., hastings, C., Kendall, St. C., Posamentier, H., Ross, C., and Van Wagoner, J., eds., Sea-level changes: An integrated approach: Society of Economic Petrologists and Minerologists Special Publication, 42. Pg. 71-109. 1988.

Herbin, J., Montadert, L., Muller, R., Gomez, R., Thurow, J., and Wiedmann, J. Organic-rich sedimentation at the Cenomanian-Turonian boundary in oceanic and coastal basins in the North Atlantic and Tethys. North American Paleoceanography. Summerhayes, C., and Shackelton, N., eds. Blackwell, Oxford. Pg. 389-422. 1986.

Ho, A., and Cashman, K. Temperature constraints on the Ginkgo flow of the Columbia River Basalt Group. Geology, 28. Pg. 403-406. 1997.

Jacobs, L., and Emerson, S. Trace metal solubility in and anoxic fjord. Earth and Planetary Science Letters, 60. Pg. 237-252. 1982.

Johnson, K. The MBARI Chemical Sensor Program, Summary Table of Mean Ocean Concentrations and Residence Times. Webpage. Accessed, 02/15/06. Available: http://www.mbari.org/chemsensor/summary.html

Kerr, A.C. Oceanic Plateaus. Treatise on Geochemistry, 3. Eds Rudnick R., Holland, H., and Turekian, K. Pg. 537-561. 2003.

Kroenke, L., Wessel, P., and Sterling, A. Motion of the Ontong Java Plateau in the hotspot frame of reference: 122 Ma-present. *In* Fitton, J., Mahoney, J., Wallace, P., and Saunders, A. (Eds.), *Origin and Evolution of the Ontong Java Plateau.* Geol. Soc. Spec. Publ., 229. Pg. 9-20. 2004.

Kuypers, M., Blokker, P., Erbacher, J., Kinkel, H., Pancost, R., Schouten, S., Damste, S. Massive expansion of marine Archea during a mid-Cretaceous oceanic anoxic event. Science, 293. Pg. 92-94. 2001.

Lancelot, Y., and Larson, R. Sedimentary and tectonic evolution of the northwestern Pacific. In Larson, R., Moberly, R., et al., Intl. Rpts. DSDP, 32: Washington (U.S. Govt. Printing Office). Pg. 925-939. 1975.

Larson, R. Geological consequences of superplumes. Geology, 19a. Pg. 547-550. 1991.

Larson, R. Latest pulse of the Earth: Evidence for a mid-Cretaceous superplume. Geology, 19b. Pg. 547-550. 1991.

Leary, P., Carson, G., Cooper, K., Hart, M., Horne, D., Jarvis, I., Rosenfeld, A., and Tocher, B. The biotic response to the late Cenomanian anoxic event; integrated evidence from Dover, SE England. Journal of the Geological Society of London, 146. Pg. 311-317. 1989.

Leckie, R., Bralower, T., and Cashman, R. Ocean anoxic events and planktonic evolution: Biotic response to tectonic forcing during the mid-Cretaceous. Paleoceanography, 17. Pg 13-1 -13-27. 2002.

Lupton, J., Feely, R., Cowen, J., Greene, R., Rago, T., Baker, E., Garfield, N., and Massoth, G. Tracking the evolution of a hydrothermal event plume with a RAFOS neutrally buoyant drifter. Science, 280. Pg. 1052-1055. 1998.

Mahoney, J., Storey, M., Duncan, R., Spencer, K., and Pringle, M. Geochemistry and age of the Ontong Java oceanic plateaus. *In* Pringle, M., Sager, W., Sliter, W., and Stein, S. (Eds.), *The Mesozoic Pacific: Geology, Tectonics, and Volcanism.* Geophys. Monogr., 77. Pg. 233-261. 1993.

Milnes, A., and Fitzpatrick, R. Titanium and Zirconium Minerals in Minerals and Soil Environments. Eds: Dixon, J., and Weed,B. Soil Science Society of America. Madison, Wisconsin, 23. Pg. 1131-1205. 1989.

Morford, J., and Emerson, S. The Geochemistry of redox sensitive trace metals in sediments. Geochimica et Cosmochimica Acta, 63. Pg. 1735-1750. 1999.

Nameroff, T., Balistrieri, L., and Murray, J. Suboxic Trace Metal Geochemistry in the Eastern Tropical North Pacific. Geochimica Cosmochimica Acta, 66. Pg. 1139-1158. 2002.

Nijenhuis, I., Bosch, H., Damste, S., Brumsack, H., and De Lange, G. Organic Matter and Trace Element Rich Sapropels and Black Shales: A Geochemical Comparison. Earth and Planetary Science Letters, 169. Pg. 277-290. 1999.

Orth, C., Attrep, M., Quintana, L., Elder, W., Kauffman, E., Diner, R., and Villamil, T. Elemental abundance anomalies in the late Cenomanian extinction interval: a search for the source(s). Earth and Planetary Science Letters, 117. Pg. 189-204. 1993.

Petterson, M. The geology of north and central Malaita, Solomon Islands: the thickest and most accessible part of the world's largest (Ontong Java) ocean plateau. *In* Fitton, J., Mahoney, J., Wallace, P., and Saunders, A. (Eds), *Origin and Evolution of the Ontong Java Plateau.* Geol. Soc. Spec. Publ, 229. Pg. 63-81. 2004.

Piper, D. Seawater as the source of minor elements in black shales, phosphorites and other sedimentary rocks. Chemical Geology, 114. Pg. 95-114. 1994.

Pilson, M. An Introduction to the Chemistry of the Sea. Prentice Hall. Pg. 316-339. 1998.

Pirie, G (ed.). Diagenesis. Schlumberger Oilfield Glossary. Web-accessed 06/30/06. Web available http://www.glossary.oilfield.slb.com/

Poulsen, C., Barron, E., Arthur, M., and Peterson, W. Response of the mid-Cretaceous global oceanic circulation to tectonic and CO_2 forcings. Paleoceanography, 16. Pg. 576-592. 2001.

Price, G. New constraints upon isotope variation during the early Cretaceous (Barremian-Cenomanian) from the Pacific Ocean. Geology Magazine, 140. Pg. 513-522. 2003.

Richards, M., Duncan, R., and Courtillot, V. Flood basalts and hotspot tracks: Plume heads and tails. Sicence, 246. Pg. 103-107. 1989.

Rubin, K. Degassing of metals and metalloids from erupting seamount and mid-ocean ridge volcanoes: Observations and predictions. Geochimica Cosmochimica Acta, 61. Pg. 3525-3545. 1997.

Saltzmann, E., and Barron, E. Deep circulation in the late Cretaceous: oxygen isotope paleotemperature from Inoceramus remains in D.S.D.P. cores. Paleogeography, Paleoclimatology, Paleoecology, 40. Pg. 167-181. 1982.

Sarmiento, J., Herbert, T., and Toggweiler, J. Causes of anoxia in the world oceans. Global Geochemical Cycle, 2. Pg 115-128. 1988.

Schlanger, S., and Jenkyns, H. Cretaceous oceanic anoxic events: Causes and consequences. Geologica Minjbouw, 55. Pg. 179-184. 1976.

Schlanger, S., Jenkyns, H., and Premoli-Silva, I. Volcanism and vertical tectonics in the Pacific Basin related to the global Cretaceous transgressions. Earth and Planetary Science Letters, 52. Pg. 435-449. 1981.

Schlesinger, W. Biogeochemistry: An Analysis of Global Change. Second Edition. Academic Press. Pg. 226-230. 1997.

Segar, D. Introduction to Ocean Sciences. Wadsworth Publishing Company. Pg 114-115, 217.1998.

Sinton, C., and Duncan, R. Potential links between ocean plateau volcanism and global ocean anoxia at the Cenomanian-Turonian boundary. Economic Geology, 92. Pg. 836-842. 1997.

Snow, L. Hydrothermal links between ocean plateau formation and global anoxia at the Cenomanian-Turonian boundary. Thesis, Oregon State University. Pg. 69-70. 2003.

Snow, L., Duncan, R., and Bralower, T. Trace element abundances in the Rock Canyon Anticline, Pueblo, Colorado, marine sedimentary section and their relationship to Caribbean Plateau construction and Ocean Anoxic Event 2. Paleoceanography, 20. Pg. PA 3005 (1-14). 2005.

Swanson, D., Wright, T., and Helz, R. Linear vent systems and estimated rates of magma production and eruption for the Yakima basalt on the Colombia plateau. American Journal of science, 275. Pg. 877-905. 1975.

Tarduno, J., Sliter, L., Kroenke, L., Leckie, M., Mayer, H., Mahoney, J., Musgrave, R., Storey, M., and Winterer, E. Rapid formation of the Ontong Java Plateau by Aptian mantle plume volcanism. Science, 254. Pg. 399-403. 1991.

Tejada, M., Mahoney, J., Duncan, R., and Hawkins, M. Age and geochemistry of basement and alkalic rocks of Malaita and Santa Isabel, Solomon Islands, southern margin of the Ontong Java Plateau. J. Petrol., 37. Pg. 361-394. 1996.

Tejada, M., Mahoney, J., Neal, C., Duncan, R., and Petterson, M. Basement geochemistry and geochronology of Central Malaita, Solomon Islands, with implications for the origin and evolution of the Ontong Java Plateau. J. Petrol., 43. Pg. 449-484. 2002.

Thiede, J, Vallier, T, and Others. Site 463: Western Mid-Pacific Mountains Site Summary. In Initial Reports of the Deep sea Drilling Project LXII. Pg. 33-156. 1978.

Veeh, H. Deposition of uranium from the ocean. Earth and Planetary Science Letters, 3. Pg. 145-150. 1967.

Vogt, P. Volcanogenic upwelling of anoxic, nutrient-rich water: A possible factor in Carbonate-bank/reef demise and benthic faunal extinctions? Geological Society of America Bulletin, 101. Pg. 1225-1245. 1989.

Wagner, T., Damste, J., Hofmann, P., Beckmann, B. Euxinia and primary production in Late Cretaceous eastern equatorial Atlantic surface waters fostered orbitally driven formation of marine black shales. Paleoceanography, 19. Pg. 3009-3022. 2004.

Wilson, P., Jenkyns, H., Elderfield, H., and Larson, R. The paradox of drowned carbonate platforms and the origin of Cretaceous Pacific guyouts. Nature, 392. Pg. 889-894. 1998.

Winterer, E., Ewing, J., Douglas, R., Jarrard, R., Lancelot, Y., Moberly, R., Moore, T., Roth, P., and Schlanger, S. Site 167 Site Summary. In, Initial Reports of the Deep Sea Drilling Project XVII. Pg. 145-234. 1971.

Appendix 1: Trace Metal Patterns in Marine Sediments

Plankton and Trace Metals:

Particles are produced primarily by phytoplankton in surface waters, and thus the uptake of some trace metals in the ocean can be attributed to their function as essential micro-nurtients (Bruland, 1983). The table below shows the average chemical composition of plankton/marine organisms. One would expect the chemical composition of a biogenic sediment (and black shales are known for their high organic carbon) to have some relationship to the constitution of the organisms that it is comprised of. Indeed, Piper (1994) showed that some minor element ratios found in several black shale formations matched minor element ratios found in modern plankton, demonstrating that seawater could be the source of minor elements to some black shales. However, in their comparison of the geochemistry of organic matter, sapropels (organic matter-rich marine sediments), and black shales, Nijenhuis et al. (1999) concluded that this may not always be the case. As an example they demonstrated that the globally distributed Cenomanian/Turonian Boundary Event (CTBE) black shale (and its attendant metal enrichment) was too massive to be attributed to seawater trace metal enrichment alone; seawater could not have provided the needed trace element reservoir. The ratios seen are also different from those seen in the table below.

Element	Mean Value (ppm dry matter)
Ag	0.1
As	5
Ba	80
Bi	0.1
Cd	12
Co	1
Cr	1
Cu	10
Mo	2
Ni	8
Pb	6
Sb	0.5
Se	1
Tl	0.1
V	3
Zn	80

Table demonstrates the average chemical composition of modern plankton/marine organisms. Data from this table can be seen graphically in figure 14. After Brumsack (1989).

Further validation of this conclusion can be found in Brumsack and Thurow's (1986) study which found that the abundance of metals seen in CTBE sediments could not be explained by the deposition of plankton-derived, organic matter-rich particles. As OAE1a was at least as large (see Figure 1), if not larger than OAE2, it seems reasonable to assume that normal seawater is not the primary trace element source for the OAE1a shales analyzed in this study. Further, biogenic sediments cannot account for the trace metal enrichments seen.

In addition, the Figures A2-A5 below to seem to indicate that the elements present in seawater/biology have a different abundance pattern than marine sediments that accumulated during OAE1a. Algeo and Maynard (2004) add validity to this observation by noting that the trace elements Zn, Cu, and Ni exhibit trace element patterns indicative of biogenic uptake, while the metals Mo, U, V, and Cr show no evidence of a bionutrient role in modern marine systems. Finally, Brumsack (1989) noted that sediments from modern high productivity environments are not characterized by high trace metal concentrations, due to high water column metal regeneration, low trace metal concentration of marine plankton, and the high accumulation rates for these areas.

Figure A1. This cartoon demonstrates the path that many elements take through seawater. First the elements are either used by biological processes. Next, as the biological particles die and sink, additional particles are adsorbed onto the particles via a process known as scavenging. Ultimately most of the elements in seawater reach the sediment in this manner.

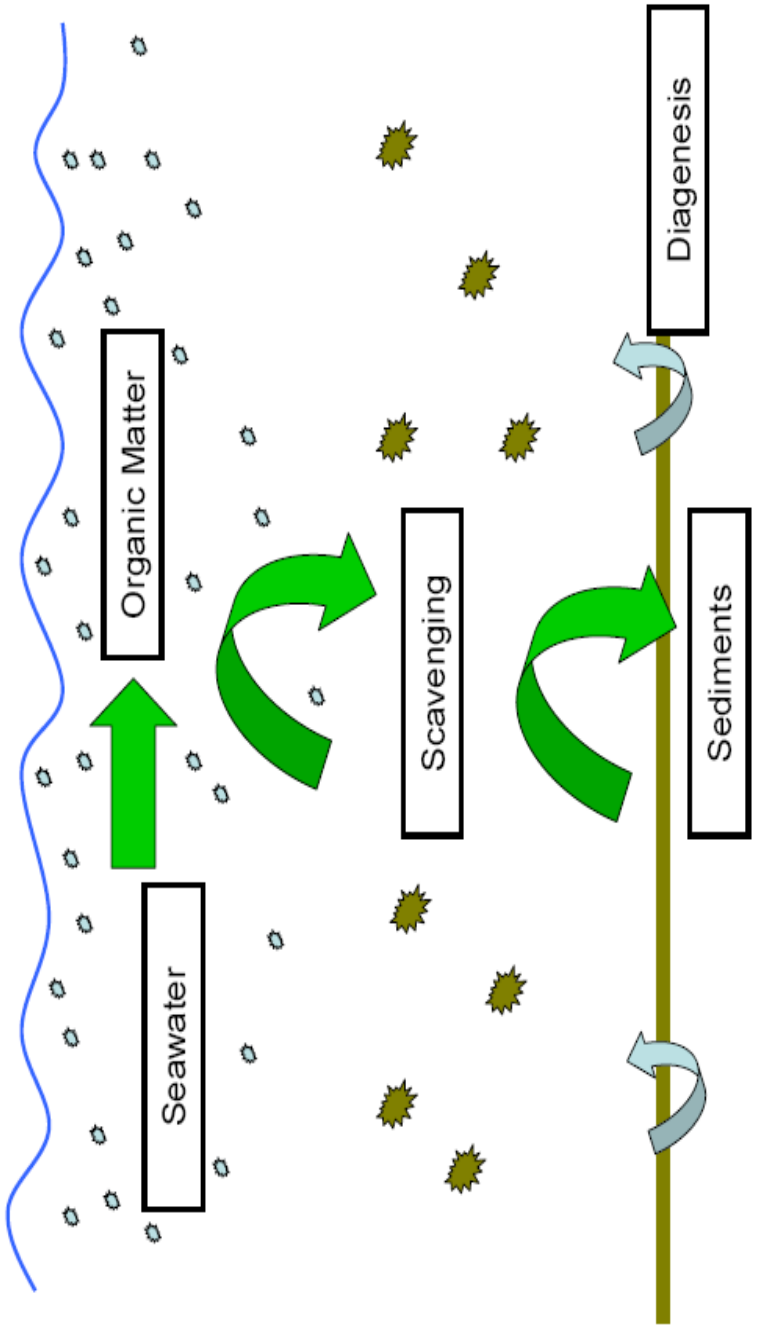
Diagenesis
Organic Matter
Scavenging
Sediments
Seawater

Water Column Oxygen and Trace Metals

In the modern ocean anoxic water column conditions are ideal sinks for many redox-sensitive and stable sulfide forming elements (Brumsack, 1989). Oxic water column conditions can also affect the chemical composition of sediments. For example, those elements coupled with labile nutrients (like Cd and Zn) will have lower concentrations in oxic sediments than expected from the chemical composition of marine plankton because they are regenerated into the water column (Brumsack, 1989). Previous studies have shown that the elements Cd, Cu, Mo, Re, U, and V are enriched in anoxic sediments and not enriched in those that are anoxic (Veeh, 1967; Bertine and Turekian, 1973; Jacobs and Emerson, 1982; Colodner et al., 1993; Calvert and Pederson, 1993). Brumsack (1989) concluded that Cretaceous black shale layers, however, represent periods of enhanced preservation of organic matter rather than periods of excessively high productivity. This conclusion is based on the premise that seawater is generally very metal-poor, making long time periods and low sediment accumulation rates necessary to generate trace metal peaks (Brumsack, 1986). As seen in the data for ocean drilling sites 167 and 463, this study indicates that there may be an anomalously high flux of trace metals to the Cretaceous ocean, generating the peaks seen. It seems that while the biological makeup of plankton itself lacks the necessary chemistry to provide trace element signatures seen in the OAE1a sediments, particle scavenging made possible by the sinking of these organisms is an important additional source of metal removal from the water column. Yet, it still remains to be seen where the elements seen in this study come from, as continental source fluxes

would not appear to be large enough to maintain the trace metal enrichment necessary for the large temporal and global distribution seen in OAE1a (Morford and Emerson, 1999).

Diagenesis and Trace Metals

Trace element distributions seen in sediments are also affected by diagenetic processes. Is it possible that the diagenetic remobilization of trace elements in sediments (having arrived as biological particles complete with their load of scavenged elements) could provide the peaks that are seen in the results of this study? Diagenetic processes can do two things: generate metal peaks in the sediment record (essentially concentrating the metals from an interval into one horizon), or cause them to diffuse across the sediment-water interface (depending on the redox potential of the surrounding water column) and be lost from the sediment record (Froelich et al., 1999, Nameroff et al., 2002). Redox potential is used by chemists to express the tendency of an environment to receive or supply electrons (Schlesinger, 1997). Oxic environments are said to have a high redox potential because O_2 is available as an electron acceptor (Schlesinger, 1997). An understanding of the redox potential of the environment is pertinent because it can have a noticeable effect on the authigenic enrichment or depletion factors in sediments.

Brumsack and Thurow (1986) evaluated the possibility of diagenetic enrichment to black shales and concluded that an enrichment due exclusively to these processes seems highly unlikely. While it seems clear that these elements will be enriched during periods of anoxia, it should also be noted that under the same

conditions any redistribution will occur on a centimeter scale (Algeo and Maynard, 1999., Brumsack and Thurow, 1986). All of the high abundance metal signatures seen in this study occur over intervals of several meters.

Modern seawater does not have a sufficient inventory of the necessary elements to maintain the rate of metal deposition seen in this study, so we must look at additional sources to explain the abundances and patterns. One possibility is that increased volcanic activity would have increased global levels of CO_2, increasing the acidity of the environment, and thus increasing terrestrial weathering and runoff. If this were the case, all river-borne elements would increase together, including the inert (low residence time) elements such as Zr and Al. Our normalizations to Zr and Al (see methods) should account for this possible extra runoff. In addition, if aluminum levels in seawater had varied with time, this variation would have been reflected in the plots of major elements. This is not the case.

Appendix 12: Figures comparing Metal Fluxes

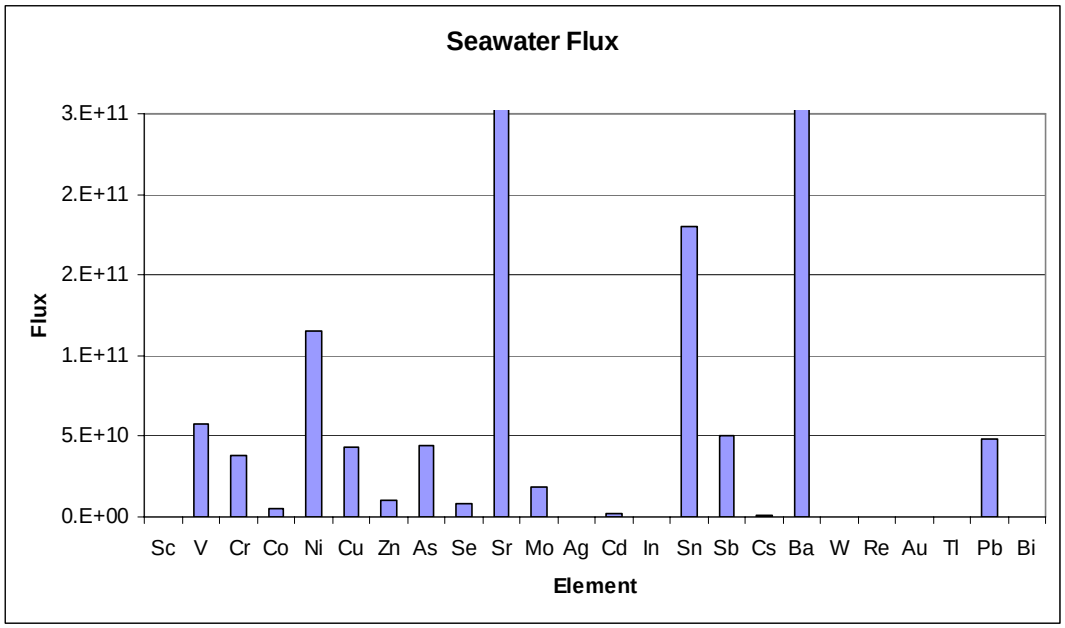

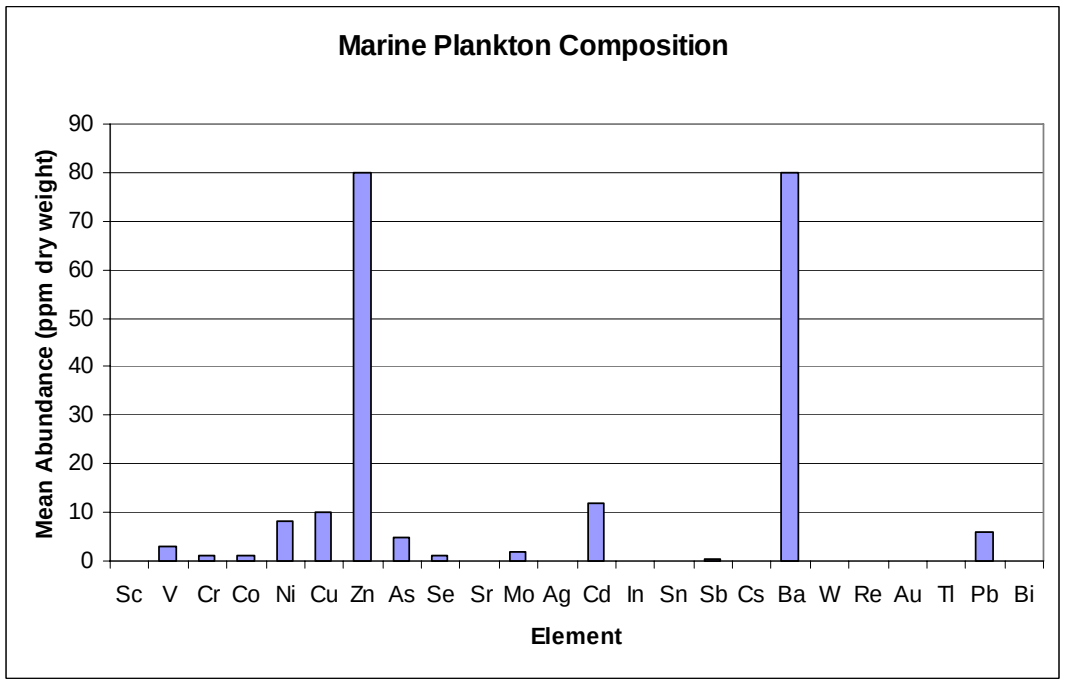

Figure A2. Seawater flux and planktonic composition. Seawater flux (element in ocean (g)/ residence time (yr) data developed using information from Johnson (2005). Some of the residence times were calculated using riverine input, others by accumulation rate in sediment, and through other means. Marine plankton (entire organism) chemical composition (no data for elements Sr, In, Sn, W, Re and Au) from Brumsack (1989).

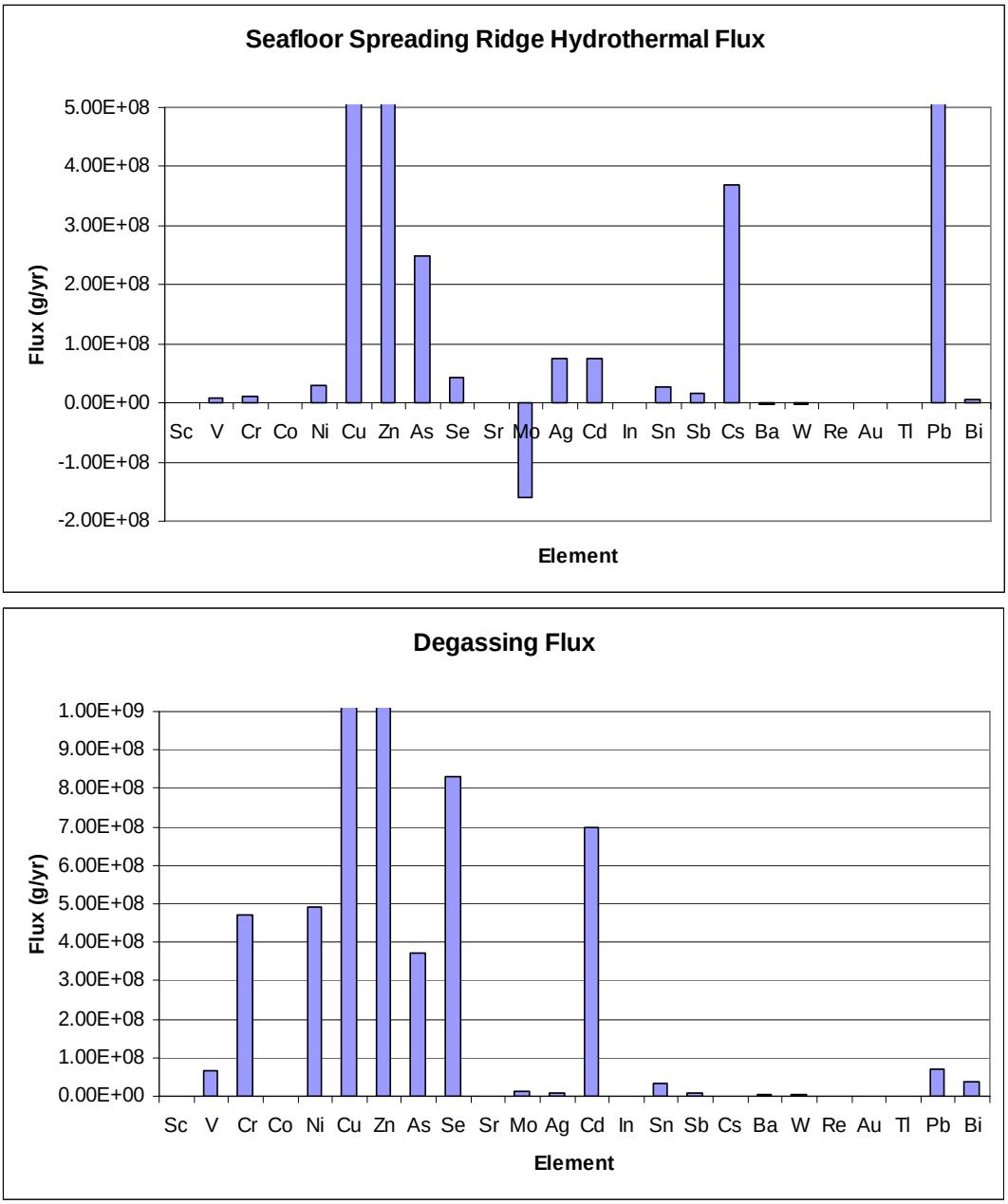

Figure A3. Hydrothermal and degassing fluxes. Data from Rubin (1997). Degassing flux calculated using parameters developed from known subaerial volcanic production and emanation coefficients.

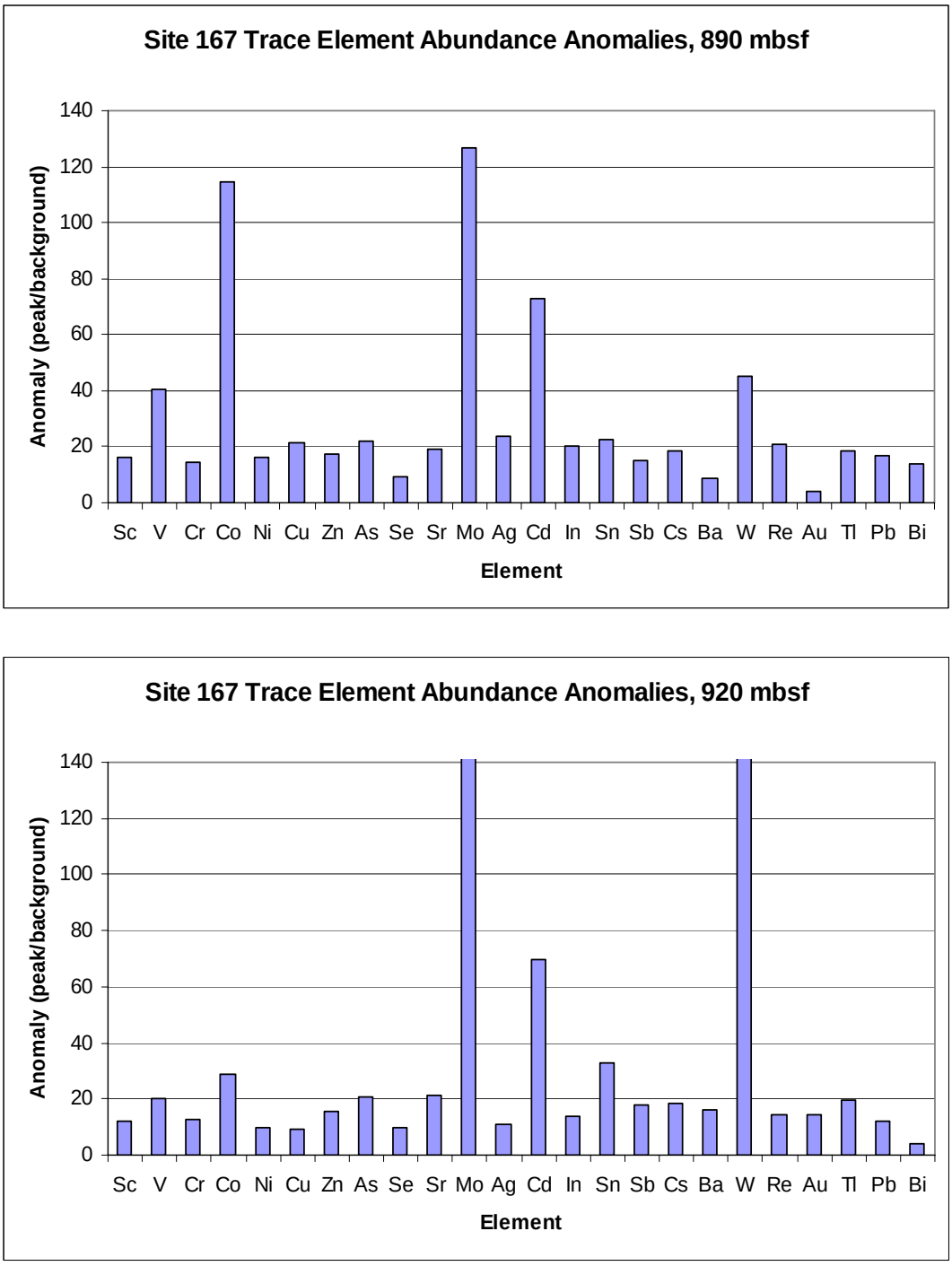

Figure A4.Trace element abundance anomalies found in Deep Sea Drilling Project Site 167 during this study.

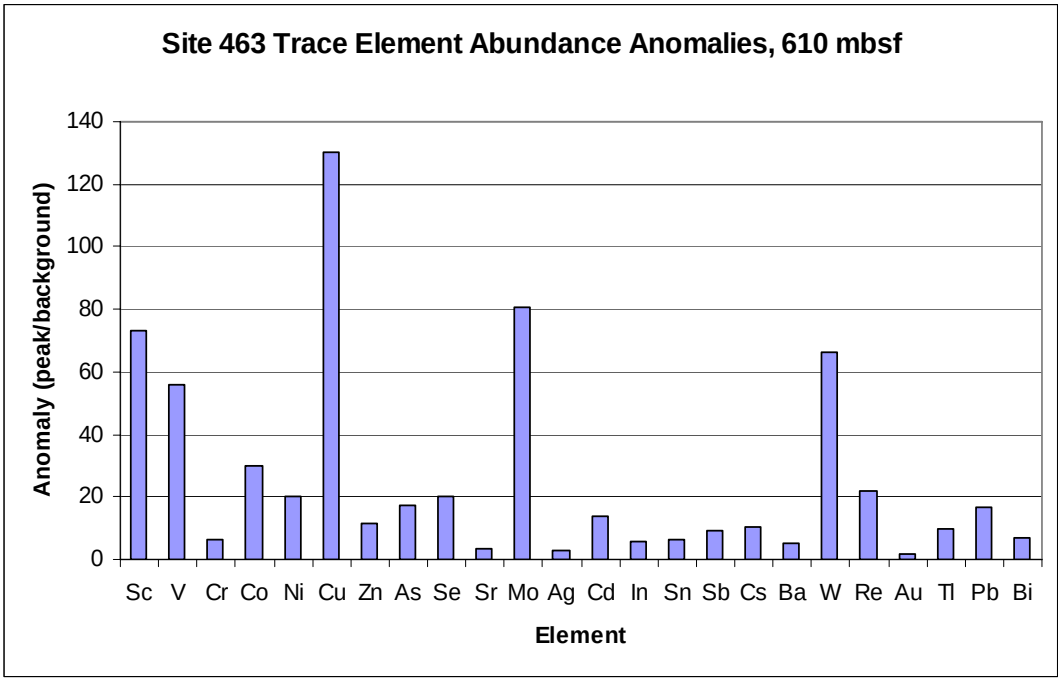

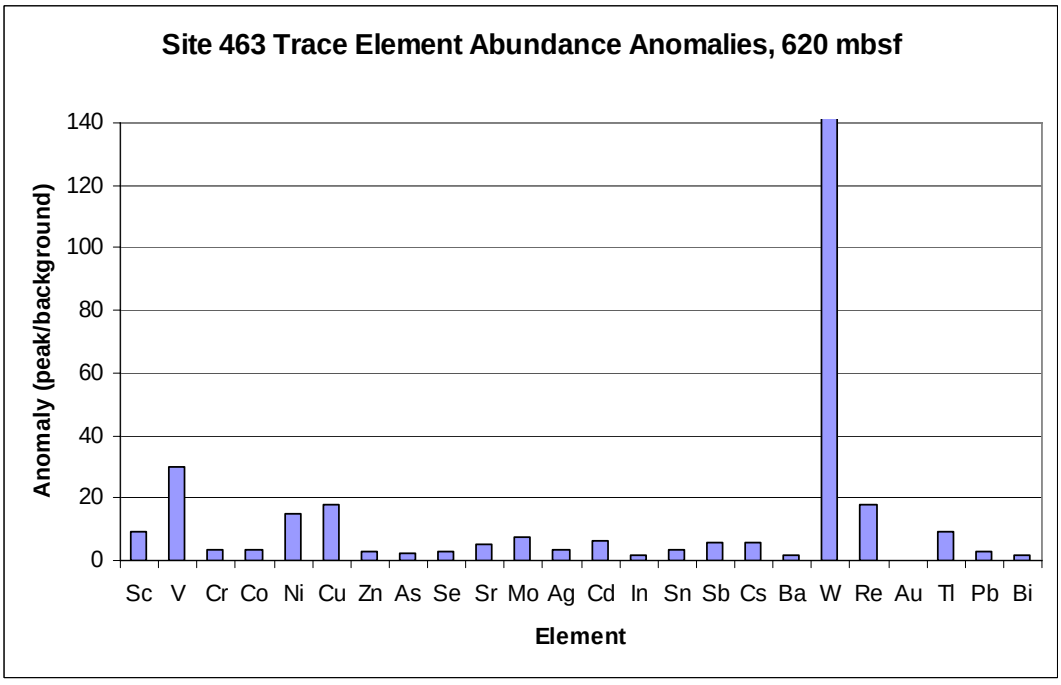

Figure A5. Trace element abundance anomalies found in Deep Sea Drilling Project Site 463 during this study.

Appendix 2. Deep Sea Drilling Project Site 167 and Site 463 normalized element abundances.

Site 167 Minor Element Data

Depth (mbsf)	Sc/Zr	V/Zr	Cr/Zr	Co/Zr	Ni/Zr
870.29	23.94	63.53	31.22	103.8	105.8
870.29	23.94	58.26	32.94	114.5	105.6
870.48	42.50	52.00	82.00	164.5	120.5
870.64	27.75	65.11	36.54	161.4	127.8
870.82	23.13	61.87	33.35	136.9	102.6
870.99	28.63	54.43	29.60	226.8	108.2
871.21	50.00	98.33	104.11	305.8	191.1
871.50	51.82	71.64	72.73	253.8	148.9
871.50	38.13	49.87	51.07	183.7	100.6
871.71	30.54	42.67	48.79	121.5	94.7
871.91	25.82	53.55	31.77	144.9	110.3
872.10	35.79	52.58	37.29	185.0	98.5
872.31	23.33	61.02	30.40	196.9	104.8
872.52	22.78	66.27	29.78	177.1	99.7
872.52	22.26	59.92	30.54	174.8	101.7
872.70	24.69	59.76	30.38	182.2	102.8
873.00	21.83	59.25	28.07	164.7	98.4
873.22	85.00	232.80	136.20	835.8	342.0
873.42	21.53	66.73	28.16	145.2	81.0
873.60	29.20	52.00	44.13	144.8	77.9
873.79	31.29	52.64	41.93	153.6	74.4
874.00	25.74	81.74	36.87	285.6	110.9
874.20	23.03	32.38	25.90	33.8	24.0
874.40	24.63	76.75	34.05	112.1	73.0
874.60	19.91	54.41	28.20	94.7	70.2
874.80	30.32	87.53	39.21	134.7	71.7
875.00	75.00	227.20	124.40	577.4	167.8
875.21	40.27	107.18	54.91	279.2	80.6
875.40	30.50	135.65	48.90	258.9	80.8
875.60	28.65	92.30	42.83	235.8	79.0
875.81	29.58	66.58	46.05	225.9	79.8
875.90	25.63	82.63	40.48	181.0	79.9
879.88	35.44	205.78	132.11	440.3	248.8
879.88	25.91	56.12	41.53	135.0	78.7
880.08	133.00	756.00	408.00	2265.0	778.0
880.28	32.13	53.67	133.13	272.2	80.3
880.50	43.20	107.80	84.90	481.8	152.1
880.71	242.00	842.00	553.00	5685.0	814.0
880.89	34.60	83.40	46.60	382.5	90.9
881.11	81.50	407.75	239.25	1678.0	495.8
881.28	83.75	297.00	159.25	1755.0	315.8
881.50	120.50	428.00	274.50	3240.5	453.0
881.69	206.00	454.00	571.00	5589.0	540.0
881.87	211.00	389.00	445.00	6582.0	461.0
882.11	138.00	663.00	409.00	4276.5	723.5
882.28	83.25	155.75	149.25	1749.8	231.8

Site 167 Minor Element Data (cont.)

Depth (mbsf)	Sc/Zr	V/Zr	Cr/Zr	Co/Zr	Ni/Zr
882.50	37.91	68.18	58.09	590.4	98.3
882.70	34.33	50.93	45.67	311.4	98.9
882.88	65.20	137.00	123.60	1295.8	192.8
883.10	32.46	58.92	47.92	450.6	80.0
882.70	34.33	50.93	45.67	311.4	98.9
882.88	65.20	137.00	123.60	1295.8	192.8
883.10	32.46	58.92	47.92	450.6	80.0
883.28	26.42	57.16	45.26	308.6	96.2
883.28	88.40	189.80	153.20	1528.0	300.2
883.50	27.14	56.55	49.95	297.3	81.0
883.70	43.56	117.78	87.78	694.4	149.4
883.91	91.67	287.33	233.33	2426.3	369.0
884.01	144.50	545.50	393.00	4957.5	683.5
884.30	20.33	52.11	35.98	233.5	69.7
884.51	234.00	567.00	498.00	8125.0	732.0
884.71	40.91	75.09	56.64	709.4	103.7
884.89	341.00	1076.00	808.00	9585.0	1306.0
885.08	18.84	51.53	38.92	263.7	67.7
885.08	20.67	50.56	41.22	265.3	69.7
885.26	50.67	181.25	121.83	814.5	264.2
885.58	24.38	49.95	39.62	349.2	67.0
885.58	47.25	123.50	98.50	884.8	165.6
885.80	86.00	209.33	192.33	2250.3	296.3
885.97	84.25	322.00	234.25	2138.3	408.5
886.18	44.44	88.00	74.44	841.2	126.9
886.29	242.00	441.50	353.00	6340.0	541.5
888.36	317.00	377.00	373.00	15030.0	549.0
888.57	483.00	951.00	726.00	19490.0	1444.0
888.75	93.67	340.33	278.67	5363.3	528.0
888.94	282.00	1075.00	893.00	12660.0	1445.0
889.16	139.33	448.33	171.33	5066.7	287.7
889.36	49.27	604.55	142.45	1584.5	256.7
889.61	35.68	178.32	63.42	724.7	127.1
889.80	29.25	103.25	50.38	609.4	80.8
889.80	32.67	108.33	55.53	582.3	94.7
889.99	25.58	84.39	42.55	317.0	75.2
890.20	127.50	661.50	340.50	4534.0	556.0
890.40	27.38	103.14	44.57	458.4	74.0
890.58	432.00	1677.00	706.00	13140.0	1245.0
890.79	237.00	2038.00	634.00	9982.0	1088.0
891.08	91.00	987.00	314.67	3790.0	568.3
891.30	122.33	510.33	312.33	4146.7	591.3
891.49	258.00	1861.00	746.00	11800.0	1598.0
891.69	20.11	102.84	38.21	268.7	48.1
891.69	20.36	87.43	34.82	200.3	45.2
891.93	31.63	249.93	80.72	274.6	90.1

Site 167 Minor Element Data (cont.)

Depth (mbsf)	Sc/Zr	V/Zr	Cr/Zr	Co/Zr	Ni/Zr
892.11	283.00	1743.00	777.00	9395.0	713.0
892.28	64.77	337.23	243.88	430.0	78.1
892.50	81.84	515.78	343.56	410.7	114.4
892.69	72.65	361.63	646.33	427.1	147.2
898.22	34.53	161.11	187.19	103.4	61.6
898.43	48.16	234.08	238.16	150.0	72.3
898.62	49.44	231.60	348.20	172.9	114.3
898.82	30.21	196.64	226.93	247.6	53.8
899.01	40.03	248.17	908.87	163.5	140.4
899.23	41.26	314.75	966.39	180.2	182.5
899.23	40.85	289.02	925.74	182.0	180.7
899.40	41.25	246.23	784.06	160.9	135.5
899.61	40.54	284.33	560.60	158.5	125.8
899.81	36.48	235.36	466.31	121.2	81.1
900.02	29.66	294.11	952.68	210.7	194.5
900.22	42.36	308.18	642.12	180.2	146.1
900.42	39.42	300.31	578.91	162.3	121.8
900.62	46.50	406.92	564.42	226.7	137.2
900.79	46.70	313.48	579.86	160.4	100.8
901.01	44.32	323.51	437.03	162.6	109.0
908.17	16.00	45.97	40.97	58.1	37.4
908.17	16.28	43.24	42.45	62.3	36.3
908.37	16.24	47.00	55.76	71.5	48.7
908.61	18.35	74.77	43.50	68.0	44.3
908.81	18.60	47.88	41.32	66.2	45.0
909.00	13.33	49.48	34.73	52.5	45.6
909.22	21.31	52.50	58.13	84.8	49.3
909.40	17.64	58.24	49.88	62.0	47.4
909.60	23.86	99.79	52.57	90.8	54.9
909.80	360.00	997.00	680.00	2548.0	696.0
910.03	24.33	84.00	57.83	228.3	68.8
910.21	23.50	68.08	58.17	167.1	65.7
910.42	22.93	62.36	51.14	132.6	61.1
910.42	104.00	409.00	359.00	1094.0	419.5
910.60	60.25	195.25	206.00	679.0	251.3
911.03	24.33	67.80	63.93	229.3	81.6
911.21	128.00	450.00	434.00	1780.5	527.5
911.40	36.71	101.00	115.57	506.7	131.0
911.59	25.50	85.36	65.57	243.5	75.2
911.80	48.67	232.00	207.67	702.0	265.7
912.01	178.00	645.00	754.00	3996.0	860.0
912.23	18.30	45.78	45.78	165.5	61.5
912.40	20.31	44.63	48.75	181.3	58.0
912.40	208.00	592.00	693.00	3352.0	851.0
912.60	116.00	348.50	378.50	2177.5	522.5
912.81	100.00	375.00	411.50	2163.0	512.0

Site 167 Minor Element Data (cont.)

Depth (mbsf)	Sc/Zr	V/Zr	Cr/Zr	Co/Zr	Ni/Zr
912.90	110.00	463.50	451.50	2243.0	549.5
917.35	50.60	206.00	176.20	714.4	229.4
917.84	67.33	372.67	330.33	1394.3	422.3
918.35	235.00	929.00	826.00	4877.0	997.0
918.83	105.00	436.00	403.50	2410.5	475.0
919.36	25.18	48.45	57.55	340.6	69.0
919.36	23.29	44.50	51.71	231.0	63.9
919.84	20.39	93.78	105.83	187.7	69.3
920.33	15.73	63.95	39.73	111.1	50.4
920.86	16.54	51.08	42.77	136.5	54.4
921.35	183.00	641.00	615.00	3003.0	717.0
921.85	27.00	107.69	76.92	269.7	81.8
922.34	17.15	42.25	44.60	156.2	51.3
922.83	44.67	131.67	123.50	501.3	122.5
923.33	14.53	70.69	45.19	122.4	46.9
925.10	20.47	50.67	57.73	70.3	118.5
925.21	16.83	50.42	48.38	84.0	80.8
925.31	19.00	53.13	77.20	51.7	542.9
925.31	18.59	49.53	52.12	57.1	98.6
925.41	83.67	62.33	714.67	347.3	330.3
925.50	21.62	60.38	63.08	92.5	127.6
925.70	21.06	52.94	58.00	101.9	106.4
925.80	48.83	150.00	163.00	274.3	298.8
925.90	20.15	52.46	66.23	115.8	126.3
926.10	37.40	64.20	134.80	237.2	295.2
926.30	23.89	55.89	126.89	96.1	138.1
926.71	23.64	69.00	69.64	93.4	162.4
926.80	30.14	80.43	112.86	175.1	203.3
927.00	14.10	51.90	48.21	60.0	71.3
927.20	17.50	48.41	55.27	126.0	90.5
927.39	19.90	58.00	55.48	136.2	83.1
927.61	39.25	199.25	121.38	290.0	215.1
927.80	25.50	97.90	75.10	107.3	153.0
928.10	62.00	320.25	229.00	648.0	436.8
928.30	93.75	198.25	1556.50	348.3	221.0
928.50	42.50	193.00	214.00	331.5	371.5
928.50	24.10	63.90	79.40	129.8	146.2
928.71	24.00	58.20	88.60	142.6	147.2
928.90	23.31	58.62	76.85	104.5	129.5
929.10	20.00	48.27	59.53	102.5	113.0
929.10	21.64	55.07	66.93	143.0	126.9
929.10	21.36	52.29	62.07	127.6	119.4
929.30	13.75	52.62	41.52	58.6	55.3
929.30	13.57	47.65	42.28	61.0	55.4
929.60	21.95	51.89	57.11	97.7	87.5
929.80	18.80	66.80	60.73	91.2	128.1

Site 167 Minor Element Data (cont.)

Depth (mbsf)	Sc/Zr	V/Zr	Cr/Zr	Co/Zr	Ni/Zr
929.80	19.79	68.00	65.36	91.7	115.4
930.01	13.84	65.73	45.11	54.7	61.4
930.21	28.00	109.29	98.71	133.0	202.1
930.40	27.93	120.50	73.64	196.0	111.8
930.60	30.86	68.71	114.57	193.7	197.9
930.80	30.63	58.88	101.63	169.0	169.8
935.70	22.73	53.45	76.91	133.5	147.5
935.91	14.31	46.94	43.63	70.6	55.0
936.10	11.55	47.30	40.29	62.4	50.6
936.30	19.69	63.69	79.54	75.2	105.6
936.61	12.25	70.02	40.04	72.9	60.5
936.61	12.59	66.94	41.55	69.9	54.6
936.61	12.13	67.61	41.02	72.4	54.2
936.79	25.50	147.07	83.36	186.1	131.6
937.00	26.11	179.78	91.22	169.3	174.6
937.40	13.70	94.00	44.72	61.9	60.3
937.60	15.11	71.51	47.80	59.0	66.1
937.80	24.77	132.54	109.31	213.3	166.5
938.10	18.18	50.27	53.64	81.5	84.0
938.30	38.00	129.50	157.17	299.3	259.0
938.50	15.41	48.82	44.91	78.1	67.4
938.71	19.85	48.15	73.85	103.7	220.5
938.71	23.36	48.36	77.64	118.2	121.8
938.89	14.35	46.84	46.84	84.3	72.7
939.11	23.33	59.50	84.00	126.7	120.8
939.30	34.33	77.17	111.50	151.2	232.8
939.59	31.86	63.29	94.43	125.3	211.9
939.80	18.09	49.70	58.57	89.1	78.9
940.01	22.64	61.00	87.18	115.8	155.1
940.19	26.67	59.44	87.33	147.4	323.4
940.60	58.67	94.67	204.33	665.7	549.3
940.79	15.13	54.48	48.29	74.0	68.5
940.90	15.46	60.49	50.78	78.6	70.6

Site 167 Minor Element Data (cont.)

Depth (mbsf)	Cu/Zr	Zn/Zr	Se/Zr	As/Zr	Se/Zr
870.3	909	1.33	1601	147.6	11.39
870.3	917	1.18	1539	154.9	10.29
870.5	966	1.00	1388	679.3	6.67
870.6	1028	1.29	1726	197.1	12.50
870.8	920	1.13	1035	224.2	4.78
871.0	896	1.10	1092	181.5	3.67
871.2	1208	1.89	2415	508.3	11.11
871.5	1085	2.18	2005	416.3	9.09
871.5	751	1.13	1413	298.1	7.33
871.7	713	1.08	1148		5.42
871.9	825	1.05	1206	131.9	4.77
872.1	737	0.96	1172	209.6	4.17
872.3	808	1.07	1203	137.6	4.89
872.5	789	1.09	1200	136.9	5.11
872.5	805	1.26	1167	132.1	4.60
872.7	803	1.02	1169	137.3	4.67
873.0	786	1.08	1144	116.0	4.83
873.2	2534	3.20	4356	978.2	22.00
873.4	594	0.87	1047	141.0	4.67
873.6	521	0.80	1170	315.4	5.33
873.8	524	0.71	977	330.1	4.29
874.0	696	1.06	1245	199.3	5.81
874.2	193	0.52	1013	103.0	7.59
874.4	413	0.95	1437	111.8	7.25
874.6	371	0.81	1387	80.0	8.41
874.8	426	1.00	1656	211.1	10.53
875.0	925	2.80	3933	793.6	22.00
875.2	512	1.18	1886	373.6	12.73
875.4	398	1.10	1343	244.1	7.50
875.6	430	1.09	1379	199.4	7.39
875.8	319	0.95	1232	224.2	7.37
875.9	379	1.26	912	173.0	6.90
879.9	1394	3.89	3770	583.0	17.78
879.9	410	1.06	1879	163.2	13.53
880.1	3598	9.50	12443	2287.5	75.00
880.3	319	1.00	1347	272.4	10.67
880.5	933	2.30	2457	447.8	14.00
880.7	4352	12.00	12420	4233.0	90.00
880.9	493	1.13	1218	302.1	8.67
881.1	2960	6.25	11025	1285.5	37.50
881.3	1817	4.00	4208	1140.5	32.50
881.5	2847	6.50	805	2242.0	6.21
881.7	2655	12.00	6255	4218.0	40.00
881.9	2597	8.00	3195	3955.0	50.00
882.1	5570	10.00	8438	2355.5	35.00
882.3	1077	3.00	3150	1133.3	20.00

Site 167 Minor Element Data (cont.)

Depth (mbsf)	Cu/Zr	Zn/Zr	Se/Zr	As/Zr	Se/Zr
882.5	507	1.36	1301	413.9	9.09
882.7	718	1.48	977	188.9	3.70
882.9	1056	2.60	3150	850.0	28.00
883.1	489	1.08	1284	350.8	9.23
882.7	718	1.48	977	188.9	3.70
882.9	1056	2.60	3150	850.0	28.00
883.1	489	1.08	1284	350.8	9.23
883.3	366	1.21	1149	252.3	4.74
883.3	1293	3.80	600	926.6	4.72
883.5	513	1.14	1381	234.2	7.27
883.7	928	2.11	1845	533.6	7.78
883.9	2748	5.00	3210	1446.3	13.33
884.0	5595	10.00	5085	2283.5	0.00
884.3	473	0.96	948	135.1	3.91
884.5	4917	11.00	7380	4388.0	50.00
884.7	694	1.36	1743	448.7	12.73
884.9	10650	19.00	6165	4939.0	0.00
885.1	434	0.89	894	136.3	3.95
885.1	441	0.92	790	156.9	5.17
885.3	2418	3.33	2768	449.9	13.33
885.6	330	1.00	911	216.9	6.19
885.6	818	2.13	2109	603.9	10.00
885.8	1219	4.00	2895	1494.0	23.33
886.0	4250	5.25	4894	1291.5	20.00
886.2	632	1.44	1630	496.3	8.89
886.3	2747	8.00	1845	2266.0	0.00
888.4	2674	6.00	0	4154.0	0.00
888.6	9583	15.00	5625	4752.0	0.00
888.8	2957	6.00	847	1667.3	7.50
888.9	5852	19.00	8865	4914.0	10.00
889.2	600	3.33	2205	1352.7	13.33
889.4	574	3.45	3514	375.5	8.18
889.6	362	1.79	2667	227.8	9.47
889.8	180	1.38	1547	253.3	6.25
889.8	209	1.20	1767	265.7	6.00
890.0	184	1.03	1365	125.4	3.03
890.2	950	6.50	9180	1982.5	20.00
890.4	124	1.05	1080	190.0	3.81
890.6	1885	15.00	720	4035.0	6.90
890.8	2193	14.00	14310	3686.0	40.00
891.1	1239	7.33	6345	1334.7	20.00
891.3	2674	7.33	5985	1327.3	16.67
891.5	1630	15.00	15885	3824.0	70.00
891.7	274	1.00	1155	105.1	5.00
891.7	208	0.75	1025	95.3	4.32
891.9	728	0.97	278	38.5	0.36

Site 167 Minor Element Data (cont.)

Depth (mbsf)	Cu/Zr	Zn/Zr	Se/Zr	As/Zr	Se/Zr
892.1	1945	13.00	13275	3700.0	40.00
892.3	2029	1.31	1848	145.8	3.85
892.5	648	1.93	615	91.6	-0.67
892.7	768	1.71	1772	75.3	0.35
898.2	883	0.86	1620	91.8	0.82
898.4	665	0.92	1437	97.2	1.20
898.6	820	1.24	2141	98.7	0.71
898.8	316	0.57	1060	336.6	0.56
899.0	1328	0.94	1104	65.2	0.98
899.2	634	1.11	1169	76.5	0.98
899.2	586	1.05	815	76.9	1.01
899.4	568	0.90	735	67.5	0.90
899.6	548	0.91	658	69.7	1.07
899.8	617	0.76	1124	61.4	1.25
900.0	714	1.29	834	81.0	0.91
900.2	651	1.11	893	71.7	1.25
900.4	983	0.92	929	69.0	1.35
900.6	713	1.17	852	81.5	1.01
900.8	725	1.07	864	66.2	0.95
901.0	735	1.07	1230	63.2	3.82
908.2	359	0.74	1221	122.1	3.45
908.2	430	0.69	1357	142.3	2.80
908.4	572	0.84	1374	173.2	3.46
908.6	286	0.81	1273	169.8	3.20
908.8	300	0.72	1121	170.5	1.79
909.0	4720	0.99	1266	75.0	4.38
909.2	511	0.88	1253	257.4	2.80
909.4	421	0.88	1392	170.3	4.29
909.6	209	1.00	11790	306.6	0.00
909.8	2877	12.00	1316	4110.0	4.17
910.0	207	1.25	1245	358.2	3.33
910.2	255	1.17	1244	358.8	4.29
910.4	247	1.14	7718	306.4	20.00
910.4	1819	7.00	4928	2204.0	15.00
910.6	1190	4.00	0	1093.5	0.00
911.0	658	1.33	8618	291.8	5.00
911.2	3620	9.00	2385	2233.0	8.57
911.4	538	2.14	1437	599.6	5.00
911.6	374	1.29	4988	308.4	8.33
911.8	943	4.50	13770	741.8	30.00
912.0	2754	14.00	1186	4308.0	3.91
912.2	326	1.09	1223	199.4	3.75
912.4	258	1.13	12645	284.6	20.00
912.4	4482	14.00	7245	4378.0	10.00
912.6	3271	9.50	8078	2240.0	25.00
912.8	3005	10.00	9923	2173.5	20.00

Site 167 Minor Element Data (cont.)

Depth (mbsf)	Cu/Zr	Zn/Zr	Se/Zr	As/Zr	Se/Zr
912.9	2393	9.50	4140	2248.5	14.00
917.4	891	5.60	7440	925.2	13.33
917.8	2161	8.00	14490	1490.0	30.00
918.4	3591	17.00	7470	4335.0	15.00
918.8	1344	10.00	1096	2202.5	5.45
919.4	282	1.09	1093	398.5	4.29
919.4	270	1.07	1365	332.1	3.33
919.8	190	1.06	1046	281.2	2.70
920.3	233	1.03	1083	153.4	2.69
920.9	287	1.12	8280	198.7	0.00
921.4	2949	12.00	1637	4634.0	5.38
921.9	319	1.77	918	387.4	3.50
922.3	332	1.10	2093	259.9	5.00
922.8	455	2.50	982	765.2	1.25
923.3	259	1.00	1321	166.6	19.47
925.1	272	1.20	1316	278.2	15.04
925.2	266	1.04	1713	201.1	25.47
925.3	311	1.60	1438	265.7	20.24
925.3	310	1.24	5007	243.2	0.00
925.4	1104	2.67	1512	1456.3	20.38
925.5	383	1.62	1306	319.7	15.81
925.7	327	1.44	3813	257.0	24.00
925.8	786	3.50	1291	728.2	6.69
925.9	293	1.38	838	313.2	10.40
926.1	832	3.00	1927	761.2	6.22
926.3	592	1.11	1408	509.6	15.09
926.7	467	1.36	1266	326.2	15.00
926.8	574	1.71	1321	559.6	7.97
927.0	246	0.97	1180	173.7	16.00
927.2	411	1.14	1294	202.6	11.05
927.4	370	1.29	2338	266.2	49.00
927.6	581	2.25	1427	521.6	24.60
927.8	781	1.40	4343	395.7	49.00
928.1	941	4.75	14233	1073.3	0.00
928.3	874	0.75	3023	3065.0	3.25
928.5	1318	5.00	1162	954.5	13.70
928.5	403	1.30	1236	372.5	14.40
928.7	1910	1.30	1482	369.4	19.38
928.9	339	1.31	1115	301.9	14.33
929.1	369	1.13	1280	273.0	13.36
929.1	500	1.64	1174	294.1	14.07
929.1	382	1.14	1167	287.8	12.75
929.3	288	1.02	1127	97.8	10.72
929.3	283	0.91	1364	104.4	12.58
929.6	832	1.21	1053	242.6	15.20
929.8	977	1.80	1384	262.3	16.00

Site 167 Minor Element Data (cont.)

Depth (mbsf)	Cu/Zr	Zn/Zr	Se/Zr	As/Zr	Se/Zr
929.8	1086	1.79	1191	284.4	7.27
930.0	345	0.89	1118	133.7	11.00
930.2	470	2.00	1137	543.0	2.14
930.4	378	1.14	1057	321.9	9.57
930.6	689	2.29	1093	541.0	8.25
930.8	402	2.63	1015	478.8	11.45
935.7	605	1.82	1159	364.4	12.63
935.9	423	0.82	1165	106.8	7.53
936.1	344	0.79	1441	85.2	10.69
936.3	619	0.92	1085	361.8	8.94
936.6	458	1.08	1033	110.4	10.10
936.6	425	0.82	1037	104.7	8.07
936.6	450	0.87	1475	101.2	17.36
936.8	666	1.86	1096	293.1	20.33
937.0	656	2.11	0	440.9	0.00
937.4	402	1.09	1207	119.4	13.26
937.6	353	0.91	2503	134.4	13.15
937.8	861	2.15	1162	371.6	18.00
938.1	360	0.91	2258	202.5	10.50
938.3	901	2.50	1177	693.3	16.85
938.5	408	0.88	1031	146.1	10.69
938.7	544	1.54	1054	333.0	8.73
938.7	602	1.36	1092	366.8	8.74
938.9	328	0.84	1251	148.0	10.00
939.1	545	1.08	1058	372.3	25.33
939.3	678	2.83	1128	632.5	31.00
939.6	610	2.71	1119	562.9	2.87
939.8	513	1.13	976	207.9	11.18
940.0	408	1.27	768	345.0	9.56
940.2	502	2.56	0	441.2	0.00
940.6	925	5.67	1190	1270.7	17.52
940.8	388	0.84	1345	151.0	12.76
940.9	407	1.00	0	142.5	0.00

Site 167 Minor Element Data (cont.)

Depth (mbsf)	Rb/Zr	Sr/Zr	Y/Zr	Mo/Zr	Ag/Zr
870.29	271.28	139.0	2422	1941	692
870.29	280.41	136.0	2282	1840	697
870.48	502.83	203.0	2332	1493	7017
870.64	296.14	149.5	2714	2644	1004
870.82	299.70	160.6	1232	2296	1109
870.99	279.43	100.7	752	2327	3083
871.21	740.00	327.2	1882	1133	2944
871.50	558.55	213.4	2071	1323	3236
871.50	396.73	152.0	1567	890	2447
871.71	338.96	121.7	1319	656	1683
871.91	335.23	62.8	977	1183	1275
872.10	349.88	71.3	1026	1114	2200
872.31	316.22	96.6	1024	1805	993
872.52	301.33	103.3	1110	1814	887
872.52	310.40	100.5	1039	1834	818
872.70	314.22	98.7	1030	1782	896
873.00	304.83	90.8	1040	1708	817
873.22	1307.80	631.8	4052	5090	3500
873.42	306.89	96.8	1200	1176	816
873.60	396.00	171.1	1529	808	1073
873.79	372.93	172.1	1243	794	1064
874.00	363.55	127.8	1526	1754	868
874.20	323.62	80.6	865	411	1052
874.40	414.25	105.8	934	1355	1218
874.60	283.33	72.8	990	1398	1139
874.80	564.74	143.0	1281	2501	1174
875.00	1744.00	583.4	3480	19956	2780
875.21	792.55	308.5	2003	3568	1491
875.40	607.50	136.5	1233	4626	1485
875.60	507.39	112.7	1197	2851	1683
875.81	578.42	178.5	1268	1008	1558
875.90	494.81	131.1	1053	1470	1300
879.88	1371.11	218.4	1581	2182	1733
879.88	430.29	100.5	1614	549	1182
880.08	5520.00	1533.5	4697	12345	5650
880.28	618.07	207.7	1728	1369	1473
880.50	1036.00	280.8	1833	2185	1860
880.71	8209.00	2090.0	6627	12950	16400
880.89	635.07	201.6	1459	1575	1767
881.11	3062.50	698.5	3098	9630	4225
881.28	2301.00	655.8	5098	4008	5000
881.50	4076.50	1197.0	2979	6745	1610
881.69	7212.00	2056.0	7640	5445	17900
881.87	6715.00	1701.0	5800	26130	21500
882.11	5430.00	1040.0	2419	6345	10450
882.28	1991.25	676.3	4943	3115	4900

Site 167 Minor Element Data (cont.)

Depth (mbsf)	Rb/Zr	Sr/Zr	Y/Zr	Mo/Zr	Ag/Zr
882.50	812.91	216.6	1910	732	2000
882.70	450.00	111.8	932	622	1459
882.88	1724.60	512.4	4028	1203	3660
883.10	696.46	202.4	1795	475	1877
882.70	450.00	111.8	932	622	1459
882.88	1724.60	512.4	4028	1203	3660
883.10	696.46	202.4	1795	475	1877
883.28	540.00	115.0	1023	665	1916
883.28	2054.00	357.6	1289	1436	1664
883.50	535.45	115.3	1408	449	1786
883.70	1200.00	259.3	2026	934	2622
883.91	3223.33	576.0	1679	3262	7900
884.01	5490.00	841.0	914	3977	14050
884.30	419.13	58.9	639	709	1650
884.51	7907.00	1861.0	4628	6162	25000
884.71	845.45	241.5	2099	568	2991
884.89	11290.00	1279.0	1370	9663	27800
885.08	410.26	61.3	632	352	1400
885.08	438.06	62.7	624	338	1469
885.26	1412.50	172.3	669	1091	2408
885.58	500.00	115.0	987	1724	1771
885.58	1346.25	255.5	1831	3938	2400
885.80	2773.33	621.3	2223	1811	5700
885.97	3095.00	503.5	2180	2155	5125
886.18	1079.00	242.7	1950	783	2411
886.29	5150.00	547.0	1008	3728	16850
888.36	7010.00	1009.0	1519	8092	33900
888.57	10410.00	1036.0	1153	16920	47200
888.75	3650.00	584.0	1070	3024	2014
888.94	11630.00	1556.0	1363	6953	29800
889.16	2644.33	471.7	2163	1744	11267
889.36	1656.36	165.9	399	1299	4327
889.61	826.84	151.9	1001	2843	2263
889.80	654.38	144.3	1038	1049	1963
889.80	742.00	159.8	1187	842	1820
889.99	496.67	75.2	561	488	1524
890.20	4890.50	973.0	2772	5120	9800
890.40	577.14	91.8	717	1673	1814
890.58	10440.00	1262.0	1212	9173	1824
890.79	9766.00	1800.0	2589	190100	23400
891.08	4076.67	630.7	1130	2783	8300
891.30	4523.33	740.7	945	3903	10033
891.49	11400.00	2278.0	2683	10230	25300
891.69	525.00	72.0	636	900	1571
891.69	491.82	67.9	626	540	1377
891.93	107.55	17.8	85	512	1287

Site 167 Minor Element Data (cont.)

Depth (mbsf)	Rb/Zr	Sr/Zr	Y/Zr	Mo/Zr	Ag/Zr
892.11	11950.00	1813.0	2306	13130	29100
892.28	785.38	355.5	618	1795	2546
892.50	186.47	65.4	142	605	2262
892.69	196.67	71.6	157	442	909
898.22	355.96	87.2	259	210	1422
898.43	317.76	137.8	300	240	1692
898.62	364.20	180.8	292	196	18079
898.82	536.36	53.5	420	572	1439
899.01	161.97	66.0	159	193	1592
899.23	187.21	129.5	261	569	1648
899.23	186.56	120.9	247	196	1526
899.40	112.33	84.7	242	276	1675
899.61	103.37	96.6	230	184	1569
899.81	86.98	73.3	220	185	2027
900.02	159.27	63.6	254	5298	1520
900.22	108.91	53.8	236	192	1534
900.42	135.42	75.3	244	191	1773
900.62	164.02	70.0	246	196	1430
900.79	144.42	43.2	257	285	1278
901.01	146.89	43.0	249	262	1274
908.17	402.94	109.3	958	1434	986
908.17	441.03	106.8	937	746	1408
908.37	483.20	107.3	777	356	885
908.61	471.54	147.8	991	413	900
908.81	454.80	144.2	992	346	1049
909.00	420.00	33.3	477	240	925
909.22	486.31	228.9	1395	499	656
909.40	464.00	152.3	971	1719	629
909.60	494.43	253.9	1566	520	11700
909.80	6294.00	1559.0	1787	3998	1667
910.03	518.58	218.9	1969	650	900
910.21	533.42	229.4	1698	554	850
910.42	493.50	229.1	1582	1347	2650
910.42	3593.00	1502.0	3707	2028	2400
910.60	2074.50	784.3	3353	3268	0
911.03	636.80	216.5	1582	379	7600
911.21	4584.50	1365.5	1470	306500	2686
911.40	1012.29	459.4	2176	5144	1279
911.59	609.93	244.9	1697	6676	2617
911.80	2213.33	478.0	1414	5552	13300
912.01	6745.00	2212.0	2924	11100	1165
912.23	476.09	157.2	1218	486	1200
912.40	444.44	209.2	1480	1301	10800
912.40	6867.00	2433.0	3518	6122	9850
912.60	3897.00	1206.5	1790	5250	7750
912.81	3737.50	1529.0	3672	3576	8250

Site 167 Minor Element Data (cont.)

Depth (mbsf)	Rb/Zr	Sr/Zr	Y/Zr	Mo/Zr	Ag/Zr
912.90	4315.50	1531.5	3217	2704	3020
917.35	1829.40	821.4	3754	1622	5133
917.84	3440.00	1064.3	1470	6000	21900
918.35	8481.00	2571.0	2411	11410	9850
918.83	3889.00	1273.5	2350	3958	1782
919.36	481.36	265.8	1912	5172	1179
919.36	461.79	260.7	1904	477	1067
919.84	445.39	157.1	1545	1548	781
920.33	424.05	133.4	889	345	892
920.86	424.62	139.8	1054	326	11700
921.35	4923.00	1727.0	6618	4085	1192
921.85	707.77	224.8	2065	766	935
922.34	415.05	166.7	1241	479	1533
922.83	1037.67	367.2	2948	1455	722
923.33	428.75	78.1	668	373	1678
925.10	663.33	164.6	1901	384	1743
925.21	547.50	119.9	1289	415	1915
925.31	678.00	172.2	1903	967	1664
925.31	614.71	161.0	1751	397	4737
925.41	2067.00	153.3	1705	1476	1701
925.50	744.54	188.8	2079	538	1894
925.70	662.50	146.0	1614	419	2922
925.80	1833.33	385.5	2717	993	1951
925.90	724.00	142.9	1485	423	2752
926.10	1417.60	317.0	3700	2094	2402
926.30	921.44	120.1	1407	745	1816
926.71	797.91	172.9	1806	428	2460
926.80	1098.71	257.3	2850	706	1299
927.00	516.21	75.5	851	332	2309
927.20	568.64	138.7	1411	707	2247
927.39	569.05	105.5	1053	587	3448
927.61	1263.75	458.1	4175	1974	1524
927.80	862.60	292.6	2783	764	4745
928.10	2468.75	758.5	6890	3190	4283
928.30	1421.50	91.5	1588	2640	2326
928.50	2227.75	374.0	1915	2868	1629
928.50	865.30	184.8	1897	716	2167
928.71	861.10	190.9	2037	564	1798
928.90	774.62	213.0	2325	439	1835
929.10	659.40	165.5	1812	801	2141
929.10	732.14	187.2	2116	1200	1724
929.10	720.71	179.3	1954	1054	1614
929.30	422.69	67.0	908	448	1525
929.30	439.57	63.8	858	470	1861
929.60	609.47	129.4	1333	768	1955
929.80	620.53	146.5	1733	439	2655

Site 167 Minor Element Data (cont.)

Depth (mbsf)	Rb/Zr	Sr/Zr	Y/Zr	Mo/Zr	Ag/Zr
929.80	710.00	161.6	1858	440	1385
930.01	483.24	65.8	863	338	1389
930.21	1097.71	249.4	2626	669	2429
930.40	747.86	116.7	1245	1000	3064
930.60	1105.71	235.3	2537	712	2395
930.80	992.75	226.3	2249	633	1781
935.70	821.18	202.2	2142	1151	1590
935.91	456.12	71.6	937	463	1443
936.10	426.82	44.1	572	277	2638
936.30	748.31	128.8	1368	600	1557
936.61	427.50	69.8	761	1560	1478
936.61	423.53	69.4	738	386	1453
936.61	421.30	69.7	746	411	2599
936.79	832.14	198.6	1755	1114	2008
937.00	910.00	238.3	2557	1468	0
937.40	452.56	79.0	1053	392	1327
937.60	506.86	92.0	1151	355	1628
937.80	1160.77	196.8	1045	894	1402
938.10	582.73	113.7	1424	477	2485
938.30	1756.67	293.0	1875	1395	1523
938.50	501.18	90.1	1273	495	1739
938.71	682.85	124.4	1422	555	1755
938.71	793.82	128.5	1401	432	1570
938.89	501.94	94.8	988	347	2458
939.11	741.83	167.5	1717	1099	1461
939.30	1245.17	329.7	3602	904	1554
939.59	1122.57	359.4	3434	871	7443
939.80	567.83	75.7	732	316	1723
940.01	833.91	201.8	1885	1051	2003
940.19	901.44	239.1	2583	1373	0
940.60	2085.33	548.0	5930	3957	1532
940.79	500.32	87.0	1204	315	1668
940.90	515.95	58.8	914	288	0

Site 167 Minor Element Data (cont.)

Depth (mbsf)	Cd/Zr	In/Zr	Sn/Zr	Sb/Zr	Cs/Zr
870.29	10133	25.58	22100	4583	23.22
870.29	13959	26.97	22492	4628	24.26
870.48	54000	151.67	16304	4625	61.17
870.64	13314	32.39	22065	5223	25.89
870.82	18765	38.35	24827	5498	27.39
870.99	3040	29.50	23303	6295	25.97
871.21	40556	94.67	57886	5750	70.33
871.50	127364	79.91	43698	5768	54.18
871.50	25267	59.00	32717	3460	39.13
871.71	14067	36.54	26339	3813	31.00
871.91	4905	19.80	28895	5185	28.32
872.10	6583	36.96	25716	5156	32.33
872.31	5782	19.31	26924	5827	26.24
872.52	6609	18.89	26859	5760	24.89
872.52	6456	17.12	27502	5778	25.64
872.70	5676	19.87	28405	6037	26.24
873.00	6640	14.52	27598	5788	24.70
873.22	93280	187.60	100100	16050	124.00
873.42	6493	19.82	26917	4153	25.49
873.60	33667	61.00	27343	2970	39.80
873.79	21714	68.00	26696	2904	37.86
874.00	11542	30.10	27635	6740	32.10
874.20	4834	37.52	10075	1283	20.38
874.40	6135	25.93	24440	3420	30.93
874.60	3200	14.81	18464	2737	21.48
874.80	10737	53.37	25692	3829	37.11
875.00	48960	208.20	56745	8970	104.20
875.21	15709	94.27	24700	3532	47.55
875.40	11610	51.95	27934	4800	43.30
875.60	14096	43.91	23838	3509	34.57
875.81	14705	52.47	24358	2700	37.53
875.90	5110	37.63	9559	1329	34.85
879.88	22889	117.44	88219	12983	92.11
879.88	8282	31.85	26076	3159	31.62
880.08	147300	545.50	279825	40650	365.50
880.28	14347	75.27	21688	2270	38.53
880.50	37220	115.10	45825	20145	67.80
880.71	149800	1159.00	230100	33600	481.00
880.89	20627	75.93	25415	6560	40.93
881.11	68500	288.50	146819	45788	206.50
881.28	61650	288.50	74019	17700	145.00
881.50	4566	601.00	9291	1221	240.00
881.69	293600	1144.00	166400	19500	397.00
881.87	342400	1234.00	122200	10800	352.00
882.11	301800	590.00	213850	23850	362.50
882.28	133000	294.50	51513	9900	115.50

Site 167 Minor Element Data (cont.)

Depth (mbsf)	Cd/Zr	In/Zr	Sn/Zr	Sb/Zr	Cs/Zr
882.50	33764	108.55	40064	3450	49.36
882.70	14015	43.22	19512	4861	29.48
882.88	364960	229.20	48360	8160	106.20
883.10	30538	88.85	21725	2815	43.00
882.70	14015	43.22	19512	4861	29.48
882.88	364960	229.20	48360	8160	106.20
883.10	30538	88.85	21725	2815	43.00
883.28	10537	61.63	29951	3213	35.00
883.28	4017	245.60	7610	1004	135.20
883.50	12345	54.23	21657	3143	36.36
883.70	28200	132.11	42178	5900	78.00
883.91	99400	415.00	104217	12050	200.33
884.01	184800	639.00	198413	23475	356.50
884.30	3622	27.15	20779	2876	31.09
884.51	300200	1223.00	195975	25200	457.00
884.71	22182	111.82	26768	3477	53.27
884.89	168200	1253.00	470600	41400	717.00
885.08	4747	34.00	19859	2582	27.58
885.08	4855	36.81	9156	1459	31.36
885.26	15000	109.42	76538	9025	96.75
885.58	10638	60.86	21419	4200	31.10
885.58	20575	168.13	54722	5100	84.00
885.80	86667	453.67	81142	8100	162.33
885.97	28950	335.25	157788	15113	206.75
886.18	26578	147.89	33547	3300	65.33
886.29	111000	708.00	176475	17925	315.00
888.36	232800	1519.00	169975	12600	376.00
888.57	196400	1503.00	490100	34950	654.00
888.75	4693	482.33	10818	1527	224.00
888.94	155000	1392.00	570050	45900	742.00
889.16	52467	482.00	82658	7100	147.67
889.36	10655	126.73	81280	9586	109.73
889.61	5853	68.58	40779	5092	57.00
889.80	11088	80.00	27666	2888	39.56
889.80	15000	88.80	31027	3500	45.93
889.99	4267	40.73	33613	3114	32.82
890.20	80600	679.50	143813	15900	289.00
890.40	7448	64.95	32160	3279	36.62
890.58	5807	1375.00	10691	1402	627.00
890.79	156200	1334.00	333125	31800	577.00
891.08	40667	460.00	156325	17900	252.00
891.30	34600	463.00	184817	16500	290.00
891.49	102600	1364.00	402675	37350	712.00
891.69	4121	35.32	48878	2554	34.55
891.69	2141	31.52	62267	2659	33.86
891.93	2374	10.39	12645	1347	3.60

Site 167 Minor Element Data (cont.)

Depth (mbsf)	Cd/Zr	In/Zr	Sn/Zr	Sb/Zr	Cs/Zr
892.11	114400	1517.00	434525	43500	695.00
892.28	1123	57.23	19375	1696	27.46
892.50	8316	31.22	13253	1020	8.04
892.69	165	30.18	21992	1547	6.69
898.22	2302	16.40	19036	1267	15.84
898.43	1504	20.84	21912	1200	14.82
898.62	614	21.28	78627	16832	15.86
898.82	2685	76.43	12872	547	39.50
899.01	2439	14.97	26032	750	4.86
899.23	2698	18.36	16740	615	6.92
899.23	730	18.11	11992	589	6.77
899.40	842	16.20	12224	549	5.84
899.61	1371	16.93	11534	650	5.51
899.81	696	13.63	13464	600	5.30
900.02	173	20.13	12478	561	6.68
900.22	925	16.29	14361	480	5.82
900.42	977	17.34	20919	473	5.94
900.62	530	21.06	16344	604	7.21
900.79	595	15.91	14441	594	6.06
901.01	7765	15.00	30215	1725	5.53
908.17	7186	30.62	23557	1557	28.53
908.17	7880	34.72	24219	5526	31.93
908.37	8746	40.84	25338	1881	34.76
908.61	8840	36.96	25142	1722	35.19
908.81	5898	38.52	25164	4263	33.72
909.00	16200	11.25	25919	1538	27.68
909.22	9152	57.69	23517	1752	40.81
909.40	17271	36.88	37491	1543	35.36
909.60	272400	65.07	456625	17550	43.07
909.80	27417	987.00	41302	2650	563.00
910.03	25483	77.25	36454	1525	46.33
910.21	17471	76.08	39534	1864	46.67
910.42	110800	66.07	264225	11625	42.29
910.42	50150	457.00	131544	5888	301.50
910.60	0	240.00	0	#DIV/0!	167.00
911.03	92600	63.07	316225	14850	50.47
911.21	41457	462.50	78975	2507	364.00
911.40	15443	132.43	48657	1886	85.00
911.59	19700	66.00	142079	9800	50.57
911.80	345200	157.33	551850	20250	160.67
912.01	11122	963.00	37389	2374	590.00
912.23	15188	40.35	42311	1903	35.87
912.40	302000	57.88	815100	18150	37.50
912.40	348100	943.00	282750	13950	582.00
912.60	174400	480.00	364000	15150	319.00
912.81	106000	477.00	351163	12450	317.50

Site 167 Minor Element Data (cont.)

Depth (mbsf)	Cd/Zr	In/Zr	Sn/Zr	Sb/Zr	Cs/Zr
912.90	52280	483.50	124540	6810	358.00
917.35	77800	192.00	225333	11750	151.80
917.84	231800	317.00	708175	32550	276.67
918.35	109400	981.00	359613	14100	732.00
918.83	25945	501.50	51645	2059	345.00
919.36	24571	90.64	59104	2121	45.82
919.36	13656	68.21	104939	4350	41.50
919.84	5470	55.44	36409	2534	38.28
920.33	13762	25.92	34925	1863	32.08
920.86	346800	37.12	0	17250	33.65
921.35	69600	1025.00	128450	4223	474.00
921.85	17440	75.31	44769	1830	60.00
922.34	106633	48.55	68846	3125	35.60
922.83	10488	170.33	31413	2475	95.83
923.33	17133	31.56	17200	2751	33.13
925.10	4867	64.60	23542	2929	41.40
925.21	11333	40.13	14913	4885	35.67
925.31	11529	64.13	12600	2439	42.87
925.31	6230	56.94	85900	24453	39.12
925.41	10738	329.67	27762	2740	119.00
925.50	13763	74.62	19513	2566	46.31
925.70	23350	61.44	97917	8438	43.31
925.80	17615	164.33	13646	3222	118.33
925.90	78200	78.00	0	3216	44.54
926.10	65	203.40	23356	15256	82.40
926.30	15500	108.44	17000	2739	55.67
926.71	19286	90.91	42114	3806	48.27
926.80	2310	141.29	21966	4652	67.00
927.00	801818	33.55	2236	2253	34.14
927.20	693810	44.05	2669	8919	39.50
927.39	960375	47.38	0	3399	38.67
927.61	12190	121.75	40150	2345	82.75
927.80	1685500	97.90	0	7458	52.00
928.10	5035	246.75	0	54475	160.00
928.30	49525	255.00	170675	7748	78.00
928.50	12000	246.75	41750	2129	135.75
928.50	10190	97.50	29220	3081	53.30
928.71	11200	99.10	50231	2288	53.00
928.90	36760	75.92	0	2087	48.69
929.10	16064	65.60	4720	2961	42.40
929.10	19379	71.57	0	2364	46.43
929.10	287308	72.93	6881	2321	46.14
929.30	221739	18.56	5913	2110	30.56
929.30	11126	21.15	0	6642	31.70
929.60	15640	51.63	30627	2429	38.53
929.80	13421	64.73	20793	2539	38.73

Site 167 Minor Element Data (cont.)

Depth (mbsf)	Cd/Zr	In/Zr	Sn/Zr	Sb/Zr	Cs/Zr
929.80	2371	69.50	16438	3562	45.07
930.01	18429	26.05	38186	2659	33.24
930.21	6948	140.29	0	9200	65.43
930.40	19500	70.93	72271	2773	52.00
930.60	22775	141.71	37713	3411	66.86
930.80	25845	125.88	0	2563	60.38
935.70	148653	92.27	6776	2267	49.82
935.91	1612	19.29	7132	2105	33.10
936.10	3738	14.52	14885	9015	29.71
936.30	5242	74.85	7867	3121	46.15
936.61	8392	20.04	5749	2212	28.85
936.61	4135	19.08	6231	2348	28.94
936.61	920714	18.69	1445	3716	29.20
936.79	28167	69.50	0	2821	56.36
937.00	0	119.67	0	0	55.56
937.40	5077	22.79	24109	3091	31.72
937.60	8977	29.91	37000	7474	34.91
937.80	11800	74.15	16595	2554	72.69
938.10	32500	44.59	0	7387	37.91
938.30	12721	162.67	5050	2907	113.50
938.50	10746	28.62	19715	4975	35.09
938.71	9800	75.31	39209	4381	41.46
938.71	6990	89.09	3448	2382	48.09
938.89	32908	31.55	0	5599	33.06
939.11	68000	82.33	32450	3590	45.58
939.30	22986	164.17	40871	3884	74.33
939.59	4604	141.57	22626	5965	67.57
939.80	17418	42.96	49164	3367	37.13
940.01	45700	89.82	0	4863	50.73
940.19	0	109.89	0	0	54.33
940.60	5155	331.33	17948	2658	125.33
940.79	4592	31.35	19873	3438	33.39
940.90	0	25.95	0	0	31.84

Site 167 Minor Element Data (cont.)

Depth (mbsf)	Ba/Zr	W/Zr	Re/Zr	Au/Zr	Hg/Zr
870.29	1829.4	27229	23.8	3.17	69.78
870.29	1833.8	24860	25.4	3.68	86.88
870.48	2191.7	25288	148.0	16.33	175.67
870.64	1692.9	32196	30.0	3.96	90.46
870.82	2275.7	30783	36.9	3.39	116.91
870.99	1535.0	36400	28.3	5.00	124.80
871.21	1730.0	20300	92.1	6.78	140.67
871.50	1448.2	20141	77.6	6.82	83.00
871.50	1052.0	12695	56.5	2.47	89.13
871.71	681.3	10009	35.1	4.29	48.08
871.91	960.5	21341	19.0	5.55	79.00
872.10	480.4	19341	36.3	4.54	116.88
872.31	916.7	27317	18.0	4.20	99.80
872.52	914.7	30100	17.8	5.04	108.64
872.52	932.2	28080	16.0	5.20	97.06
872.70	948.2	27467	18.2	5.00	105.60
873.00	878.5	26388	13.4	5.42	83.47
873.22	2258.0	82380	179.8	19.80	515.80
873.42	840.7	19433	18.4	5.09	71.84
873.60	334.1	14125	59.7	4.67	40.93
873.79	118.6	13859	64.4	4.93	85.14
874.00	528.7	36073	27.9	4.81	95.48
874.20	520.0	5527	36.0	0.90	0.00
874.40	416.0	17856	25.7	5.10	38.40
874.60	227.4	14228	14.4	3.75	27.97
874.80	247.8	20195	51.0	5.00	13.95
875.00	687.8	72750	203.0	10.00	99.40
875.21	170.4	30798	91.6	6.82	15.55
875.40	352.1	32565	50.1	6.10	63.00
875.60	209.1	26592	42.3	9.48	51.00
875.81	95.3	11637	50.8	5.37	11.47
875.90	191.7	5366	36.7	6.11	60.22
879.88	488.0	31342	113.3	19.22	33.89
879.88	174.7	8874	29.8	5.68	17.29
880.08	603.0	159225	522.5	39.00	98.00
880.28	93.9	6045	71.1	4.80	0.00
880.50	212.6	15083	107.5	12.00	103.00
880.71	1232.0	141225	1111.0	50.00	0.00
880.89	158.2	16180	71.8	9.27	
881.11	951.5	68681	269.3	40.00	147.75
881.28	912.0	110269	274.3	33.75	41.00
881.50	1284.5	5519	566.0	59.50	382.00
881.69	1704.0	46650	1081.0	28.00	0.00
881.87	2792.0	34200	1168.0	66.00	0.00
882.11	2458.0	111713	569.0	31.50	25.00
882.28	518.3	21938	278.5	12.25	0.00

Site 167 Minor Element Data (cont.)

Depth (mbsf)	Ba/Zr	W/Zr	Re/Zr	Au/Zr	Hg/Zr
882.50	292.3	10364	100.6	2.64	0.00
882.70	351.1	12481	41.5	4.52	20.11
882.88	2576.0	22005	218.6	7.00	83.20
883.10	973.1	9254	82.5	9.77	0.00
882.70	351.1	12481	41.5	4.52	20.11
882.88	2576.0	22005	218.6	7.00	83.20
883.10	973.1	9254	82.5	9.77	0.00
883.28	443.7	12963	58.1	40.74	59.79
883.28	1423.4	4298	228.8	16.00	9.00
883.50	545.5	10913	51.0	7.73	5.91
883.70	1028.1	19208	123.2	9.22	50.33
883.91	1680.3	40750	384.7	24.00	135.33
884.01	2649.0	89925	607.5	42.00	235.50
884.30	395.2	8948	25.3	5.22	28.15
884.51	7124.0	84525	1125.0	59.00	164.00
884.71	1433.6	12443	106.3	12.55	58.91
884.89	3908.0	168225	1186.0	120.00	0.00
885.08	173.6	9051	31.9	7.97	0.00
885.08	173.5	5351	33.9	5.94	4.06
885.26	650.3	33950	102.8	25.67	73.08
885.58	147.6	8507	57.4	1.57	0.00
885.58	348.6	18459	154.0	18.50	0.00
885.80	660.0	30775	425.7	35.33	149.67
885.97	1293.0	43106	307.8	25.50	217.75
886.18	254.9	11425	140.1	9.00	0.00
886.29	859.5	69225	675.0	44.00	0.00
888.36	2528.0	41325	1417.0	84.00	0.00
888.57	2501.0	134025	1425.0	91.00	0.00
888.75	834.3	5721	450.3	31.00	899.33
888.94	2970.0	172200	1283.0	156.00	0.00
889.16	1105.0	898500	447.7	34.33	2038.00
889.36	518.6	30075	118.5	19.36	27.00
889.61	513.9	16792	65.6	8.11	0.00
889.80	223.2	10894	76.0	7.13	0.00
889.80	244.0	11300	83.0	7.87	19.33
889.99	202.2	8420	38.2	6.79	0.00
890.20	1419.5	528000	637.0	44.50	688.50
890.40	237.0	7286	61.2	5.33	0.00
890.58	2834.0	5571	1268.0	81.00	0.00
890.79	2786.0	100050	1245.0	103.00	0.00
891.08	828.3	62950	424.7	34.67	0.00
891.30	2424.0	87675	428.7	43.00	0.00
891.49	5159.0	133950	1283.0	73.00	0.00
891.69	333.7	8816	32.7	7.18	0.00
891.69	310.0	7376	29.3	8.86	0.00
891.93	1.0	23827	9.4	3.16	58.46

Site 167 Minor Element Data (cont.)

Depth (mbsf)	Ba/Zr	W/Zr	Re/Zr	Au/Zr	Hg/Zr
892.11	4781.0	117525	1346.0	171.00	0.00
892.28	118.7	18868	52.3	13.58	28.73
892.50	2.2	1423	29.3	3.58	0.00
892.69	5.7	2943	27.0	4.14	0.00
898.22	197.2	13459	15.9	5.12	16.35
898.43	208.2	2637	19.8	4.67	32.92
898.62	188.1	3474107	20.3	5.48	3.88
898.82	438.4	1858	73.4	7.79	8678.57
899.01	9.3	25820	14.1	4.04	4.97
899.23	57.4	24492	16.8	3.85	61.13
899.23	59.0	11011	16.8	3.72	61.69
899.40	10.7	1613	14.9	5.13	22.10
899.61	24.4	1515	15.5	3.99	169.55
899.81	3.5	1918	12.6	3.63	2.55
900.02	19.5	1638	18.5	2.55	0.00
900.22	6.5	2481	15.2	4.44	3.33
900.42	32.1	5391	15.9	3.39	2.45
900.62	23.1	7617	19.6	3.60	2.94
900.79	9.1	15618	14.9	3.86	13.29
901.01	7.8	9964	13.9	4.32	30.36
908.17	823.8	8992	27.9	7.26	23.41
908.17	788.6	191550	31.7	5.17	17.24
908.37	515.6	11161	37.1	6.12	470.00
908.61	981.5	10557	34.4	5.69	33.08
908.81	783.2	8226	35.5	5.96	31.88
909.00	675.1	14053	10.3	5.52	29.64
909.22	1241.3	11601	53.6	7.56	79.69
909.40	1232.8	16645	34.5	5.92	44.68
909.60	1438.6	182400	61.3	5.00	68.64
909.80	9098.0	14638	951.0	45.00	924.00
910.03	1052.5	14381	72.9	3.25	35.42
910.21	999.2	15943	72.3	4.25	35.42
910.42	1082.9	102863	61.0	6.29	65.07
910.42	7500.0	836813	430.5	19.50	447.50
910.60	2627.5	0	223.8	20.25	2011.00
911.03	1029.3	2059875	58.5	7.07	25.47
911.21	12705.0	24429	430.5	58.00	4829.50
911.40	1947.1	1903393	122.9	11.43	77.57
911.59	1249.3	56250	61.1	5.00	4402.14
911.80	2615.0	172950	146.5	19.00	92.17
912.01	11740.0	11084	900.0	58.00	204.00
912.23	1015.7	14883	37.8	9.13	30.30
912.40	1312.5	170400	53.7	5.94	25.38
912.40	15640.0	220238	893.0	43.00	696.00
912.60	7415.0	491625	451.5	22.50	435.50
912.81	6840.0	127313	443.0	24.50	984.00

Site 167 Minor Element Data (cont.)

Depth (mbsf)	Ba/Zr	W/Zr	Re/Zr	Au/Zr	Hg/Zr
912.90	10000.0	55365	449.5	26.50	192.00
917.35	4366.0	100825	175.8	27.00	150.60
917.84	7933.3	1602750	293.3	36.67	299.33
918.35	0.0	154875	900.0	92.00	3966.00
918.83	5755.0	18607	471.0	30.00	416.00
919.36	1326.4	16409	82.6	4.00	50.73
919.36	1185.7	21708	62.9	5.00	17.36
919.84	804.4	42081	49.5	4.72	32.33
920.33	1286.8	98077	23.5	7.32	98.54
920.86	773.1	152550	33.6	4.12	257.31
921.35	5116.0	31777	945.0	23.00	233.00
921.85	1511.5	166725	68.2	4.31	60.23
922.34	844.0	1268750	44.2	4.20	371.45
922.83	1375.2	45398	157.3	5.67	2918.33
923.33	389.4	27007	28.8	5.31	92.97
925.10	659.4	24113	59.1	447.40	3276.00
925.21	620.8	25793	36.2	315.21	2505.00
925.31	935.3	24082	59.8	1451.33	3194.00
925.31	890.6	438667	52.4	246.41	2617.06
925.41	176.3	26946	298.3		36100.00
925.50	888.5	39631	67.2	253.85	3407.69
925.70	696.3	67267	55.4	333.75	3508.75
925.80	1940.0	23169	147.8	643.67	5000.00
925.90	507.6	28380	70.6	422.62	3144.62
926.10	746.2	34433	192.2	396.60	3006.00
926.30	542.3	21591	102.1	325.22	6438.89
926.71	464.0	29814	80.8	498.18	2886.36
926.80	1205.9	18110	130.0	431.57	2931.43
927.00	417.6	21859	30.8	295.86	1533.45
927.20	723.6	17371	41.5	508.18	4246.82
927.39	685.2	40863	44.1	256.14	2044.29
927.61	1978.8	27220	114.9	587.75	6213.75
927.80	1127.0	82150	91.5	620.10	4143.00
928.10	2995.0	397000	233.8	1041.75	5995.00
928.30	70.3	66950	234.8	599.00	34400.00
928.50	1620.8	20610	232.5	958.75	5695.00
928.50	663.5	22720	93.5	320.30	1665.00
928.71	807.7	24031	90.2	837.50	2260.00
928.90	853.8	19873	69.0	302.08	4119.23
929.10	812.0	23293	60.7	261.80	1407.33
929.10	928.6	22307	68.0	221.71	1537.86
929.10	895.7	21481	67.9	252.57	613.14
929.30	343.3	19813	17.2	286.54	1883.08
929.30	331.1	19816	19.7	261.09	1732.17
929.60	812.1	19047	49.5	275.37	2851.58
929.80	672.0	20664	60.3	321.13	1835.33

Site 167 Minor Element Data (cont.)

Depth (mbsf)	Ba/Zr	W/Zr	Re/Zr	Au/Zr	Hg/Zr
929.80	752.9	19546	63.5	218.50	2255.00
930.01	411.9	21143	23.8	219.68	2083.51
930.21	800.0	21264	130.7	293.14	123.00
930.40	389.1	22829	66.4	277.57	2475.00
930.60	628.4	22963	131.4	343.86	1942.86
930.80	863.6	18855	115.5	149.38	3046.25
935.70	550.0	17406	86.2	260.36	3480.91
935.91	555.7	16545	17.7	227.35	1584.69
936.10	324.4	23885	13.4	303.79	1877.27
936.30	600.1	17033	69.7	380.00	2886.15
936.61	420.8	15645	18.7	260.21	1718.33
936.61	414.3	15880	17.8	211.76	1622.55
936.61	420.9	24836	17.1	288.33	1191.11
936.79	770.7	20544	65.8	274.71	2765.00
937.00	673.8	0	111.7	306.89	3866.67
937.40	534.9	22609	21.1	236.05	1290.70
937.60	407.7	48569	27.3	342.29	2112.86
937.80	1506.9	19773	68.8	666.08	7090.00
938.10	615.0	54350	41.2	192.09	2549.09
938.30	1488.8	18912	151.8	326.00	1966.67
938.50	563.8	24869	25.9	298.53	1748.82
938.71	640.7	24009	69.4	502.15	2047.69
938.71	650.8	16516	80.5	305.73	2836.36
938.89	418.4	22483	29.4	253.35	1136.77
939.11	648.8	30150	76.4	301.83	3403.33
939.30	1365.2	20943	150.7	371.67	7115.00
939.59	1418.3	20317	129.7	384.86	1507.14
939.80	312.8	18445	39.1	305.09	2015.22
940.01	596.1	18178	83.4	420.09	1650.91
940.19	853.0	0	103.6	210.67	313.56
940.60	964.7	18142	320.0	321.67	5126.67
940.79	534.5	23522	28.4	260.32	1977.74
940.90	511.9	0	23.5	358.92	2424.05

Site 167 Minor Element Data (cont.)

Depth (mbsf)	Tl X/Zr	Pb/Zr	Bi/Zr	Th/Zr	U/Zr
870.29	5514	20.53	689.3	20208	920.0
870.29	5160	20.29	671.6	20109	932.1
870.48	5050	14.50	0.0	38155	1700.0
870.64	5774	18.82	513.0	21664	917.5
870.82	5773	24.52	650.1	18639	818.7
870.99	5408	19.10	647.2	16700	1264.3
871.21	9920	15.44	0.0	19687	2192.2
871.50	8373	17.73	0.0	18824	1656.4
871.50	5560	10.73	0.0	22640	1171.3
871.71	4829	5.96	0.0	22275	1095.4
871.91	6302	18.55	753.0	20905	1419.1
872.10	5125	17.17	457.0	23213	1681.3
872.31	5647	19.00	773.6	19980	1211.6
872.52	5899	16.82	753.1	20827	1196.2
872.52	5675	16.86	769.0	20382	1242.4
872.70	5602	17.44	780.5	20567	1267.3
873.00	5540	18.43	862.0	20160	1260.7
873.22	19488	57.00	880.8	37026	4772.0
873.42	5555	13.91	608.0	21547	1320.9
873.60	5692	10.73	0.0	28540	1270.7
873.79	5014	12.93	182.6	26293	1100.7
874.00	6642	34.13	1344.0	23487	1381.3
874.20	1818	10.03	574.3	31484	556.2
874.40	4915	15.43	691.8	26921	1294.5
874.60	4003	9.45	531.8	21722	947.1
874.80	6033	13.74	890.5	27805	1258.4
875.00	12816	24.80	1128.0	13965	2886.0
875.21	5291	10.45	385.1	27095	1280.0
875.40	6816	17.85	654.6	8498	1473.5
875.60	5692	14.61	550.4	27483	1205.2
875.81	5885	5.42	317.1	27600	1241.1
875.90	1867	17.96	644.7	31655	1280.4
879.88	19980	31.78	1161.3	24617	4113.3
879.88	5373	5.79	492.0	24428	1204.4
880.08	72555	111.50	4542.0	4673	12265.0
880.28	5832	3.07	327.2	25190	1158.7
880.50	9393	8.20	961.2	16800	2211.0
880.71	50010	79.00	2916.0	0	10480.0
880.89	5172	13.00	419.2	25730	1212.7
881.11	28538	50.25	2433.0	7035	7647.5
881.28	19905	152.50	2238.0	5010	4285.0
881.50	1822	88.50	595.9	31841	5860.0
881.69	35880	26.00	960.0	0	8113.0
881.87	25170	40.00	0.0	0	5939.0
882.11	38460	200.50	3156.0	1545	12530.0
882.28	12758	20.25	498.0	5453	2897.5

Site 167 Minor Element Data (cont.)

Depth (mbsf)	Tl X/Zr	Pb/Zr	Bi/Zr	Th/Zr	U/Zr
882.50	5926	10.09	279.3	9012	1349.1
882.70	3601	10.41	251.1	20717	1136.7
882.88	9180	27.80	362.4	2211	2940.0
883.10	4272	9.62	104.3	27900	1277.7
882.70	3601	10.41	251.1	20717	1136.7
882.88	9180	27.80	362.4	2211	2940.0
883.10	4272	9.62	104.3	27900	1277.7
883.28	4179	9.89	279.2	26439	1484.7
883.28	1464	34.60	458.3	26113	5760.0
883.50	4330	10.41	294.0	13023	1314.1
883.70	8063	17.89	321.3	8258	2882.2
883.91	19610	42.67	736.0	18405	6130.0
884.01	38025	83.00	1116.0	3098	13090.0
884.30	3935	8.20	243.9	14592	1315.9
884.51	45870	94.00	360.0	24345	11660.0
884.71	5995	12.00	162.5	8028	1547.3
884.89	78720	198.00	2340.0		28540.0
885.08	3994	7.29	191.7	27426	1189.7
885.08	1762	6.86	528.8	31029	1313.1
885.26	12078	31.67	1401.0	7926	4177.5
885.58	4416	7.10	262.3	24264	960.5
885.58	9664	16.13	466.5	10418	2650.0
885.80	15830	27.00	572.0	13995	4053.3
885.97	22583	39.25	1275.0	9131	6652.5
886.18	6773	11.00	236.0	6358	1782.2
886.29	29580	50.50	798.0	6525	8870.0
888.36	24240	48.00	0.0	0	6723.0
888.57	56250	120.00	444.0	0	18080.0
888.75	1874	50.67	584.6	31216	7050.0
888.94	81060	148.00	3240.0	0	22200.0
889.16	17310	25.00	48.0	21355	2891.0
889.36	13293	24.36	1081.1	6282	4563.6
889.61	9246	17.26	672.0	4989	2030.5
889.80	5256	10.25	318.0	23822	1226.3
889.80	5806	11.13	347.2	12670	1558.0
889.99	4028	8.09	229.8	16518	1356.7
890.20	36315	59.50	1422.0	15263	8325.0
890.40	5490	7.38	198.9	23129	1561.4
890.58	1734	140.00	544.1	30538	23320.0
890.79	67920	93.00	936.0	11070	18420.0
891.08	34500	50.00	1268.0	7795	9116.7
891.30	38810	43.33	1764.0	9505	9710.0
891.49	83880	74.00	756.0	4140	21340.0
891.69	6318	4.13	295.6	22950	1397.4
891.69	5530	3.80	289.9	23414	1270.5
891.93	1771	11.93	28.1	1685	4115.8

Site 167 Minor Element Data (cont.)

Depth (mbsf)	Tl X/Zr	Pb/Zr	Bi/Zr	Th/Zr	U/Zr
892.11	83490	54.00	2760.0	2880	23840.0
892.28	4047	4.62	300.5	8804	1088.8
892.50	1252	4.47	8.3	1574	191.5
892.69	2256	4.00	221.3	49368	230.4
898.22	2044	2.35	99.2	3139	787.9
898.43	2140	2.29	472.3	3272	640.4
898.62	2681	3.02	0.0	8764	695.2
898.82	1139	7.79	475.3	1399	20314.3
899.01	1281	3.10	162.9	1739	1203.7
899.23	1193	2.02	78.1	1703	230.0
899.23	945	1.87	0.0	1385	211.8
899.40	1107	1.51	0.0	1458	198.0
899.61	1199	1.24	0.0	1226	249.6
899.81	1405	1.42	0.0	1546	322.9
900.02	1207	1.20	0.0	1415	245.5
900.22	1124	1.30	78.9	1494	237.1
900.42	1461	1.53	0.0	1582	313.4
900.62	1206	0.94	0.0	1266	269.6
900.79	988	0.93	0.0	1180	238.7
901.01	5053	0.70	17.3	8082	207.3
908.17	5014	9.68	0.0	8069	1489.4
908.17	4420	9.24	0.0	9192	1604.1
908.37	5848	4.80	0.0	9362	2376.0
908.61	4796	6.00	0.0	9100	2000.8
908.81	8918	7.16	616.4	7363	1855.2
909.00	4905	56.81	0.0	10538	2879.8
909.22	5465	7.00	0.0	9200	2906.9
909.40	5638	3.96	0.0	10893	2046.8
909.60	63960	9.79	0.0	55720	3054.3
909.80	5515	75.00	0.0	11500	29920.0
910.03	5360	6.33	0.0	11392	2183.3
910.21	4980	6.58	0.0	10236	2051.7
910.42	34350	6.79	0.0	31365	1997.1
910.42	22643	44.00	0.0	16873	14165.0
910.60	0	24.25	0.0	0	8412.5
911.03	55455	7.60	0.0	30500	2564.0
911.21	10667	121.50	0.0	13493	17735.0
911.40	6431	26.71	0.0	6356	3907.1
911.59	21450	13.36	0.0	11028	2455.7
911.80	67890	25.33	0.0	54830	8475.0
912.01	4263	108.00	0.0	8809	23320.0
912.23	5698	7.00	0.0	9256	1774.3
912.40	79170	7.88	0.0	58640	1508.8
912.40	38145	109.00	0.0	31135	22580.0
912.60	39705	68.00	0.0	31460	13310.0
912.81	54210	53.50	0.0	33145	13555.0

Site 167 Minor Element Data (cont.)

Depth (mbsf)	Tl X/Zr	Pb/Zr	Bi/Zr	Th/Zr	U/Zr
912.90	19422	52.50	0.0	15206	16185.0
917.35	44370	26.00	0.0	19457	6818.0
917.84	88620	54.00	0.0	56340	12876.7
918.35	39285	143.00	0.0	32800	33490.0
918.83	5755	110.00	0.0	10836	18035.0
919.36	5331	6.18	0.0	10507	1722.7
919.36	5400	5.93	0.0	9722	1780.0
919.84	5218	5.89	84.3	8470	2463.3
920.33	4236	5.59	0.0	8408	1964.3
920.86	47400	29.46	0.0	61630	1795.8
921.35	7555	75.00	0.0	7085	17730.0
921.85	4692	11.31	0.0	4482	3106.2
922.34	12020	10.35	0.0	10685	1777.5
922.83	3601	28.83	0.0	8741	3905.0
923.33	3049	4.75	518.4	10153	1968.4
925.10	2776	7.93	1482.5	10600	1913.3
925.21	3403	6.75	644.2	10460	1986.7
925.31	3205	7.33	516.8	9394	1992.0
925.31	3837	5.35	816.7	15863	1832.4
925.41	3059	49.33	555.6	10415	6236.7
925.50	2584	12.00	477.5	6161	2033.8
925.70	6980	6.19	1060.3	3778	2060.6
925.80	2199	16.00	400.1	10346	5596.7
925.90	4052	6.69	550.2	13584	1999.2
926.10	2337	14.80	439.7	11933	2700.0
926.30	2715	5.56	359.0	10000	4150.0
926.71	3389	7.27	396.9	12676	2067.3
926.80	1805	9.71	226.9	10810	2395.7
927.00	2817	5.14	401.7	10636	2139.3
927.20	2435	34.23	477.1	11019	2220.5
927.39	5656	69.86	1030.0	4068	3042.4
927.61	3490	63.50	610.0	11040	3930.0
927.80	11178	8.20	1507.0	4380	2122.0
928.10	2935	90.00	574.0	12165	7625.0
928.30	8953	18.25	0.0	9415	22862.5
928.50	2961	22.50	869.4	11160	6260.0
928.50	3674	5.50	331.0	11540	2243.0
928.71	3565	26.90	425.0	11923	2473.0
928.90	3066	6.31	269.9	10273	2396.9
929.10	3504	5.60	370.5	8736	2082.7
929.10	3199	8.00	298.4	9843	2469.3
929.10	2673	5.57	345.4	11540	2309.3
929.30	2541	14.35	305.0	10741	2103.8
929.30	2707	12.48	418.6	10042	2159.3
929.60	3197	5.00	369.0	10200	2463.2
929.80	3609	12.27	296.1	10964	1936.7

Site 167 Minor Element Data (cont.)

Depth (mbsf)	Tl X/Zr	Pb/Zr	Bi/Zr	Th/Zr	U/Zr
929.80	2613	10.29	316.2	10381	2335.7
930.01	4150	5.46	310.3	12046	2246.5
930.21	3269	6.86	296.6	11821	2607.1
930.40	4651	17.79	277.6	11497	4922.9
930.60	3544	7.57	388.8	12105	2702.9
930.80	3231	12.75	359.0	11436	2970.0
935.70	2302	10.82	355.5	10841	2356.4
935.91	1897	13.08	276.5	10261	2306.1
936.10	2807	5.56	351.1	11300	2177.3
936.30	2070	9.15	313.1	10156	3206.2
936.61	1967	9.17	280.4	9812	2118.8
936.61	2061	7.63	280.6	10048	2076.5
936.61	4544	8.04	512.4	7407	2229.6
936.79	4511	61.64	285.8	10166	3315.7
937.00	0	10.44			2441.1
937.40	2889	8.23	447.1	11526	2259.5
937.60	7257	20.34	902.3	7977	2419.4
937.80	2812	18.85	496.8	9718	5704.6
938.10	7453	7.95	915.8	13290	2175.9
938.30	2728	25.17	452.9	10821	6323.3
938.50	3432	18.65	443.8	10662	2220.6
938.71	3696	7.15	353.5	10555	2074.6
938.71	2031	8.64	292.0	10268	2255.5
938.89	3346	8.90	394.2	10775	2030.3
939.11	5018	10.00	492.8	13573	3105.0
939.30	6400	23.00	484.3	11753	3166.7
939.59	3328	15.57	302.6	10517	2601.4
939.80	3435	7.74	369.5	11209	3001.7
940.01	3848	11.55	337.4	10734	2290.0
940.19	0	17.89	0.0	0	2236.7
940.60	2678	132.67	446.8	9800	3169.7
940.79	2878	9.16	467.8	10132	1851.3
940.90	0	11.16	0.0	0	2349.2

Site 167 Minor Element Figures

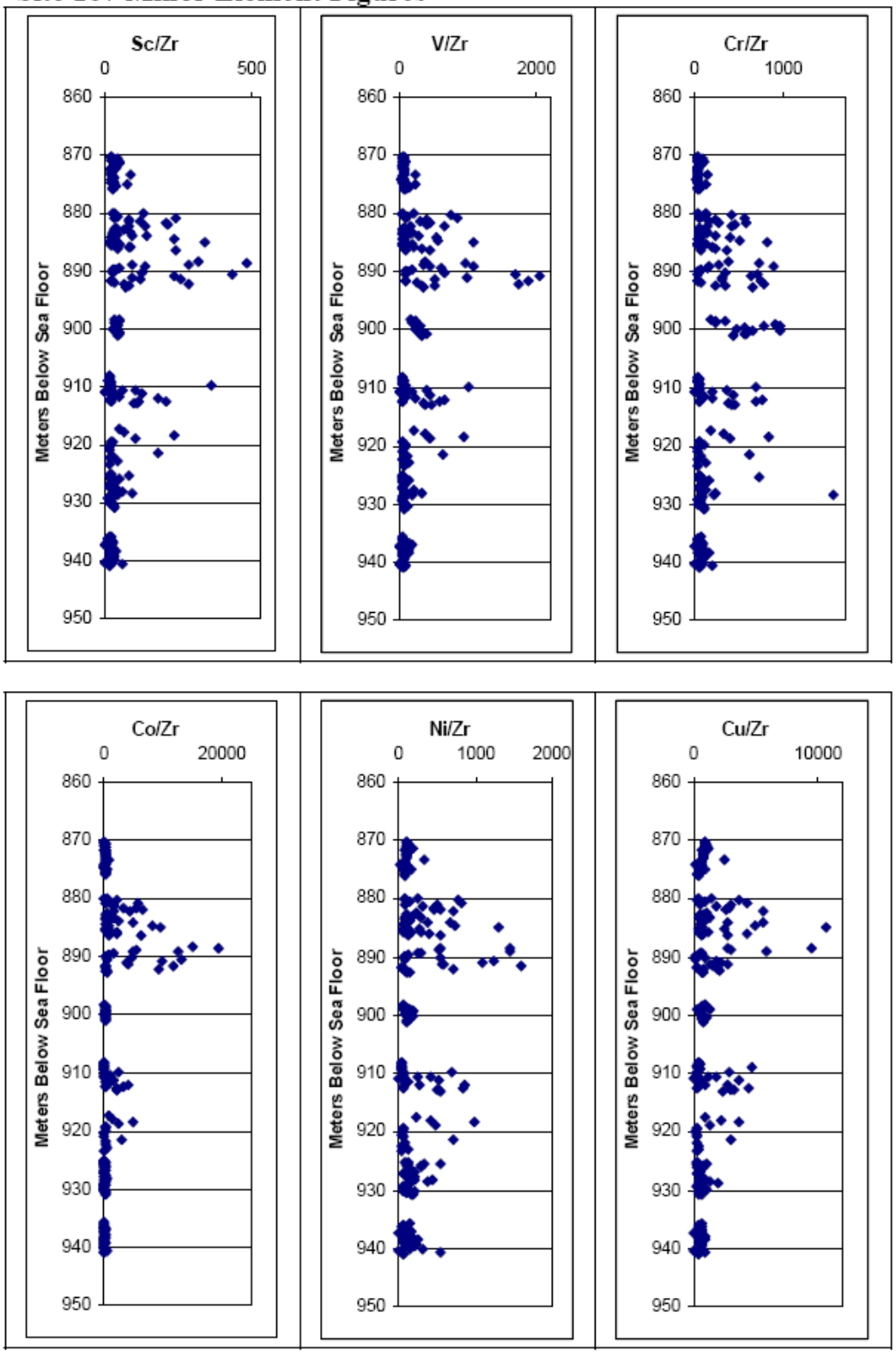

Site 167 Minor Element Figures

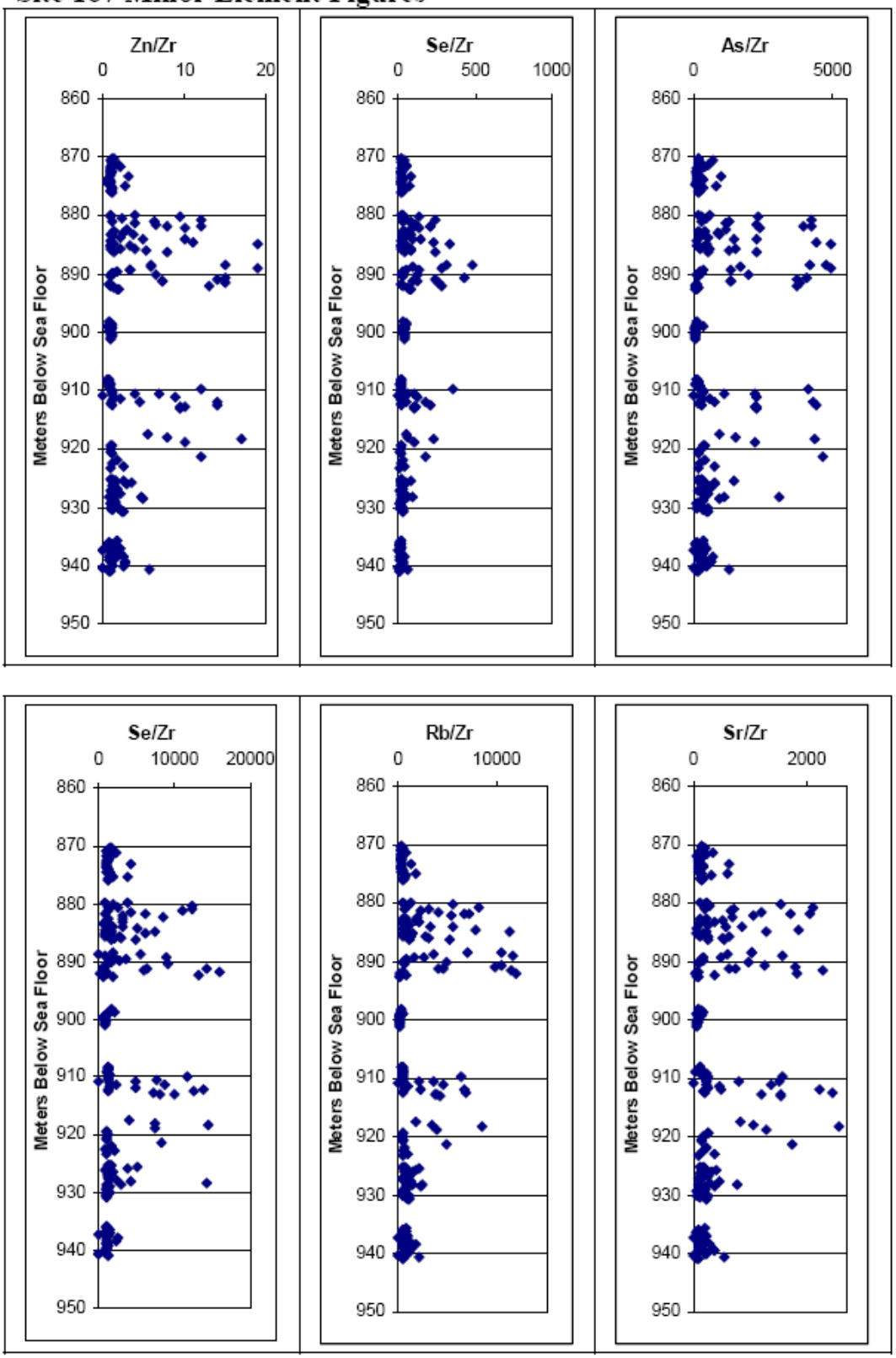

Site 167 Minor Element Figures

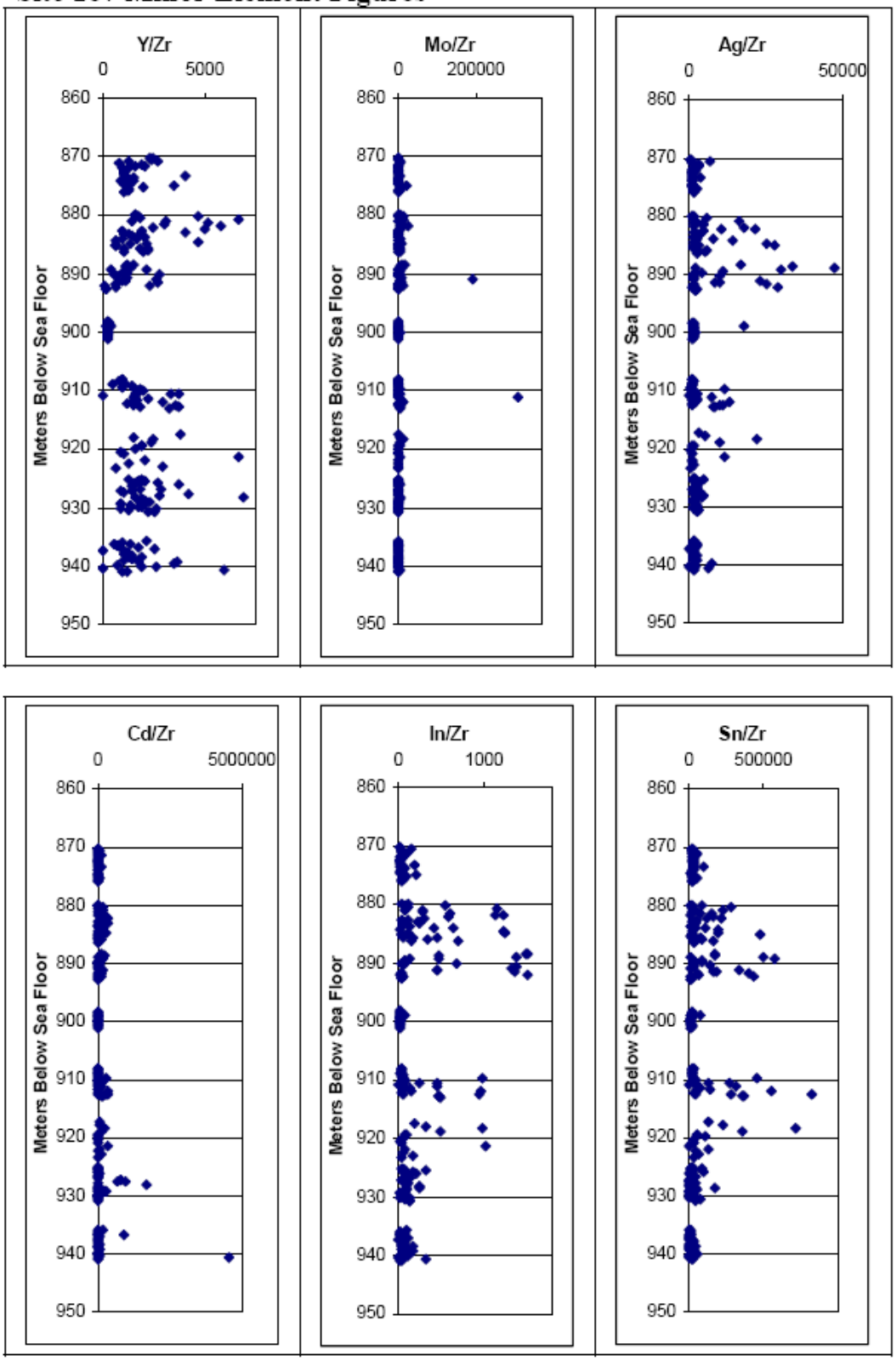

Site 167 Minor Element Figures

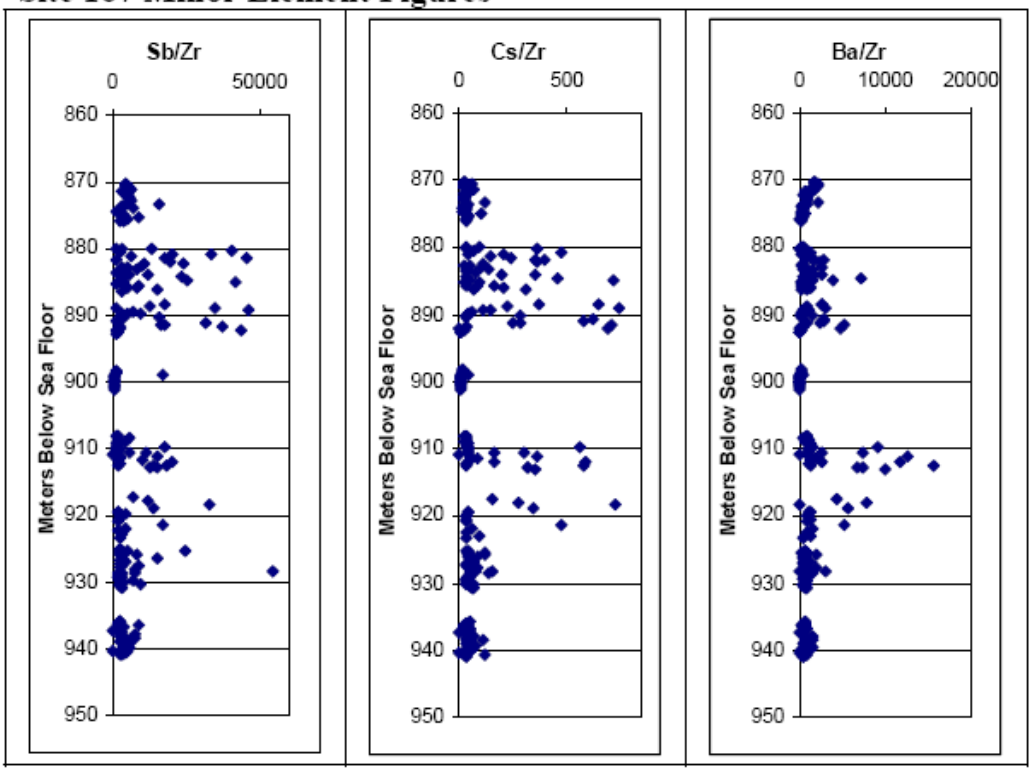

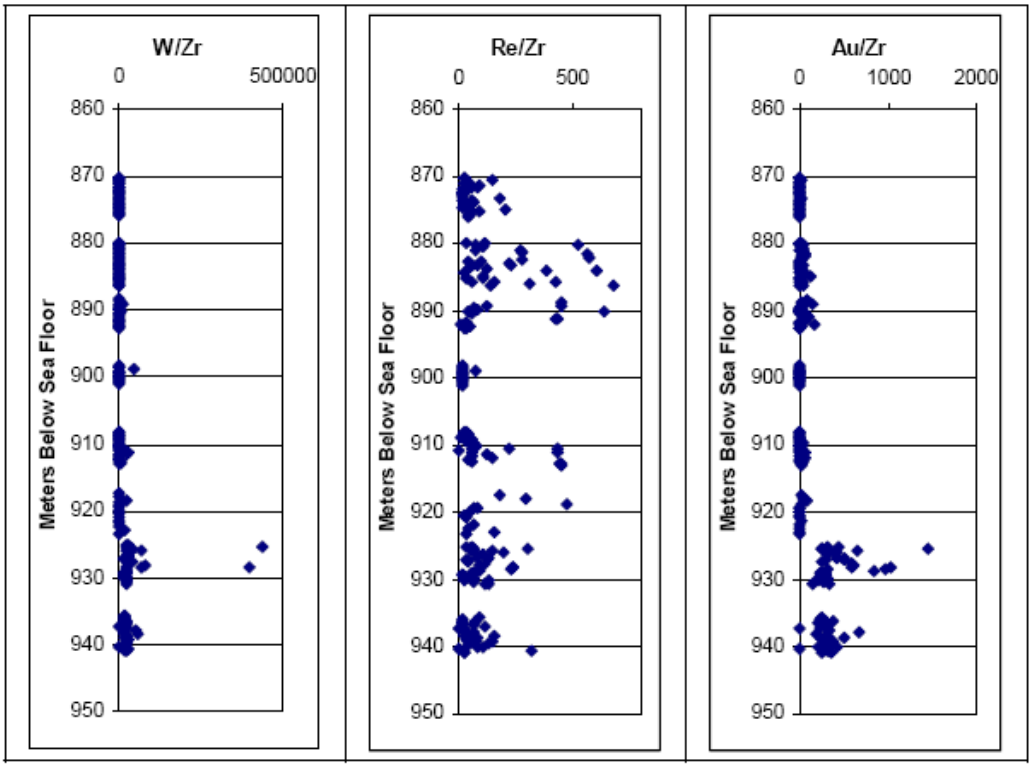

Site 167 Minor Element Figures

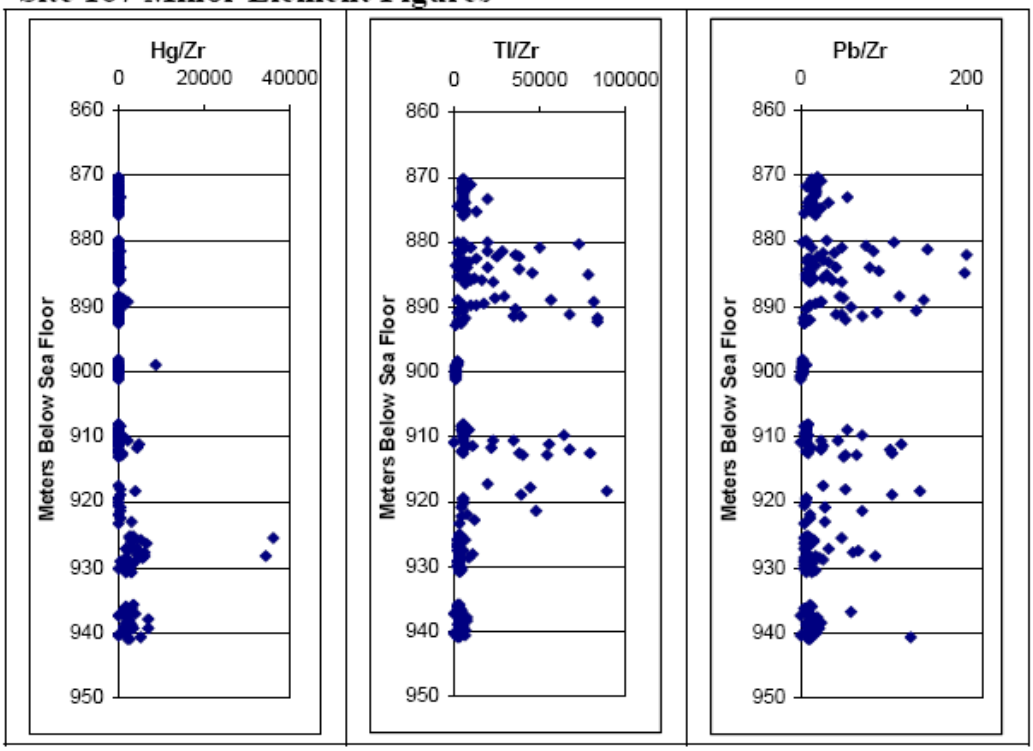

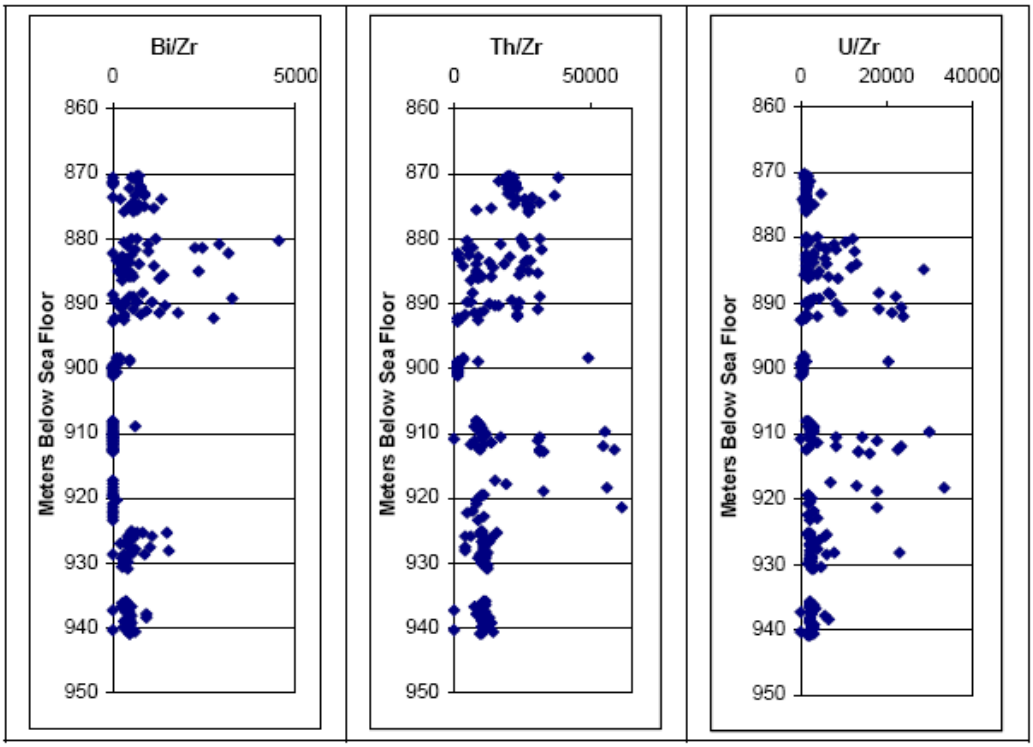

Site 167 Major Element Data

Depth (mbsf)	Ba/Al	Ca/Al	Fe/Al	K/Al	Mg/Al
870.29	0.61	19.03	4.54	1.25	4.07
870.29	0.66	19.80	4.61	1.33	4.42
870.48	0.52	76.48	4.71	0.00	7.83
870.64	0.55	22.07	4.70	1.16	4.45
870.82	0.82	32.72	5.05	0.86	5.10
870.99	0.63	10.72	4.82	0.85	4.27
871.21	0.29	28.89	3.69	0.74	5.09
871.50	0.26	24.02	3.27	0.52	4.13
871.50	0.31	29.18	4.06	0.53	5.19
871.71	0.23	17.50	3.80	1.00	4.22
871.91	0.35	5.90	4.00	1.40	3.65
872.10	0.18	9.35	3.70	0.83	3.98
872.31	0.31	10.61	3.63	1.50	3.60
872.52	0.28	11.86	3.28	1.31	3.35
872.52	0.31	12.31	3.59	1.59	3.53
872.70	0.32	10.73	3.69	1.48	3.61
873.00	0.30	9.85	3.55	1.70	3.39
873.22	0.21	34.01	3.60	0.71	4.70
873.42	0.28	14.55	3.00	1.56	3.34
873.60	0.11	42.97	3.47	0.51	5.02
873.79	0.05	44.49	3.65	0.29	5.09
874.00	0.17	18.21	3.30	1.35	3.81
874.20	0.17	12.00	2.50	0.16	3.36
874.40	0.14	15.68	3.06	1.53	3.55
874.60	0.29	10.91	3.11	1.69	3.25
874.80	0.27	38.50	3.56	0.88	4.47
875.00	0.28	51.67	3.57	0.33	5.33
875.21	0.18	63.21	3.55	0.30	5.25
875.40	0.31	26.91	3.32	1.07	4.48
875.60	0.21	27.16	3.39	0.99	4.48
875.81	0.11	42.61	3.30	1.00	4.54
875.90	0.20	32.40	3.27	1.30	4.30
879.88	0.30	23.69	5.92	2.12	5.27
879.88	0.19	25.81	3.54	1.44	4.09
880.08	0.08	43.42	3.56	1.06	4.57
880.28	0.11	55.72	3.28	0.59	4.74
880.50	0.13	42.76	3.85	0.90	4.77
880.71	0.13	45.50	3.78	0.11	5.49
880.89	0.17	53.70	3.66	0.66	4.91
881.11	0.17	32.20	3.70	1.22	4.30
881.28	0.27	52.31	3.91	0.51	5.09
881.50	0.27	67.53	4.12	0.00	6.05
881.69	0.24	78.61	4.10	0.00	6.75
881.87	0.41	80.52	4.26	0.00	7.70
882.11	0.27	33.11	3.67	1.01	5.16
882.28	0.22	85.61	3.97	0.00	6.37

Site 167 Major Element Data (cont.)

Depth (mbsf)	Ba/Al	Ca/Al	Fe/Al	K/Al	Mg/Al
882.50	0.25	60.05	3.54	0.45	5.54
882.70	0.28	23.29	3.75	1.14	4.22
882.88	0.89	62.70	3.55	0.37	5.49
883.10	0.82	60.86	3.46	0.53	5.44
883.28	0.32	23.05	2.57	0.65	3.37
883.28	0.39	25.30	3.45	0.86	4.48
883.50	0.51	36.29	3.60	1.19	4.72
883.70	0.47	38.13	3.40	0.99	4.87
883.91	0.36	44.57	3.79	0.68	5.65
884.01	0.40	32.82	4.77	1.35	6.56
884.30	0.37	13.81	3.04	1.73	3.65
884.51	0.74	72.27	4.55	0.00	7.19
884.71	0.99	56.52	3.71	0.61	5.24
884.89	0.33	24.40	5.02	1.45	6.94
885.08	0.17	18.69	2.78	1.33	3.65
885.08	0.18	19.57	3.12	1.54	4.00
885.26	0.21	13.38	3.87	1.65	3.99
885.58	0.13	33.48	2.53	0.65	3.52
885.58	0.17	38.44	3.63	0.89	5.02
885.80	0.21	65.06	4.01	0.03	6.29
885.97	0.24	26.50	3.61	1.24	4.76
886.18	0.17	52.32	3.46	0.62	5.11
886.29	0.23	21.53	6.31	1.22	8.39
888.36	0.51	49.36	5.60	0.00	9.94
888.57	0.29	20.45	5.78	1.17	7.92
888.75	0.18	30.81	4.10	1.09	5.48
888.94	0.23	28.74	4.76	1.31	6.06
889.16	0.49	52.11	5.76	1.36	8.07
889.36	0.17	11.22	3.39	2.42	3.56
889.61	0.31	24.34	3.93	2.32	3.91
889.80	0.17	32.92	3.01	1.36	3.65
889.80	0.21	42.03	3.93	1.90	4.69
889.99	0.19	18.40	3.42	2.19	3.92
890.20	0.23	47.99	4.41	1.66	5.51
890.40	0.23	21.23	3.47	1.82	3.98
890.58	0.33	26.11	7.26	2.64	7.22
890.79	0.25	43.87	4.66	1.76	6.05
891.08	0.16	31.65	4.52	2.23	5.10
891.30	0.37	21.97	6.24	2.60	5.41
891.49	0.33	34.56	5.67	2.14	5.65
891.69	0.33	16.02	4.23	2.88	3.80
891.69	0.33	16.45	4.42	2.92	3.97
891.93	0.02	1.44	4.34	1.19	2.18
892.11	0.35	36.39	1.37	2.59	0.57
892.28	0.25	29.47	4.28	2.63	1.97
892.50	0.02	26.01	6.19	2.11	5.66

Site 167 Major Element Data (cont.)

Depth (mbsf)	Ba/Al	Ca/Al	Fe/Al	K/Al	Mg/Al
892.69	0.03	27.62	5.92	2.65	5.89
898.22	0.65	14.50	5.97	2.09	2.75
898.43	0.56	16.50	5.02	1.52	2.77
898.62	0.17	3.01	0.99	1.75	0.64
898.82	0.53	4.06	1.11	1.53	0.42
899.01	0.09	20.89	5.69	0.98	5.08
899.23	0.31	18.76	5.33	0.85	5.83
899.23	0.35	18.67	5.75	0.95	5.90
899.40	0.09	24.23	5.31	0.64	5.15
899.61	0.17	34.06	4.98	0.63	5.24
899.81	0.05	24.13	4.70	0.70	3.80
900.02	0.03	5.76	1.59	0.20	1.26
900.22	0.07	21.34	6.04	0.70	6.12
900.42	0.22	28.18	6.19	0.95	5.79
900.62	0.15	22.78	7.26	1.12	6.81
900.79	0.07	20.39	5.41	1.26	4.91
901.01	0.07	21.05	6.01	1.18	5.43
908.17	0.25	17.93	2.86	2.19	3.36
908.17	0.27	19.15	3.39	2.51	4.06
908.37	0.16	16.34	3.44	2.25	4.03
908.61	0.29	22.79	3.19	2.42	3.92
908.81	0.25	24.35	3.40	2.33	4.03
909.00	0.22	0.27	3.41	2.76	3.52
909.22	0.35	39.53	3.23	1.90	4.43
909.40	0.36	23.92	3.36	2.29	4.04
909.60	0.40	45.08	3.56	1.80	4.69
909.80	0.36	25.84	5.88	2.18	7.67
910.03	0.30	52.24	3.53	1.54	5.27
910.21	0.28	51.60	3.59	1.58	5.17
910.42	0.25	33.42	2.68	1.36	3.54
910.42	0.35	42.55	3.93	1.89	5.12
910.60	0.20	38.66	3.68	1.98	4.66
910.80	0.46	52.29	4.52	1.35	6.36
911.03	0.26	33.70	3.53	2.10	4.42
911.21	0.55	24.29	5.12	2.70	5.84
911.40	0.30	47.29	3.67	1.74	5.02
911.59	0.30	39.49	3.24	1.91	4.43
911.80	0.19	19.96	3.53	2.38	4.11
912.01	0.30	42.93	4.15	1.76	5.70
912.23	0.29	33.72	3.47	2.21	4.20
912.40	0.29	34.40	2.81	1.30	3.53
912.40	0.45	38.46	4.72	1.97	5.95
912.60	0.38	31.94	4.69	2.21	5.89
912.81	0.29	41.53	3.92	1.95	5.23
912.90	0.36	32.74	3.85	2.10	4.90
917.35	0.34	38.52	3.76	2.04	4.59

Site 167 Major Element Data (cont.)

Depth (mbsf)	Ba/Al	Ca/Al	Fe/Al	K/Al	Mg/Al
917.84	0.36	26.47	3.91	2.37	4.81
918.35	0.46	26.87	4.07	2.29	5.42
918.83	0.25	34.98	3.54	2.00	5.09
919.36	0.27	37.92	2.49	0.80	3.70
919.36	0.39	57.82	3.51	1.61	5.01
919.84	0.25	31.76	3.96	1.78	4.62
920.33	0.39	20.66	3.36	2.48	3.78
920.86	0.25	33.01	3.60	2.50	4.31
921.35	0.17	70.81	3.63	1.45	6.30
921.85	0.27	36.50	2.90	2.17	4.43
922.34	0.29	40.39	3.40	2.02	4.65
922.83	0.19	57.74	3.24	1.67	5.42
923.33	0.13	22.69	3.18	2.37	4.13
925.10	0.18	38.08	3.62	1.91	4.85
925.21	0.18	20.18	3.80	2.24	4.12
925.31	0.22	30.69	3.45	1.66	4.27
925.31	0.26	35.60	3.92	2.01	4.78
925.41	0.03	11.42	3.11	0.44	3.63
925.50	0.23	38.70	4.07	1.88	4.96
925.70	0.19	34.58	3.50	1.97	4.59
925.80	0.18	31.00	3.63	2.06	4.66
925.90	0.14	41.62	3.60	1.74	5.14
926.10	0.13	87.87	3.67	1.05	6.90
926.30	0.11	14.23	3.38	1.20	4.37
926.71	0.12	45.70	3.61	1.61	5.30
926.80	0.23	61.46	3.59	1.31	5.89
927.00	0.12	12.04	3.56	2.21	3.95
927.20	0.20	29.12	3.44	2.21	4.21
927.39	0.18	15.58	3.09	1.89	3.89
927.61	0.28	48.65	3.60	1.93	4.73
927.80	0.27	53.69	4.06	1.60	5.39
928.10	0.23	50.24	4.19	1.95	5.15
928.30	0.01	0.76	2.05	0.00	2.15
928.50	0.18	35.96	4.19	2.01	5.96
928.50	0.16	46.31	3.52	1.58	5.41
928.71	0.19	47.80	3.28	1.49	5.24
928.90	0.20	44.43	3.45	1.93	4.86
929.10	0.22	49.56	3.49	1.86	5.13
929.10	0.10	12.18	3.00	2.46	3.47
929.10	0.10	12.12	3.22	2.57	3.62
929.80	0.17	37.86	3.13	1.39	4.45
929.80	0.19	41.47	3.46	1.82	4.97
930.01	0.12	11.36	3.46	2.42	3.84
930.21	0.16	67.81	3.73	1.24	6.13
930.40	0.10	26.55	3.85	1.80	4.75
930.60	0.13	60.51	3.72	1.18	5.92

Site 167 Major Element Data (cont.)

Depth (mbsf)	Ba/Al	Ca/Al	Fe/Al	K/Al	Mg/Al
930.80	0.19	50.27	3.47	1.21	5.54
935.91	0.17	13.08	3.22	2.64	3.61
936.10	0.10	8.08	3.33	2.78	3.53
936.30	0.14	20.74	3.31	1.55	4.32
936.61	0.13	12.83	2.94	2.54	3.53
936.61	0.13	12.84	3.16	2.53	3.57
936.79	0.15	31.98	3.34	2.05	4.31
937.20	0.21	37.30	3.38	1.88	4.63
937.40	0.16	16.13	3.15	2.49	3.73
937.40	0.16	16.02	3.15	2.58	3.67
937.60	0.12	15.75	3.11	2.39	3.71
937.80	0.36	18.73	6.64	4.78	5.15
938.10	0.18	29.92	3.83	2.27	4.50
938.30	0.24	40.04	5.43	2.83	7.06
938.71	0.14	24.88	3.07	1.10	4.06
938.71	0.17	28.85	3.96	1.41	5.23
938.89	0.12	21.99	3.42	2.40	4.11
939.30	0.25	72.30	3.94	1.07	6.34
939.59	0.28	68.35	4.44	1.31	6.16
939.80	0.09	10.80	3.36	1.96	3.92
940.01	0.14	50.45	3.86	1.70	5.37
940.19	0.20	72.59	3.83	1.34	6.14
940.19	0.20	74.26	3.74	1.48	6.02
940.41	0.33	59.57	6.85	2.12	10.78
940.60	0.14	116.76	4.37	0.30	8.02
940.79	0.17	18.16	3.49	2.39	4.00
940.90	0.15	6.66	3.60	2.77	3.36
929.60	0.22	22.23	3.52	1.93	4.31
929.60	0.22	23.02	3.39	2.20	4.04
935.70	0.14	60.74	3.81	1.64	5.59
935.70	0.14	62.26	3.87	1.80	5.52
935.70	0.14	62.12	3.78	1.80	5.50

Site 167 Major Element Data (cont.)

Depth (mbsf)	Mn/Al	Na/Al	P/Al	Ti/Al
870.29	0.19	1.40	0.63	0.39
870.29	0.21	1.54	0.34	0.45
870.48	0.31	1.96	0.22	0.59
870.64	0.23	1.63	0.44	0.46
870.82	0.26	1.58	0.31	0.47
870.99	0.28	2.40	0.18	0.48
871.21	0.09	1.95	0.11	0.46
871.50	0.07	1.85	0.07	0.40
871.50	0.09	2.34	0.22	0.51
871.71	0.06	2.10	0.18	0.45
871.91	0.16	1.58	0.19	0.45
872.10	0.15	2.00	0.31	0.46
872.31	0.19	1.73	0.16	0.40
872.52	0.17	1.60	0.16	0.35
872.52	0.20	1.83	0.16	0.39
872.70	0.19	1.71	0.18	0.41
873.00	0.19	1.62	0.16	0.39
873.22	0.17	1.82	0.26	0.47
873.42	0.13	1.68	0.23	0.38
873.60	0.11	1.83	0.26	0.48
873.79	0.12	1.87	0.17	0.51
874.00	0.15	1.76	0.11	0.41
874.20	0.05	0.84	0.02	0.25
874.40	0.11	1.63	0.15	0.39
874.60	0.10	1.65	0.19	0.38
874.80	0.15	2.13	0.16	0.48
875.00	0.15	1.84	0.23	0.50
875.21	0.16	1.76	0.17	0.50
875.40	0.16	1.66	0.01	0.44
875.60	0.13	1.49	0.24	0.44
875.81	0.08	1.64	0.15	0.44
875.90	0.11	1.60	0.19	0.42
879.88	0.08	2.31	0.48	0.81
879.88	0.05	1.56	0.26	0.44
880.08	0.11	1.73	0.21	0.46
880.28	0.07	1.61	0.15	0.43
880.50	0.06	1.87	0.19	0.49
880.71	0.11	2.15	0.13	0.55
880.89	0.12	1.69	0.18	0.47
881.11	0.07	1.56	0.13	0.45
881.28	0.15	2.15	0.07	0.50
881.50	0.14	2.25	0.18	0.58
881.69	0.12	2.52	0.37	0.61
881.87	0.17	1.82	0.50	0.66
882.11	0.09	1.71	0.29	0.49
882.28	0.12	2.70	0.46	0.56

Site 167 Major Element Data (cont.)

Depth (mbsf)	Mn/Al	Na/Al	P/Al	Ti/Al
882.50	0.09	1.95	0.34	0.50
882.70	0.05	1.64	0.13	0.45
882.88	0.10	1.69	0.37	0.50
883.10	0.11	1.64	0.34	0.48
883.28	0.04	1.63	0.05	0.34
883.28	0.06	2.21	0.07	0.49
883.50	0.07	1.51	0.30	0.47
883.70	0.07	1.63	0.19	0.47
883.91	0.10	1.64	0.29	0.54
884.01	0.11	2.07	0.29	0.70
884.30	0.03	1.31	0.15	0.41
884.51	0.19	2.04	0.55	0.65
884.71	0.11	1.57	0.29	0.51
884.89	0.11	2.37	0.27	0.77
885.08	0.04	1.11	0.12	0.37
885.08	0.04	1.26	0.15	0.42
885.26	0.04	1.39	0.09	0.50
885.58	0.06	1.09	0.12	0.33
885.58	0.08	1.54	0.17	0.50
885.80	0.14	1.85	0.30	0.58
885.97	0.07	1.70	0.15	0.49
886.18	0.11	1.61	0.27	0.48
886.29	0.14	3.22	0.33	1.00
888.36	0.30	2.38	0.64	0.95
888.57	0.14	2.42	0.16	0.90
888.75	0.11	1.83	0.18	0.59
888.94	0.10	2.15	0.19	0.69
889.16	0.21	2.44	0.06	0.89
889.36	0.03	1.51	0.08	0.47
889.61	0.06	1.46	0.11	0.46
889.80	0.08	1.49	0.11	0.37
889.80	0.10	1.89	0.14	0.50
889.99	0.05	1.67	0.05	0.41
890.20	0.15	2.01	0.08	0.58
890.40	0.04	1.75	0.20	0.45
890.58	0.15	3.25	0.00	0.88
890.79	0.16	2.06	0.09	0.62
891.08	0.12	1.99	0.17	0.55
891.30	0.08	1.77	0.03	0.61
891.49	0.13	2.00	0.13	0.55
891.69	0.05	1.42	0.16	0.41
891.69	0.05	1.44	0.11	0.43
891.93	0.01	1.34	0.17	1.05
892.11	0.25	1.90	0.03	0.15
892.28	0.17	1.94	0.07	0.35
892.50	0.04	1.83	0.03	0.44

Site 167 Major Element Data (cont.)

Depth (mbsf)	Mn/Al	Na/Al	P/Al	Ti/Al
892.69	0.03	1.67	0.09	0.44
898.22	0.05	1.56	0.26	0.46
898.43	0.05	1.79	0.17	0.42
898.62	0.01	0.35	0.13	0.07
898.82	0.01	0.30	0.02	0.07
899.01	0.04	1.52	0.04	0.58
899.23	0.04	1.43	0.13	0.44
899.23	0.04	1.62	0.17	0.48
899.40	0.04	1.69	0.13	0.51
899.61	0.04	1.68	0.13	0.51
899.81	0.04	1.65	0.19	0.61
900.02	0.01	0.42	0.13	0.13
900.22	0.04	1.64	0.23	0.49
900.42	0.06	1.71	0.24	0.56
900.62	0.04	1.80	0.23	0.52
900.79	0.03	1.50	0.15	0.52
901.01	0.03	1.59	0.27	0.53
908.17	0.11	1.30	0.22	0.41
908.17	0.13	1.52	0.22	0.45
908.37	0.07	1.60	0.14	0.41
908.61	0.12	1.62	0.12	0.44
908.81	0.11	1.67	0.03	0.43
909.00	0.01	1.07	0.16	0.36
909.22	0.20	1.79	0.08	0.48
909.40	0.10	1.61	0.12	0.42
909.60	0.18	1.84	0.05	0.50
909.80	0.31	2.71	0.07	0.89
910.03	0.20	1.59	0.05	0.49
910.21	0.20	1.76	0.18	0.48
910.42	0.10	1.26	0.08	0.37
910.42	0.16	1.77	0.22	0.53
910.60	0.13	1.79	0.12	0.49
910.80	0.21	2.04	0.23	0.66
911.03	0.11	1.64	0.18	0.45
911.21	0.12	2.14	0.01	0.68
911.40	0.15	1.92	0.06	0.51
911.59	0.12	1.61	0.11	0.47
911.80	0.07	1.46	0.05	0.44
912.01	0.18	1.98	0.07	0.59
912.23	0.10	1.53	0.07	0.41
912.40	0.08	1.32	0.20	0.38
912.40	0.14	2.06	0.10	0.64
912.60	0.13	2.11	0.17	0.63
912.81	0.12	1.87	0.03	0.54
912.90	0.11	2.08	0.06	0.53
917.35	0.09	1.68	0.14	0.46

Site 167 Major Element Data (cont.)

Depth (mbsf)	Mn/Al	Na/Al	P/Al	Ti/Al
917.84	0.09	1.50	0.20	0.52
918.35	0.10	1.60	0.06	0.62
918.83	0.11	1.36	0.26	0.56
919.36	0.08	1.12	0.13	0.36
919.36	0.13	1.83	0.18	0.50
919.84	0.08	1.67	0.19	0.45
920.33	0.05	1.50	0.10	0.40
920.86	0.07	1.63	0.06	0.43
921.35	0.17	2.19	0.16	0.55
921.85	0.09	1.80	0.13	0.44
922.34	0.09	1.75	0.29	0.47
922.83	0.13	1.90	0.18	0.48
923.33	0.06	1.72	0.03	0.40
925.10	0.09	1.90	0.05	0.47
925.21	0.04	1.78	0.14	0.42
925.31	0.07	1.81	0.33	0.40
925.31	0.08	1.97	0.13	0.47
925.41	0.03	1.96	0.19	0.42
925.50	0.11	1.89	0.18	0.49
925.70	0.09	1.78	0.19	0.46
925.80	0.08	1.80	0.25	0.45
925.90	0.10	1.97	0.14	0.47
926.10	0.22	2.35	0.70	0.55
926.30	0.03	2.21	0.19	0.45
926.71	0.11	2.06	0.40	0.49
926.80	0.17	2.20	0.40	0.52
927.00	0.03	1.80	0.12	0.39
927.20	0.07	1.75	0.10	0.42
927.39	0.03	1.83	0.17	0.41
927.61	0.10	2.06	0.28	0.47
927.80	0.12	2.34	0.08	0.51
928.10	0.13	1.94	0.23	0.47
928.30	0.01	1.70	0.08	0.29
928.50	0.12	2.58	0.47	0.63
928.50	0.09	2.17	0.17	0.50
928.71	0.09	1.86	0.47	0.50
928.90	0.08	1.84	0.25	0.46
929.10	0.09	2.04	0.25	0.45
929.10	0.02	1.49	0.13	0.35
929.10	0.03	1.58	0.07	0.39
929.80	0.07	1.79	0.33	0.40
929.80	0.09	2.11	0.20	0.46
930.01	0.03	1.44	0.08	0.38
930.21	0.15	2.38	0.43	0.53
930.40	0.04	2.19	0.17	0.44
930.60	0.11	2.20	0.37	0.52

Site 167 Major Element Data (cont.)

Depth (mbsf)	Mn/Al	Na/Al	P/Al	Ti/Al
930.80	0.08	2.00	0.17	0.52
935.91	0.03	1.49	0.05	0.38
936.10	0.02	1.31	0.06	0.36
936.30	0.04	2.06	0.25	0.45
936.61	0.02	1.37	0.11	0.37
936.61	0.02	1.37	0.08	0.37
936.79	0.06	1.95	0.16	0.43
937.20	0.08	1.94	0.16	0.45
937.40	0.04	1.44	0.11	0.37
937.40	0.04	1.43	0.07	0.37
937.60	0.03	1.40	0.04	0.39
937.80	0.06	2.98	0.24	0.82
938.10	0.08	1.94	0.16	0.44
938.30	0.14	2.69	0.34	0.72
938.71	0.05	1.46	0.18	0.36
938.71	0.07	1.93	0.36	0.49
938.89	0.04	1.53	0.06	0.39
939.30	0.16	2.30	0.37	0.56
939.59	0.11	2.39	0.11	0.53
939.80	0.02	1.92	0.27	0.41
940.01	0.08	2.08	0.34	0.47
940.19	0.11	2.06	0.34	0.50
940.19	0.11	2.10	0.34	0.48
940.41	0.19	3.59	0.64	1.02
940.60	0.17	2.78	0.62	0.61
940.79	0.03	1.79	0.23	0.41
940.90	0.02	1.33	0.07	0.44
929.60	0.04	2.21	0.23	0.43
929.60	0.04	2.22	0.05	0.40
935.70	0.11	1.86	0.25	0.47
935.70	0.11	1.87	0.18	0.46
935.70	0.11	1.89	0.26	0.46

Site 167 Major Element Figures

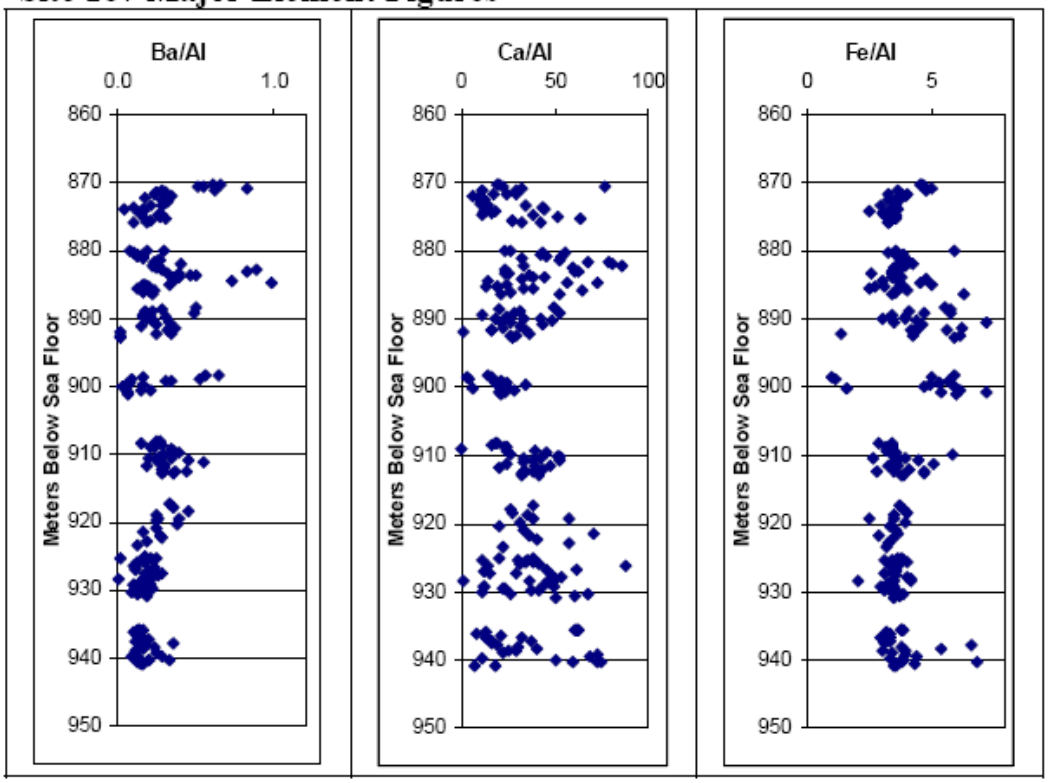

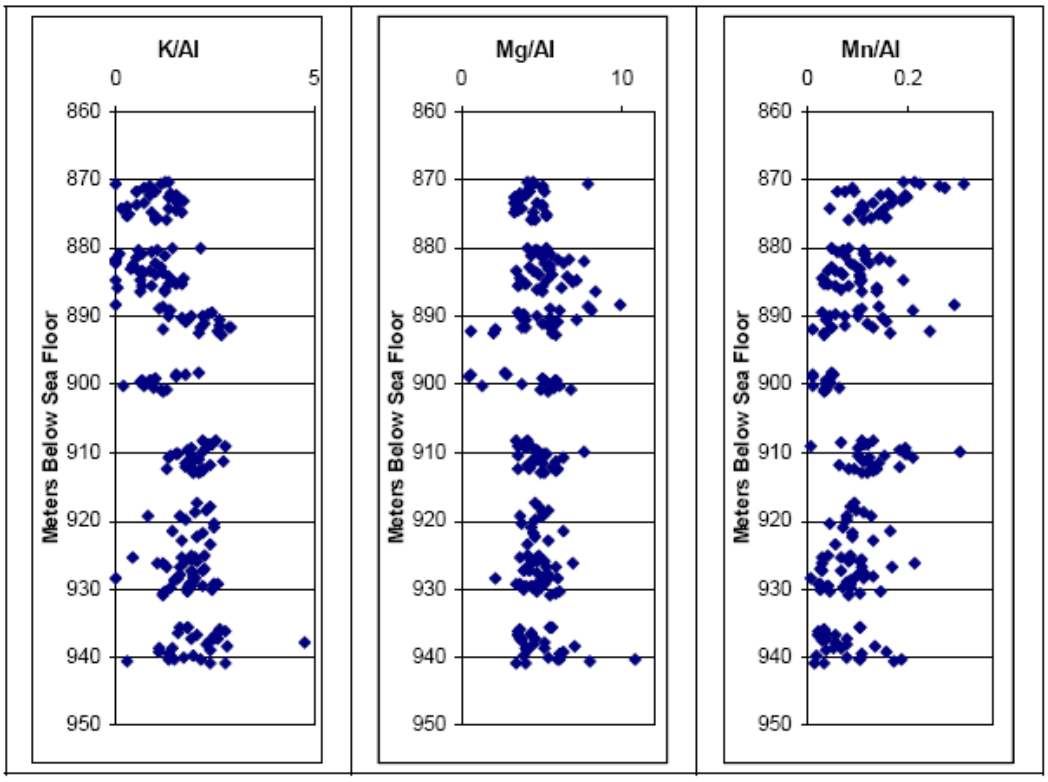

Site 167 Major Element Figures

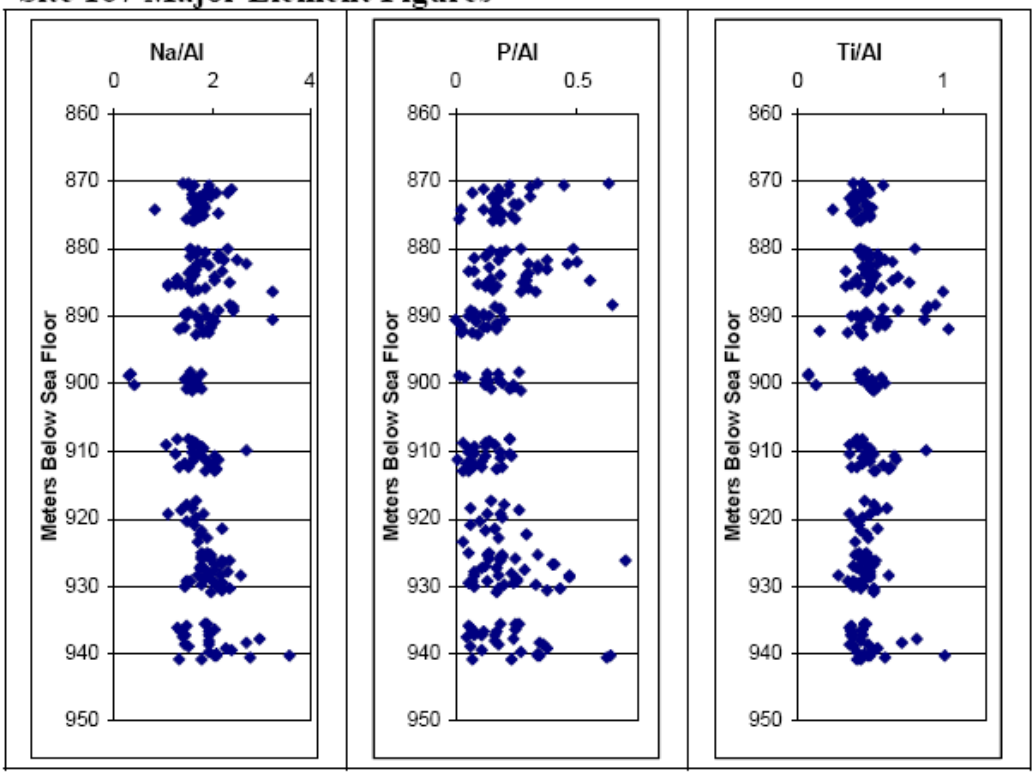

Site 463 Minor Element Data

Depth (mbsf)	Sc/Zr	V/Zr	Cr/Zr	Co/Zr	Ni/Zr
585.00	0.14	0.84	0.57	1.10	0.7
585.00	0.19	1.12	0.76	1.39	0.8
585.38	1.14	5.76	3.48	6.43	3.8
585.79	2.68	5.87	4.69	15.60	8.1
586.22	1.63	5.10	3.23	13.07	5.9
586.50	1.52	7.25	4.07	11.84	4.8
586.90	4.39	14.41	8.09	44.68	14.3
587.29	0.63	2.77	1.10	2.55	0.9
587.71	0.60	4.77	2.02	6.34	2.2
594.67	1.18	4.83	2.12	5.06	1.1
604.10	3.06	5.20	6.16	42.27	9.7
604.50	0.88	2.91	1.12	5.46	1.3
604.50	3.14	11.24	4.40	23.71	4.3
604.99	1.11	5.79	3.74	5.99	1.4
605.22	3.24	6.83	4.40	21.92	5.2
605.40	0.53	0.90	0.61	3.89	0.7
605.69	0.71	2.75	1.43	5.39	1.0
605.84	0.65	4.76	1.93	4.81	1.0
606.00	0.66	1.73	0.70	10.04	1.2
606.39	0.20	0.75	0.47	2.63	0.3
606.69	0.58	2.69	1.60	5.31	0.9
607.10	0.72	3.58	1.20	13.75	2.7
607.03	0.11	0.11	2.78	1.00	2.4
607.28	0.24	0.53	2.42	1.09	2.3
607.49	2.68	23.46	15.32	10.84	5.3
607.61	0.16		5.22	1.40	4.2
607.89	0.25	0.31	3.22	1.16	2.7
608.62	0.11	1.24	212.60	15.54	99.6
608.91	0.21	0.30	56.79	5.79	31.1
609.20	0.13	0.08	6.11	1.44	5.2
609.48	0.07	0.45	0.38	0.68	0.3
609.79	0.12	0.77	10.44	1.43	7.4
610.01	0.12	0.41	5.82	1.19	4.1
610.30	0.13	0.53	1.68	0.94	1.3
610.30	0.12	0.50	2.06	0.99	1.4
610.58	0.17	0.99	0.93	0.97	0.7
613.51	0.59	5.24	77.47	18.18	58.5
613.91	0.08	0.43	1.31	1.29	1.0
614.23	0.09	0.31	8.84	1.59	6.0
614.62	0.09	0.40	0.56	0.95	0.5
614.88	0.13	0.78	0.72	0.89	0.5
615.03	0.07	0.49	0.50	0.98	0.6
615.31	0.14	0.73	0.81	1.61	0.7
615.59	0.09	1.01	0.83	1.02	0.5
615.89	0.06	1.80	132.58	10.89	70.2
615.89	0.08	1.43	4.67	1.64	6.7

Site 463 Minor Element Data (cont.)

Depth (m)	45Sc	51V	52Cr	59Co	60Ni
615.59	0.09	1.01	0.83	1.02	0.5
615.89	0.06	1.80	132.58	10.89	70.2
615.89	0.08	1.43	4.67	1.64	6.7
616.21	0.13	0.65	0.86	0.94	0.6
616.46	0.12	0.72	0.94	1.02	0.6
616.60	0.05	0.28	0.28	0.43	0.3
616.92	0.18	1.13	1.18	1.47	0.7
617.29	0.10	0.78	0.96	0.76	0.5
617.60	0.13	1.02	0.99	1.80	0.8
617.88	0.10	0.75	0.58	1.60	0.7
618.02	0.08	0.87	0.59	0.58	0.4
618.02	0.09	0.77	0.57	0.63	0.3
618.28	0.11	0.88	1.20	1.22	0.7
618.60	0.27	1.54	2.57	1.60	0.9
618.90	0.08	0.61	0.84	1.14	0.7
619.20	0.10	0.69	1.02	1.22	0.8
619.70	0.41	3.27	2.91	5.28	1.7
619.70	0.51	3.78	3.60	4.35	2.0
620.20	0.36	2.60	1.95	3.11	2.2
620.70	0.27	12.46	2.58	1.93	2.8
621.20	0.10	6.45	1.51	0.80	1.1
621.70	0.25	2.36	1.15	1.92	1.7
622.20	0.57	3.48	2.58	5.40	2.7
622.50	0.08	0.54	0.77	2.69	1.6
622.79	0.38	1.90	3.46	2.47	1.8
623.06	0.17	1.77	2.57	2.46	1.2
623.01	0.55	3.13	2.93	2.87	1.8
623.28	0.29	2.28	3.01	2.18	1.4
623.59	0.05	0.17	0.67	0.98	0.7
623.88	0.06	0.39	0.40	0.88	0.4
623.88	0.05	0.39	0.45	0.81	0.5
624.21	0.06	0.48	4.70	2.12	2.9
624.50	0.04	0.36	1.02	0.87	0.9
624.80	0.05	0.47	1.69	1.36	1.5
625.10	0.05	0.48	1.32	0.95	1.1
625.40	0.06	0.30	1.50	0.80	1.3
625.71	0.08	0.41	3.59	1.13	2.8
626.00	0.19	0.09	2.70	4.86	3.3
626.00	0.06	0.36	3.22	1.27	2.6
626.29	0.05	0.41	25.67	2.55	13.9
626.60	0.04	0.29	15.50	1.50	8.6
627.00	0.06	0.32	12.47	1.97	9.2
627.30	0.06	0.42	47.85	4.50	28.3
627.52	0.05	0.42	2.77	0.79	2.1
627.52	0.05	0.41	2.63	0.84	2.0
627.81	0.09	0.37	10.44	2.01	7.1

Site 463 Minor Element Data (cont.)

Depth (m)	45Sc	51V	52Cr	59Co	60Ni
628.09	0.06	0.30	4.03	1.48	3.2
628.38	0.06	0.39	5.03	1.62	4.0
628.60	0.07	0.68	124.33	12.42	75.8
632.63	0.07	0.65	83.49	9.59	57.4
633.52	0.08	0.55	38.05	4.32	26.3
634.14	0.07	0.48	19.00	2.94	15.0
635.05	0.06	0.62	97.68	10.18	63.2
635.60	0.04	0.61	49.87	6.61	38.0
636.53	0.05	0.47	60.50	7.46	46.9
636.53	0.06	0.48	76.95	7.54	49.3
637.10	0.06	0.25	0.24	0.81	0.4
638.15	0.03	0.20	0.18	0.57	0.3
642.15	0.06	0.28	0.21	0.62	0.3
643.04	0.05	0.32	0.23	0.68	0.3
643.92	0.07	0.33	0.26	1.01	0.4
644.83	0.50	0.60	0.67	4.04	1.3
645.13	0.29	0.25	0.25	1.15	0.3
646.05	0.05	0.33	0.22	3.40	1.5
646.92	0.07	0.03	0.06	0.24	0.1
647.82	0.03	0.03	0.16	0.41	0.6
647.82	0.04	0.05	0.14	0.47	0.4
651.88	0.54	2.99	1.80	5.46	1.7
652.81	0.42	1.48	0.94	3.35	1.0
653.58	0.35	1.42	1.03	3.67	0.9
661.17	0.50	1.82	1.24	4.44	1.2
661.74	0.28	1.43	0.96	2.44	0.6

Site 463 Minor Element Data (cont.)

Depth (mbsf)	Cu/Zr	Zn/Zr	Se/Zr	As/Zr	Rb/Zr
585.00	7.5	1.3	5.52	2.33	0.02
585.00	9.1	1.6	7.81	2.95	0.03
585.38	46.6	12.6	44.10	9.83	0.18
585.79	92.1	19.4	41.30	32.81	0.15
586.22	179.7	23.1	34.92	20.31	0.13
586.50	60.1	23.5	51.71	22.17	0.18
586.90	196.3	40.9	99.23	86.55	0.41
587.29	18.0	1.6	13.72	5.54	0.04
587.71	57.9	10.3	25.57	14.33	0.12
594.67	23.6	4.6	25.62	11.17	0.13
604.10	43.0	22.4	49.49	81.33	0.24
604.50	19.5	3.4	10.34	10.05	0.04
604.50	73.3	7.1	43.58	40.14	0.15
604.99	63.1	6.6	17.82	8.35	0.06
605.22	42.9	7.2	30.64	29.93	0.10
605.40	5.6	1.1	4.38	5.12	0.01
605.69	13.5	2.9	16.31	7.83	0.07
605.84	30.3	4.1	20.77	5.94	0.08
606.00	9.6	2.1	8.47	11.90	0.03
606.39	6.9	0.6	4.26	2.70	0.02
606.69	20.3	2.3	18.00	4.63	0.06
607.10	43.9	4.4	10.62	9.05	0.05
607.03	7.6	0.9	7.09	0.00	0.20
607.28	9.6	0.9	6.00	0.00	0.26
607.49	51.7	3.7	4.64	4.56	0.05
607.61	13.0	1.3	35.45	0.00	0.10
607.89	14.1	1.0	7.25	0.00	0.29
608.62	71.3	1.2	2.28	6.66	0.25
608.91	37.9	1.5	6.31	0.00	0.12
609.20	10.6	1.0	19.18	0.00	0.25
609.48	10.1	0.5	5.41	0.00	0.53
609.79	28.7	0.5	6.98	0.54	0.44
610.01	13.5	1.1	9.28	0.47	0.37
610.30	13.6	0.8	10.12	0.00	0.49
610.30	13.2	0.6	3.12	0.00	0.54
610.58	19.5	0.8	10.40	0.00	0.62
613.51	63.3	2.2	0.00	8.81	0.22
613.91	16.5	0.5	10.22	0.00	0.38
614.23	10.2	0.4	9.55	0.00	0.34
614.62	8.7	0.3	7.69	0.31	0.31
614.88	10.8	0.3	3.66	1.38	0.48
615.03	12.2	0.6	5.09	2.45	0.31
615.31	12.8	1.4	6.54	1.82	0.52
615.59	17.6	7.5	8.02	1.89	0.40
615.89	52.7	1.0	3.52	13.26	0.41
615.89	11.7	0.5	3.90	9.28	0.46

Site 463 Minor Element Data (cont.)

Depth (m)	65Cu	66Zn	74Se	75As	85Rb
615.59	17.6	7.5	8.02	1.89	0.40
615.89	52.7	1.0	3.52	13.26	0.41
615.89	11.7	0.5	3.90	9.28	0.46
616.21	20.2	1.4	3.94	3.84	0.43
616.46	17.4	1.3	3.57	2.14	0.44
616.60	5.3	0.4	2.96	0.70	0.27
616.92	16.7	1.1	3.52	2.49	0.46
617.29	10.9	0.7	5.27	1.01	0.47
617.60	11.8	0.9	3.60	3.01	0.44
617.88	16.8	0.3	2.80	1.67	0.51
618.02	9.1	0.4	3.33	0.09	0.39
618.02	9.1	0.3	2.30	0.40	0.44
618.28	15.8	0.4	2.79	0.52	0.41
618.60	23.5	0.4	5.74	0.62	0.42
618.90	12.8	0.7	2.13	1.60	0.37
619.20	12.9	1.0	2.55	1.36	0.40
619.70	14.9	2.2	11.90	4.71	0.06
619.70	17.7	2.6	15.73	4.78	0.08
620.20	14.8	2.3	9.62	3.33	0.05
620.70	13.5	4.7	6.28	10.87	0.03
621.20	13.4	4.9	2.14	2.47	0.01
621.70	26.6	1.9	7.94	2.52	0.04
622.20	24.7	4.7	16.52	6.49	0.07
622.50	24.0	0.5	1.77	0.64	0.40
622.79	13.6	0.7	4.11	0.00	0.40
623.06	24.8	0.5	2.42	0.00	0.52
623.01	18.6	1.3	5.43	0.00	0.33
623.28	22.2	0.9	2.47	0.00	0.48
623.59	8.8	0.5	3.92	0.00	0.32
623.88	10.6	0.3	1.19	0.20	0.44
623.88	10.1	0.5	1.18	0.32	0.39
624.21	17.4	0.6	8.76	0.99	0.43
624.50	10.8	0.3	0.79	0.61	0.41
624.80	13.8	0.6	3.75	0.14	0.44
625.10	14.6	1.0	0.94	0.96	0.47
625.40	10.5	0.4	3.32	0.65	0.32
625.71	10.9	0.5	4.72	0.00	0.46
626.00	11.5	0.9	20.64	0.00	0.18
626.00	8.2	0.5	9.08	0.00	0.33
626.29	13.9	0.4	0.80	0.10	0.37
626.60	11.0	0.4	2.64	0.15	0.26
627.00	10.6	0.5	3.96	0.00	0.35
627.30	21.4	0.6	1.20	0.97	0.21
627.52	6.0	0.7	7.00	0.00	0.29
627.52	6.0	0.5	5.54	0.00	0.33
627.81	19.9	1.1	10.46	0.00	0.23

Site 463 Minor Element Data (cont.)

Depth (m)	65Cu	66Zn	74Se	75As	85Rb
628.09	14.8	1.1	5.28	0.51	0.34
628.38	11.0	0.7	8.55	0.00	0.23
628.60	53.4	1.4	0.00	4.16	0.07
632.63	41.9	0.9	0.11	4.20	0.26
633.52	23.0	1.0	3.00	3.77	0.39
634.14	12.2	0.6	1.39	0.00	0.25
635.05	43.3	0.8	0.00	5.44	0.18
635.60	46.4	0.6	0.17	6.52	0.24
636.53	23.7	0.7	0.74	1.18	0.12
636.53	28.9	0.7	0.00	3.35	0.11
637.10	6.5	0.5	5.12	0.68	0.23
638.15	5.1	0.3	3.93	1.18	0.26
642.15	5.2	0.4	4.22	0.00	0.32
643.04	6.3	0.4	5.69	0.49	0.39
643.92	6.7	0.3	4.94	0.00	0.33
644.83	27.0	0.7	10.51	0.00	0.56
645.13	14.3	0.3	2.01	0.00	0.29
646.05	4.9	0.6	5.32	7.15	0.00
646.92	4.2	0.1	1.66	0.00	0.02
647.82	4.7	0.4	6.90	0.00	0.03
647.82	4.6	0.3	10.81	0.00	0.06
651.88	11.8	1.9	18.99	6.99	0.12
652.81	7.1	3.7	11.55	5.07	0.11
653.58	8.7	6.6	10.55	5.86	0.06
661.17	9.2	6.9	13.78	7.52	0.07
661.74	9.0	3.0	8.70	4.18	0.04

Site 463 Minor Element Data (cont.)

Depth (mbsf)	Sr/Zr	Y/Zr	Mo/Zr	Ag/Zr	Cd/Zr
585.00	1.4	9.80	1.33	0.59	0.97
585.00	1.9	4.73	2.15	0.66	1.23
585.38	12.6	0.00	17.72	3.61	9.11
585.79	10.2	0.00	48.49	9.73	8.52
586.22	9.1	26.75	29.75	4.82	6.41
586.50	12.7	0.00	29.89	5.34	8.87
586.90	28.6	0.00	161.14	22.52	15.93
587.29	3.0	0.00	5.32	1.16	2.14
587.71	8.2	12.38	11.57	1.60	7.32
594.67	8.8	0.00	11.37	1.93	16.59
604.10	18.6	0.00	159.35	20.02	15.90
604.50	3.1	0.00	12.33	2.41	9.43
604.50	10.6	0.00	39.84	8.82	8.63
604.99	4.5	0.00	8.44	1.48	2.86
605.22	6.9	0.00	33.03	6.54	11.99
605.40	1.1	0.00	5.24	1.15	1.00
605.69	5.0	0.00	6.70	1.44	4.16
605.84	5.8	1.22	5.21	1.03	3.80
606.00	2.1	0.00	12.10	2.64	1.21
606.39	1.2	0.00	2.39	0.57	0.72
606.69	4.1	0.00	3.76	1.00	3.27
607.10	3.5	13.15	5.27	1.44	2.84
607.03	14.6	3.73	0.84	4.53	0.00
607.28	16.7	4.20	10.15	0.00	0.00
607.49	3.4	58.81	2.60	0.65	1.95
607.61	20.3	5.98	0.65	6.78	11.43
607.89	18.7	5.80	0.01	4.17	0.00
608.62	12.7	4.16	0.01	4.39	0.00
608.91	23.4	5.94	0.00	4.31	0.00
609.20	13.8	4.52	0.00	4.14	0.00
609.48	4.5	1.64	0.01	3.84	0.00
609.79	7.5	2.52	0.01	4.00	0.00
610.01	9.7	3.11	0.12		0.00
610.30	8.1	2.33	10.00	2.14	0.00
610.30	8.2	2.20	0.00	3.75	0.00
610.58	8.7	2.22	0.02	4.16	10.72
613.51	7.7	0.61	0.02	5.81	136.13
613.91	7.3	1.90	0.02	4.55	11.74
614.23	9.4	2.50	0.04	5.09	17.86
614.62	6.4	2.60	0.04	7.36	9.76
614.88	4.7	1.11	0.03	7.26	24.25
615.03	4.1	1.09	0.03	4.55	21.39
615.31	7.2	1.59	0.04	6.83	8.46
615.59	5.6	3.25	0.07	6.68	38.82
615.89	1.8	0.47	0.05	7.30	19.58
615.89	2.0	0.52	0.02	5.03	53.30

Site 463 Minor Element Data (cont.)

Depth (m)	86Sr	89Y	95Mo	107Ag	111Cd
615.59	5.6	3.25	0.07	6.68	38.82
615.89	1.8	0.47	0.05	7.30	19.58
615.89	2.0	0.52	0.02	5.03	53.30
616.21	4.0	1.66	0.03	5.30	21.97
616.46	4.4	1.64	0.08	5.99	51.12
616.60	7.8	0.66	0.02	4.86	0.00
616.92	6.4	1.56	0.03	7.85	0.00
617.29	2.9	0.93	0.04	31.55	0.00
617.60	5.1	0.97	0.01	3.69	0.00
617.88	3.1	0.96	0.02	6.61	0.00
618.02	3.1	1.04	0.02	4.40	0.00
618.02	3.3	1.09	0.03	4.76	0.00
618.28	4.6	0.97	0.02	5.62	0.00
618.60	16.2	2.57	0.04	9.87	0.00
618.90	3.5	0.78	0.04	5.56	0.00
619.20	2.9	0.85	0.03	7.66	0.00
619.70	4.5	41.73	2.85	0.97	2.93
619.70	5.3	49.55	2.92	0.90	3.44
620.20	3.7	38.53	2.51	0.68	2.42
620.70	2.0	519.85	7.98	0.44	1.52
621.20	0.7	348.77	14.84	0.18	0.60
621.70	2.6	27.37	1.48	0.36	2.65
622.20	5.0	90.21	7.66	1.33	5.54
622.50	3.3	0.61	0.04	8.56	0.00
622.79	10.9	2.25	2.20	10.19	11.87
623.06	7.2	0.87	0.21	10.29	62.15
623.01	9.0	2.47	0.03	6.19	0.00
623.28	8.6	1.45	0.03	6.34	8.70
623.59	2.8	0.67	0.01	3.69	0.00
623.88	2.1	0.58	0.15	3.81	157.54
623.88	1.8	0.49	0.04	5.18	13.51
624.21	5.5	1.33	0.00	0.00	0.00
624.50	1.9	0.46	0.82	6.09	2.75
624.80	4.8	1.29	0.01	6.10	1.07
625.10	2.7	0.52	0.01	6.41	0.61
625.40	6.2	2.07	0.01	5.62	0.28
625.71	9.1	3.57	0.72	10.06	23.72
626.00	13.4	3.90	1.31	5.12	11.15
626.00	11.9	3.14	0.00	5.67	0.24
626.29	5.2	1.22	0.00	2.84	51.67
626.60	5.5	1.18	0.00	0.37	0.00
627.00	4.5	1.06	0.00	5.59	0.19
627.30	5.9	1.99	0.01	5.57	0.94
627.52	9.4	2.14	0.01	5.87	0.00
627.52	9.2	2.16	0.05	6.72	1.03
627.81	12.4	5.23	0.09	6.74	1.80

Site 463 Minor Element Data (cont.)

Depth (m)	86Sr	89Y	95Mo	107Ag	111Cd
628.09	8.9	3.48	0.05	6.98	0.00
628.38	12.6	5.24	0.03	6.46	0.00
628.60	6.5	2.86	0.04	6.62	11.26
632.63	4.3	1.89	0.15	6.12	144.86
633.52	6.1	3.52	0.04	6.63	0.38
634.14	6.9	2.24	0.56	23.11	0.00
635.05	2.9	0.72	0.03	6.04	5.33
635.60	3.9	1.43	0.00		0.00
636.53	5.8	1.73	3.09	32.52	15.73
636.53	4.4	1.30	0.02	7.00	93.31
637.10	5.0	2.04	0.01	6.93	7.96
638.15	3.8	1.04	0.01	7.68	2.19
642.15	3.9	1.77	0.05	9.22	10.46
643.04	5.1	1.80	0.01	5.51	0.00
643.92	7.5	2.19	0.06	18.38	31.77
644.83	23.5	3.43	0.02	7.84	8.46
645.13	4.9	1.29	0.01	8.26	3.60
646.05	9.0	2.15	0.02	7.72	3.53
646.92	1.4	0.64	0.02	7.51	6.13
647.82	4.5	1.82	0.01	6.45	4.70
647.82	4.4	1.81	0.01	6.69	3.46
651.88	7.9	1.14	7.85	1.85	4.26
652.81	7.4	0.00	7.41	1.36	3.35
653.58	4.5	0.00	8.91	1.51	2.13
661.17	5.1	0.00	9.22	1.73	4.87
661.74	2.6	0.10	5.80	0.93	1.45

Site 463 Minor Element Data (cont.)

Depth (mbsf)	In/Zr	Sn/Zr	Sb/Zr	Cs/Zr	Ba/Zr
585.00	0.34	2.32	2.32	1.70	0.6
585.00	0.46	3.03	3.03	2.17	0.6
585.38	2.44	28.77	28.65	9.62	3.5
585.79	2.94	91.01	90.76	11.79	9.5
586.22	2.10	37.21	37.13	9.90	4.7
586.50	2.87	35.72	35.60	11.18	5.3
586.90	6.41	68.86	68.95	21.02	22.3
587.29	0.75	6.46	6.45	3.23	1.1
587.71	1.39	40.43	37.93	5.65	1.6
594.67	1.31	40.34	33.14	4.34	2.0
604.10	3.61	60.39	60.65	11.33	19.7
604.50	0.67	6.62	6.65	2.28	2.4
604.50	2.72	25.88	25.98	7.58	8.7
604.99	1.10	24.26	23.82	5.20	1.5
605.22	1.87	25.98	26.00	7.62	6.4
605.40	0.28	3.15	3.16	1.21	1.1
605.69	0.95	24.20	23.75	2.78	1.4
605.84	1.22	15.67	15.49	3.90	1.0
606.00	0.57	7.97	7.99	1.37	2.6
606.39	0.25	0.86	0.86	1.06	0.6
606.69	1.14	10.98	10.87	3.08	1.0
607.10	0.72	18.34	18.15	3.02	1.4
607.03	0.00	5.78	22.55	1.31	2.1
607.28	0.00	0.00	0.00	0.00	1.2
607.49	0.19	0.34	0.34	1.43	0.6
607.61	0.00	0.00	49.00	3.79	5.6
607.89	0.00	13.57	3.87	2.39	3.6
608.62	0.00	7.12	11.85	1.93	4.1
608.91	0.00	0.00	0.00	0.22	8.5
609.20	0.00	23.24	10.57	0.15	5.9
609.48	0.00	0.00	0.00	0.21	3.5
609.79	0.00	11.30	15.82	0.18	5.3
610.01	0.00	0.00	0.00	0.00	1.4
610.30	0.00	0.00	0.00	0.05	1.3
610.30	0.00	0.00	0.00	0.75	5.6
610.58	0.00	0.00	0.36	0.92	25.1
613.51	0.00	0.12	2.46	0.79	20.5
613.91	0.00	0.00	0.00	0.81	46.0
614.23	0.00	0.00	0.00	0.53	12.8
614.62	0.00	0.00	0.00	0.75	37.6
614.88	0.00	0.00	0.00	0.82	34.4
615.03	0.00	0.00	0.00	0.58	23.2
615.31	0.00	0.00	0.00	0.72	37.8
615.59	0.00	0.00	0.00	0.64	26.0
615.89	0.00	0.00	0.00	0.69	19.5
615.89	0.00	0.00	0.00	0.86	28.4

Site 463 Minor Element Data (cont.)

Depth (m)	115In	118Sn	121Sb	133Cs	135Ba
615.59	0.00	0.00	0.00	0.64	26.0
615.89	0.00	0.00	0.00	0.69	19.5
615.89	0.00	0.00	0.00	0.86	28.4
616.21	0.00	0.00	0.00	0.70	23.5
616.46	0.00	0.00	0.00	0.31	8.0
616.60	0.00	0.00	0.00	0.83	32.5
616.92	0.00	0.00	1.87	0.81	25.0
617.29	0.00	0.00	0.00	1.03	32.7
617.60	0.00	0.00	0.19	1.58	11.9
617.88	0.00	0.00	0.00	0.99	27.1
618.02	0.00	0.00	0.00	0.46	16.4
618.02	0.00	0.00	0.00	0.70	66.2
618.28	0.00	0.00	0.00	0.89	21.3
618.60	0.00	0.00	0.00	0.71	30.6
618.90	0.00	0.00	0.00	1.02	40.7
619.20	0.00	0.00	1.84	0.88	34.8
619.70	0.98	8.67	8.63	4.11	0.9
619.70	1.26	14.04	13.84	4.85	0.9
620.20	0.71	7.86	7.77	3.07	0.7
620.70	0.48	7.75	7.43	1.74	0.4
621.20	0.15	4.06	3.83	0.53	0.2
621.70	0.58	11.00	11.21	2.38	0.3
622.20	1.22	21.14	20.83	4.98	1.3
622.50	0.00	0.00	0.00	0.90	49.2
622.79	0.00	49.90	9.82	1.05	14.1
623.06	0.00	0.00	0.95	0.96	16.9
623.01	0.00	0.00	1.33	0.93	39.3
623.28	0.00	0.00	1.36	0.89	29.0
623.59	0.00	0.00	0.00	1.59	11.9
623.88	0.00	0.00	0.00	0.77	46.4
623.88	0.00	0.00	0.00	0.84	33.3
624.21	0.00	0.00	0.00	0.00	0.0
624.50	0.00	15.78	21.92	1.22	1.8
624.80	0.00	23.94	5.48	2.29	3.1
625.10	0.00	18.88	12.67	1.84	3.5
625.40	0.00	15.76	15.07	0.14	4.4
625.71	0.00	34.50	58.16	4.03	5.6
626.00	0.00	32.97	8.53	0.16	0.6
626.00	0.00	7.17	0.18	0.19	7.0
626.29	0.00	25.46	3.66	2.75	0.0
626.60	0.00	1.82	0.48	0.00	0.0
627.00	0.00	27.54	10.63	0.11	4.8
627.30	0.00	7.80	0.30	0.19	2.9
627.52	0.00	3.00	3.26	1.51	10.4
627.52	0.00	28.60	4.05	1.75	3.5
627.81	0.00	29.98	5.61	1.66	3.6

Site 463 Minor Element Data (cont.)

Depth (m)	115In	118Sn	121Sb	133Cs	135Ba
628.09	0.00	26.97	4.17	1.80	4.7
628.38	0.00	23.40	4.10	1.79	3.7
628.60	0.00	25.92	3.78	1.63	3.7
632.63	0.00	33.05	3.08	1.62	3.6
633.52	0.00	33.49	3.02	1.61	3.8
634.14	0.00	55.68	44.73	0.00	32.1
635.05	0.00	25.94	2.69	1.73	3.2
635.60	0.00	0.00	0.00	18.57	0.0
636.53	0.00	124.17	102.23	0.00	48.8
636.53	0.00	11.27	1.34	0.01	10.6
637.10	0.00	11.09	1.24	0.09	10.8
638.15	0.00	2.91	12.16	0.02	4.3
642.15	0.00	9.11	12.33	0.00	3.6
643.04	0.00	11.79	3.31	1.54	10.5
643.92	0.00	30.29	12.06	0.89	90.8
644.83	0.00	13.10	4.51	0.55	19.8
645.13	0.00	11.85	2.77	0.75	36.4
646.05	0.00	13.23	3.10	0.67	33.9
646.92	0.00	11.36	2.12	0.33	12.4
647.82	0.00	10.72	2.43	0.62	13.7
647.82	0.00	8.89	2.96	0.46	10.6
651.88	1.45	9.72	9.70	5.26	1.8
652.81	0.89	8.02	8.00	2.70	1.3
653.58	0.78	5.91	5.94	2.22	1.5
661.17	0.99	7.78	7.79	3.42	1.7
661.74	0.65	5.78	5.76	2.24	0.9

Site 463 Minor Element Data (cont.)

Depth (mbsf)	W/Zr	Re/Zr	Au/Zr	Hg/Zr	Tl/Zr
585.00	1.02	1.44	0.14	0.15	0.23
585.00	1.28	1.94	0.19	0.20	0.30
585.38	7.65	9.01	0.76	0.80	1.81
585.79	20.75	13.81	1.34	1.37	2.26
586.22	12.02	14.62	1.38	1.43	1.78
586.50	38.93	9.45	1.48	1.51	2.30
586.90	99.14	22.48	8.64	8.86	4.82
587.29	5.86	2.26	0.91	0.94	0.53
587.71	8.74	9.95	0.81	0.85	1.60
594.67	11.28	9.81	0.97	0.98	21.84
604.10	94.59	4.69	6.47	6.57	3.37
604.50	10.32	2.30	0.29	0.31	0.42
604.50	31.34	8.84	0.86	0.88	1.17
604.99	5.48	4.00	0.51	0.53	1.45
605.22	20.44	3.95	1.14	1.16	3.34
605.40	7.63	0.52	0.14	0.14	0.77
605.69	8.85	5.22	0.30	0.31	3.09
605.84	6.83	3.82	0.34	0.35	0.89
606.00	13.97	1.28	0.24	0.24	0.43
606.39	2.29	0.67	0.08	0.08	0.52
606.69	4.19	2.28	0.21	0.22	0.71
607.10	7.05	3.78	1.56	1.60	2.84
607.03	0.00	0.00	1.04	0.00	36.45
607.28	0.00	0.00	0.00	0.00	0.00
607.49	2.83	0.85	0.33	0.35	0.19
607.61	0.00	0.00	1.54	0.00	11.60
607.89	0.00	0.00	1.12	0.00	5.87
608.62	0.00	0.00	0.75	0.00	4.85
608.91	0.00	0.00	0.50	0.00	4.42
609.20	0.00	0.00	0.59	0.00	6.44
609.48	0.00	0.00	1.53	94.14	1.38
609.79	0.00	0.00	0.48	0.00	1.31
610.01	0.00	0.00	0.00	0.00	0.00
610.30	0.00	0.00	0.00	9.79	0.00
610.30	0.00	0.00	0.38	0.00	2.05
610.58	0.00	0.00	1.23	0.00	2.39
613.51	0.00	0.00	1.27	0.00	2.38
613.91	0.00	0.00	1.12	0.00	3.00
614.23	0.00	0.00	0.88	0.00	1.18
614.62	0.00	0.00	1.22	0.00	3.35
614.88	0.00	0.00	1.21	0.00	2.76
615.03	0.00	0.00	0.68	0.00	1.04
615.31	0.00	0.00	0.97	0.00	2.10
615.59	0.00	0.00	0.78	0.00	2.11
615.89	0.00	0.00	0.98	0.00	2.17
615.89	0.00	0.00	1.17	0.00	3.17

Site 463 Minor Element Data (cont.)

Depth (m)	182W	187Re	197Au	200Hg	205Tl
615.59	0.00	0.00	0.78	0.00	2.11
615.89	0.00	0.00	0.98	0.00	2.17
615.89	0.00	0.00	1.17	0.00	3.17
616.21	0.00	0.00	0.83	0.00	2.09
616.46	0.00	0.00	0.42	0.00	0.67
616.60	0.00	0.00	1.34	0.00	2.92
616.92	0.00	0.00	1.14	0.00	3.22
617.29	0.00	0.00	0.96	0.00	3.75
617.60	0.00	0.00	0.78	0.00	4.26
617.88	0.00	0.00	1.14	0.00	3.26
618.02	0.00	0.00	0.64	0.00	1.98
618.02	0.00	0.00	1.01	0.00	3.30
618.28	0.00	0.00	1.32	0.00	3.09
618.60	0.00	0.00	1.16	0.00	3.08
618.90	0.00	0.00	1.27	0.00	4.53
619.20	0.00	0.00	1.16	0.00	3.58
619.70	4.01	1.94	0.28	0.29	2.20
619.70	4.93	2.22	0.40	0.41	2.61
620.20	5.37	1.44	0.31	0.32	1.57
620.70	3.37	16.48	0.30	0.31	1.48
621.20	1.59	5.02	0.09	0.09	0.67
621.70	5.64	1.86	0.41	0.43	4.44
622.20	12.16	2.99	0.65	0.68	6.71
622.50	0.00	0.00	0.93	0.00	4.46
622.79	0.00	0.00	1.69	28.85	5.47
623.06	0.00	0.00	1.03	0.00	5.93
623.01	0.00	0.00	1.34	0.00	3.83
623.28	0.00	0.00	1.14	0.00	3.71
623.59	0.00	0.00	0.64	0.00	4.22
623.88	0.00	0.00	0.94	0.00	4.21
623.88	0.00	0.00	0.93	0.00	4.11
624.21	0.00	0.00	0.00	0.00	0.00
624.50	0.01	0.00	0.96	1.44	34.48
624.80	0.01	0.00	1.20	3.14	5.63
625.10	0.01	0.00	0.70	1.51	4.60
625.40	0.00	0.00	0.48	0.26	1.22
625.71	0.06	0.00	1.81	13.99	12.71
626.00	0.00	0.00	0.35	2.34	1.23
626.00	0.00	0.00	0.44	0.13	4.12
626.29	0.00	0.00	0.34	12.83	0.30
626.60	0.00	0.00	0.28	6.01	0.36
627.00	0.00	0.00	0.56	0.12	5.84
627.30	0.57	0.00	1.47	95.35	1.29
627.52	0.01	0.00	0.77	1.88	4.28
627.52	0.02	0.00	0.97	1.25	5.31
627.81	0.02	0.00	1.39	0.64	5.41

Site 463 Minor Element Data (cont.)

Depth (m)	182W	187Re	197Au	200Hg	205Tl
628.09	0.02	0.00	1.37	1.47	6.11
628.38	0.02	0.00	1.09	8.04	5.22
628.60	0.02	0.00	1.84	1.92	5.22
632.63	0.02	0.00	0.91	0.00	5.58
633.52	0.02	0.00	1.10	3.73	5.15
634.14	0.05	0.00	6.30	6.90	2.23
635.05	0.01	0.00	0.94	4.72	4.65
635.60	0.00	0.00	0.00	0.00	0.00
636.53	0.08	0.00	77.27	32.96	6.73
636.53	0.00	0.00	0.72	0.00	0.63
637.10	0.00	0.00	0.57	0.00	0.61
638.15	0.00	0.00	0.25	0.00	0.29
642.15	0.01	0.00	0.82	0.00	3.52
643.04	0.01	0.00	0.72	2.18	4.26
643.92	0.02	0.00	1.93	0.25	6.38
644.83	0.01	0.00	1.12	0.33	2.30
645.13	0.01	0.00	0.87	0.48	3.23
646.05	0.01	0.00	1.25	1.40	2.97
646.92	0.02	0.00	1.67	2.27	1.76
647.82	0.01	0.00	1.02	0.88	2.24
647.82	0.01	0.00	0.90	0.79	1.72
651.88	16.38	1.90	0.99	1.01	1.02
652.81	9.92	1.20	0.28	0.29	0.49
653.58	9.27	1.04	0.20	0.20	0.35
661.17	9.19	1.36	0.32	0.33	0.51
661.74	4.65	1.12	0.24	0.25	0.31

Site 463 Minor Element Data (cont.)

Depth (mbsf)	Pb/Zr	Bi/Zr	Th/Zr	U/Zr
585.00	94	238	8712	2453
585.00	117	300	11098	3530
585.38	732	1737	69360	8489
585.79	743	2757	56184	15592
586.22	584	1846	50587	10933
586.50	725	2294	64412	10128
586.90	1696	6114	127205	29818
587.29	185	523	17055	2415
587.71	389	1389	38228	7851
594.67	536	16593	52883	3904
604.10	1040	4837	63388	45020
604.50	181	585	13609	3240
604.50	657	1875	49188	13875
604.99	232	1231	21067	4483
605.22	503	3211	38112	8730
605.40	77	715	5557	1409
605.69	297	2451	28257	3895
605.84	324	776	32019	4633
606.00	157	620	10452	3799
606.39	67	453	5771	1858
606.69	300	631	29522	4240
607.10	199	2266	17844	6904
607.03	150	951	28354	243
607.28	117	0	4301	0
607.49	32	206	1870	7166
607.61	811	7563	50452	5219
607.89	196	1285	44654	1062
608.62	198	1292	34459	1033
608.91	139	541	58359	536
609.20	209	57	129143	538
609.48	43	81	15907	419
609.79	150	104	13928	396
610.01	87	0	5189	0
610.30	120	0	4296	0
610.30	61	681	16611	398
610.58	58	765	22568	274
613.51	59	1130	19534	243
613.91	102	4024	22477	491
614.23	65	1111	11152	349
614.62	93	1695	18871	672
614.88	100	1564	19741	612
615.03	84	1121	10350	315
615.31	81	2827	19070	187
615.59	81	1485	12237	569
615.89	65	2033	17916	260
615.89	53	1374	19386	602

Site 463 Minor Element Data (cont.)

Depth (m)	207Pb	209Bi	232Th	238U
615.59	81	1485	12237	569
615.89	65	2033	17916	260
615.89	53	1374	19386	602
616.21	76	2098	15537	235
616.46	67	1476	5961	384
616.60	52	1352	20409	655
616.92	107	1147	19014	966
617.29	91	1191	21759	947
617.60	128	1470	34414	828
617.88	81	1409	23843	395
618.02	30	367	11701	348
618.02	54	2311	17855	576
618.28	49	1115	21420	360
618.60	112	1143	17792	449
618.90	92	1387	22161	711
619.20	91	1619	18268	789
619.70	197	1658	18073	6971
619.70	272	1949	26050	9057
620.20	175	1189	16454	6525
620.70	114	1094	10727	20527
621.20	42	501	3941	9068
621.70	145	3185	14114	4849
622.20	290	4769	26178	13257
622.50	78	1843	19769	2040
622.79	83	736	19279	772
623.06	99	459	22011	893
623.01	100	1557	20601	851
623.28	88	1190	18380	823
623.59	128	1419	33835	824
623.88	83	2896	19027	292
623.88	60	921	20481	430
624.21		0	40143	14148
624.50	137	835	23734	14817
624.80	177	1181	38117	1064
625.10	181	1164	29015	1026
625.40	132	63	11508	348
625.71	422	8037	46070	6465
626.00	109	120	3244	482
626.00	124	487	49735	528
626.29	0	5975	32616	11483
626.60	0	1842	39741	14182
627.00	182	2	43484	489
627.30	39	59	13062	394
627.52	126	1327	29409	639
627.52	226	930	38081	0
627.81	236	1091	38749	0

Site 463 Minor Element Data (cont.)

Depth (m)	207Pb	209Bi	232Th	238U
628.09	308	207	42500	0
628.38	249	909	40188	0
628.60	236	712	37412	0
632.63	222	564	37524	0
633.52	232	410	39078	0
634.14	563	0	0	11422
635.05	177	947	38273	213
635.60	0	0	60122	0
636.53	701	0	0	9554
636.53	81	0	4019	0
637.10	60	0	4408	0
638.15	32	0	4072	384
642.15	145	0	1591	2841
643.04	126	1293	29893	660
643.92	329	0	0	0
644.83	117	0	15721	0
645.13	82	590	14058	0
646.05	107	11	10990	0
646.92	87	25	11284	0
647.82	98	49	12909	0
647.82	90	97	12194	0
651.88	266	929	23506	3630
652.81	274	495	25381	7433
653.58	182	416	15554	6043
661.17	278	550	24835	5585
661.74	129	321	11241	4536

Site 463 Minor Element Figures

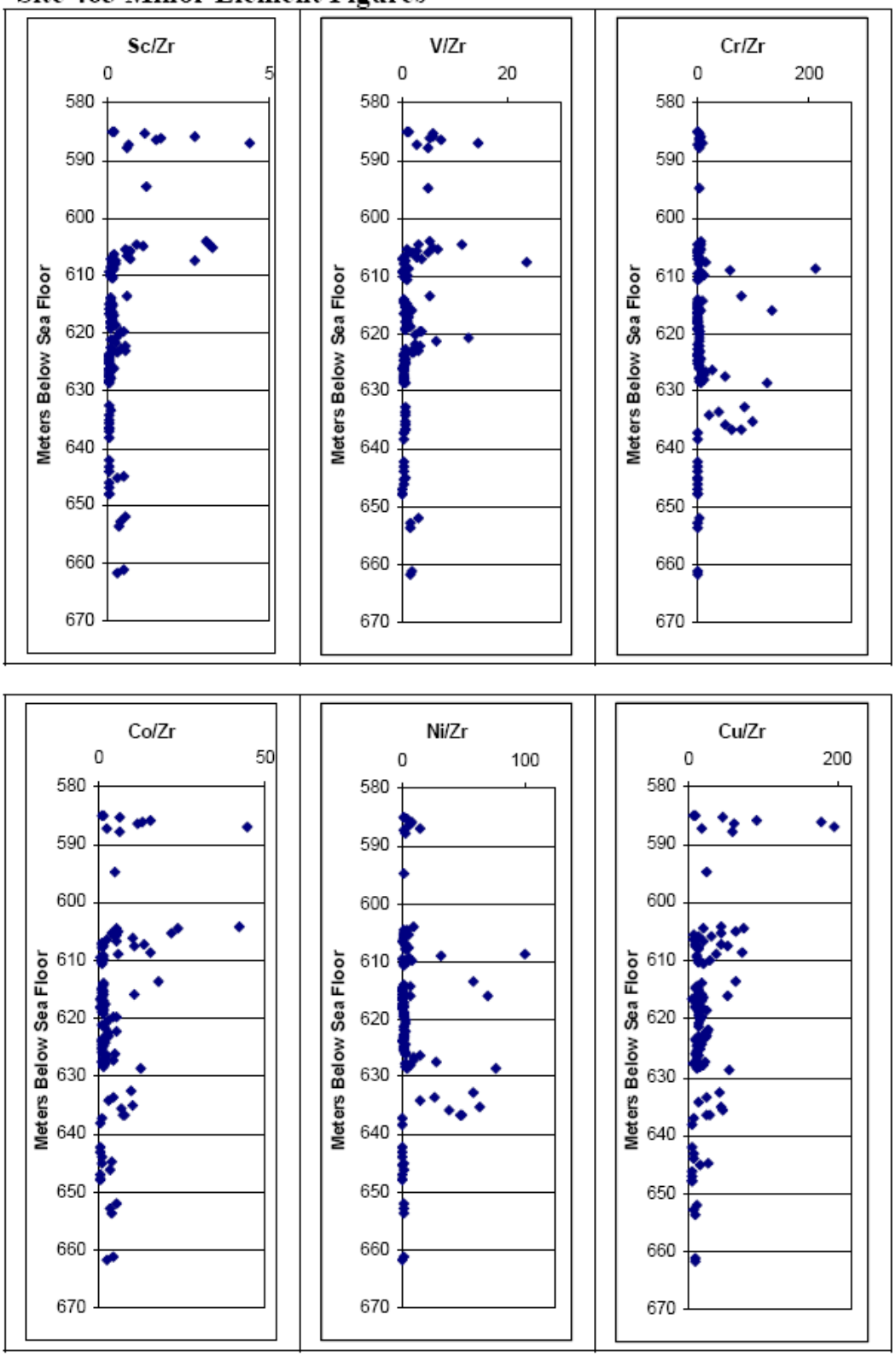

Site 463 Minor Element Figures

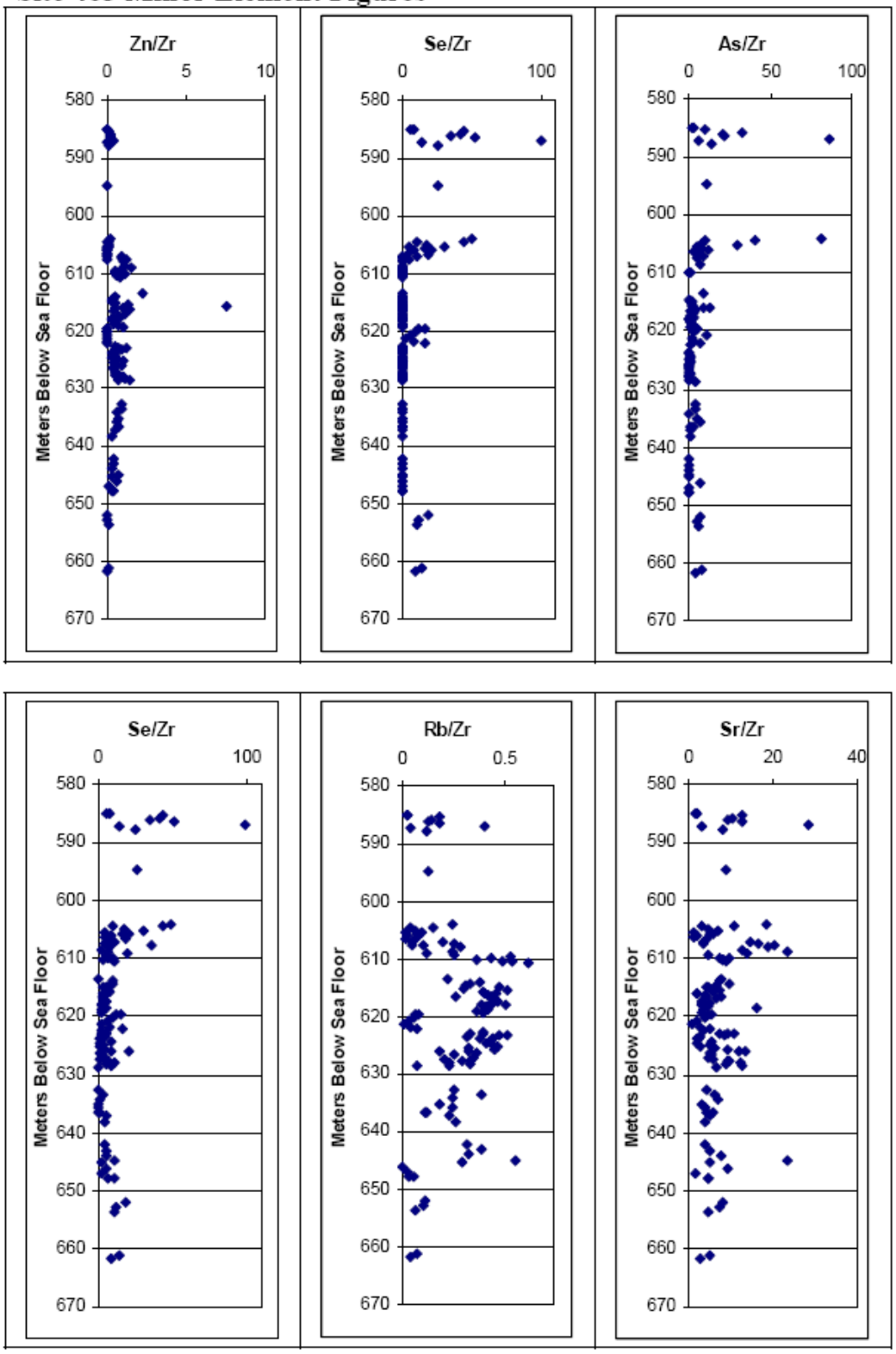

Site 463 Minor Element Figures

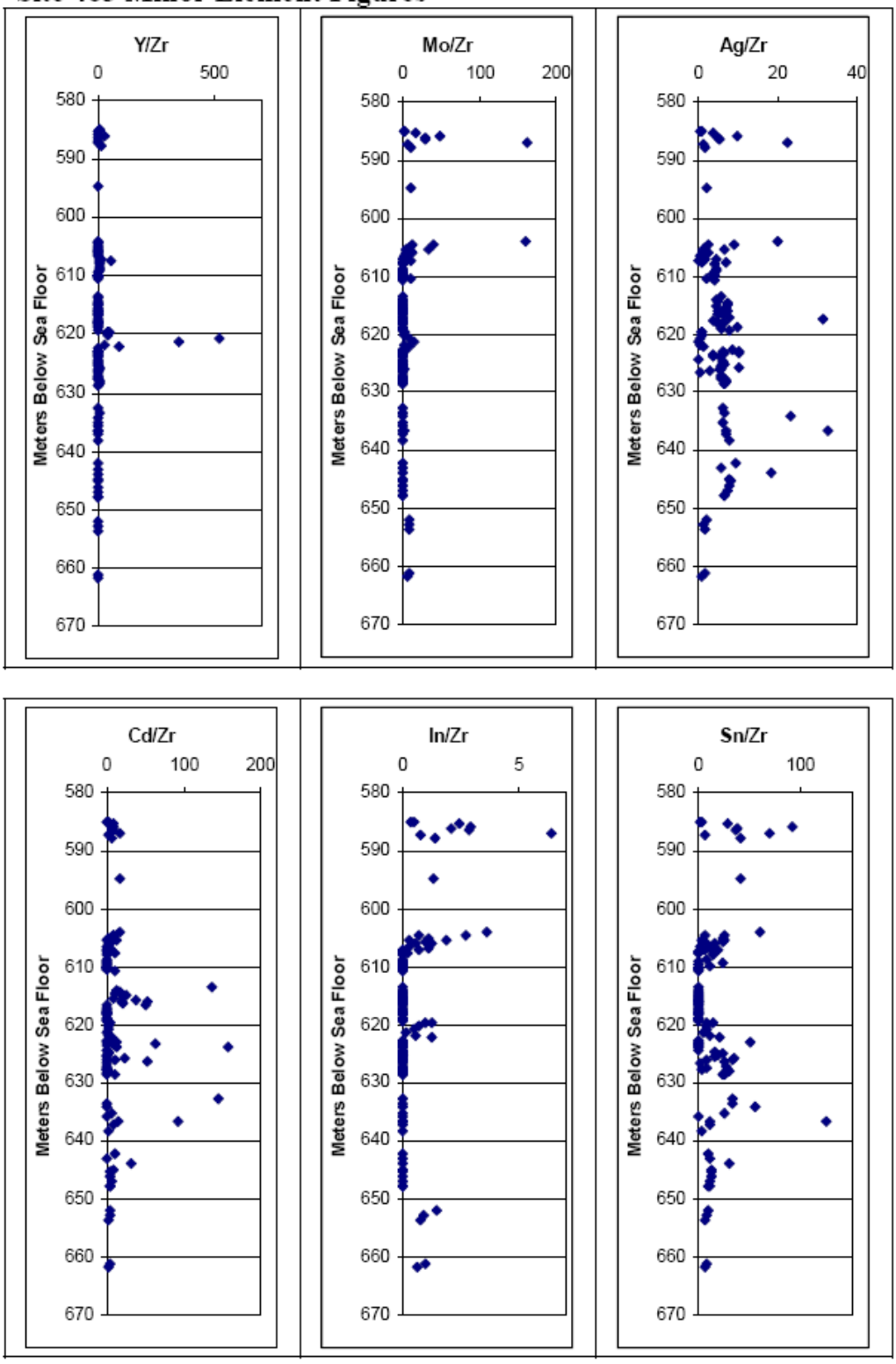

Site 463 Minor Element Figures

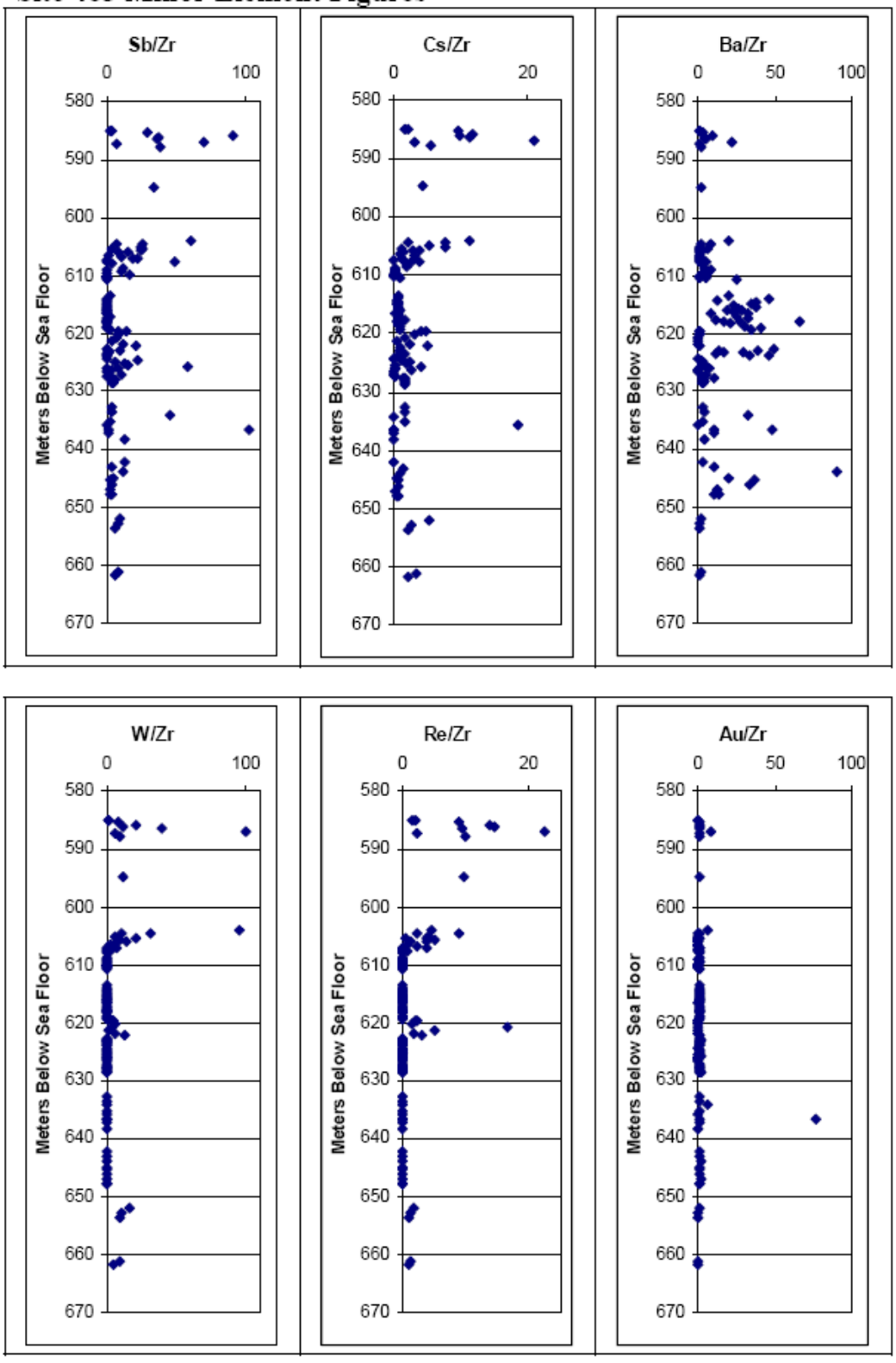

Site 463 Minor Element Figures

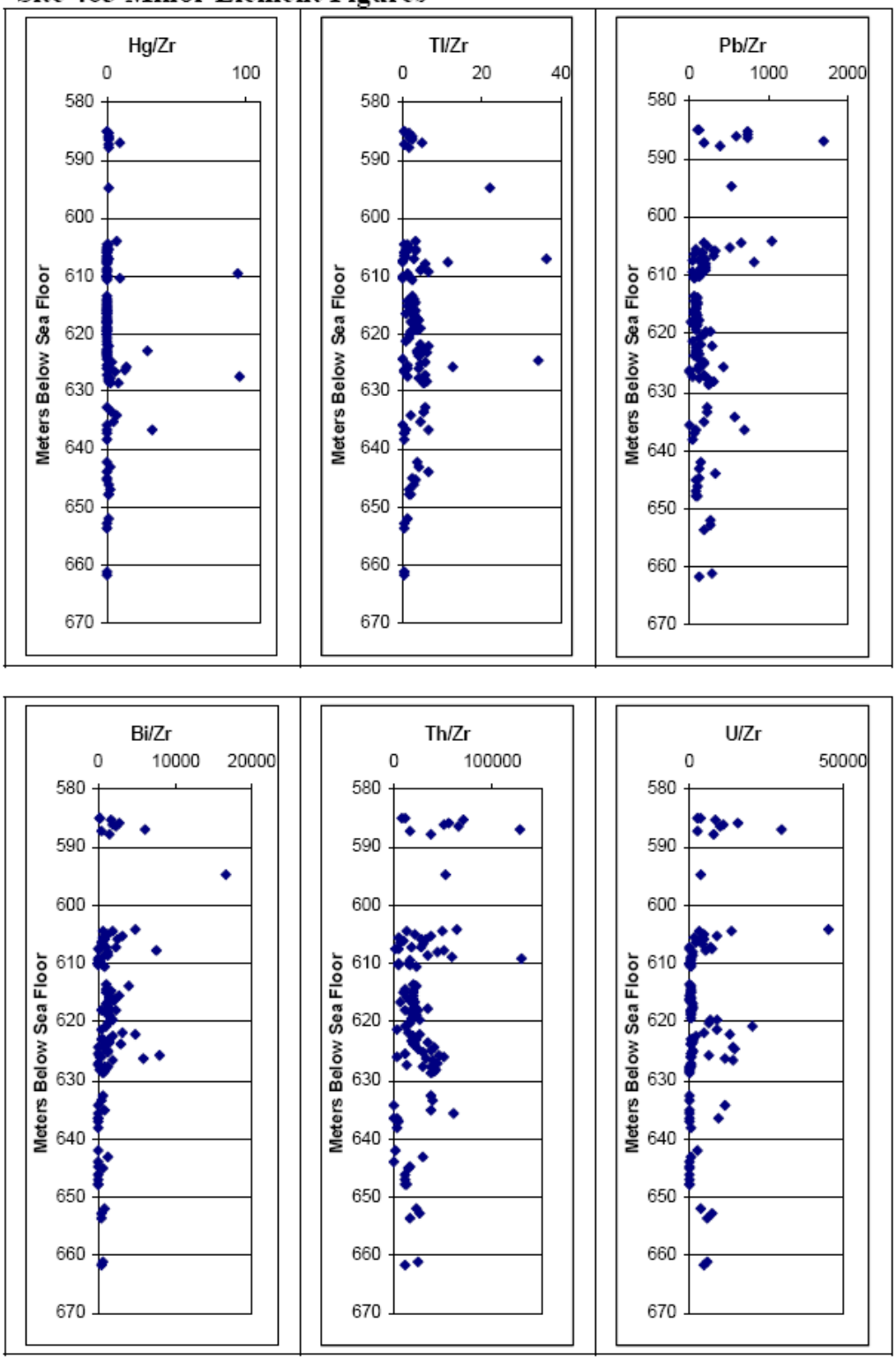

Site 463 Major Element Data

Depth (m)	Ba/Al	Ca/Al	Fe/Al	K/Al	Mg/Al	Mg/Al
585.00	0.05	21.38	0.76	0.12	0.31	0.30
585.00	0.07	28.84	1.03	0.25	0.42	0.40
585.38	0.11	33.02	1.10	0.32	0.42	0.39
585.79	0.39	118.28	2.00	0.07	0.82	0.81
586.22	0.18	63.02	2.34	0.25	0.58	0.56
586.50	0.12	48.14	1.32	0.27	0.55	0.52
586.90	0.14	120.98	2.13	0.00	0.93	0.91
587.29	0.07	23.74	0.96	0.25	0.36	0.35
587.71	0.26	20.64	1.06	0.42	0.35	0.33
594.67	0.21	28.32	1.02	0.38	0.35	0.33
604.10	0.24	186.25	2.98	0.00	1.20	1.23
604.50	0.05	42.22	0.83	0.00	0.32	0.32
604.50	0.09	66.35	1.38	0.05	0.55	0.54
604.99	0.18	27.43	1.41	0.28	0.44	0.41
605.22	0.13	81.95	2.01	0.00	0.68	0.66
605.40	0.12	109.91	2.39	0.00	0.82	0.80
605.69	0.21	32.48	1.22	0.30	0.37	0.35
605.84	0.10	14.33	0.89	0.32	0.31	0.29
606.00	0.15	120.08	1.99	0.00	0.90	0.89
606.39	0.04	17.14	1.07	0.05	0.37	0.38
606.69	0.09	11.71	0.86	0.24	0.30	0.29
607.10	0.25	37.40	1.35	0.07	0.42	0.42
607.03	0.13	83.89	1.24	1.12	0.60	0.66
607.28	0.12	56.93	1.39	0.57	0.42	0.46
607.49	0.00	0.32	0.62	0.15	0.20	0.19
607.61	0.08	132.45	1.43	1.03	0.74	0.81
607.89	0.21	62.81	1.43	0.00	0.48	0.55
608.62	0.22	60.52	6.05	1.06	0.40	0.43
608.91	0.21	91.90	2.09	0.83	0.58	0.64
609.20	0.26	71.87	1.46	0.66	0.56	0.63
609.48	0.10	6.98	0.75	0.50	0.25	0.29
609.79	0.18	13.31	0.95	0.53	0.27	0.29
610.01	0.13	23.92	0.84	0.23	0.31	0.34
610.30	0.11	9.23	0.71	0.21	0.24	0.27
610.30	0.12	9.64	0.80	0.67	0.26	0.29
610.58	0.18	8.48	0.95	0.39	0.32	0.36
613.51	0.00	0.36	0.74	0.22	0.14	0.16
613.91	0.14	13.26	0.72	0.74	0.28	0.30
614.23	0.21	20.01	0.92	0.36	0.29	0.33
614.62	0.29	7.01	0.74	0.32	0.29	0.32
614.88	0.07	3.32	0.81	0.34	0.22	0.25
615.03	0.15	6.36	1.33	0.36	0.27	0.29
615.31	0.11	6.31	1.12	0.39	0.25	0.27

Site 463 Major Element Data (cont.)

Depth (m)	Ba/Al	Ca/Al	Fe/Al	K/Al	Mg/Al	Mg/Al
615.59	0.19	6.03	0.93	0.46	0.27	0.30
615.89	0.05	0.24	3.33	0.46	0.24	0.26
615.89	0.06	0.22	1.16	0.40	0.24	0.27
616.21	0.15	4.71	1.01	0.35	0.23	0.26
616.46	0.10	3.43	1.06	0.39	0.23	0.25
616.60	0.07	2.62	0.57	0.47	0.16	0.18
616.92	0.10	0.53	0.84	0.51	0.24	0.26
617.29	0.09	2.36	0.92	0.36	0.22	0.24
617.60	0.08	1.09	0.88	0.41	0.21	0.23
617.88	0.09	1.00	0.71	0.44	0.24	0.27
618.02	0.10	0.35	0.59	0.50	0.25	0.27
618.02	0.12	0.36	0.63	0.30	0.26	0.29
618.28	0.06	1.10	0.67	0.11	0.24	0.26
618.60	0.05	4.06	0.52	0.20	0.19	0.21
618.90	0.15	0.66	1.00	0.29	0.24	0.26
619.20	0.12	0.46	0.95	0.46	0.25	0.28
619.70	0.09	1.00	0.83	0.12	0.27	0.27
619.70	0.11	1.00	0.79	0.17	0.27	0.26
620.20	0.10	7.96	0.96	0.16	0.31	0.30
620.70	0.14	7.69	2.10	0.20	0.27	0.27
621.20	0.22	12.96	0.96	0.21	0.27	0.26
621.70	0.18	1.92	0.84	0.22	0.26	0.25
622.20	0.17	0.55	1.06	0.12	0.25	0.25
622.50	0.17	0.14	0.59	0.42	0.21	0.24
622.95	0.05	0.28	0.66	0.34	0.23	0.26
623.01	0.01	4.43	1.91	0.23	0.29	0.32
623.28	0.04	0.67	1.27	0.31	0.26	0.29
623.59	0.19	0.20	0.76	0.76	0.28	0.31
623.88	0.10	0.12	0.79	0.45	0.21	0.23
623.88	0.09	0.12	0.83	0.41	0.20	0.23
624.21	0.14	8.13	0.75	0.61	0.25	0.28
624.80	0.12	6.41	0.68	0.25	0.25	0.28
625.10	0.11	0.27	0.61	0.40	0.22	0.24
625.40	0.14	14.00	0.81	0.37	0.26	0.28
625.71	0.15	19.68	0.97	0.60	0.27	0.29
626.00	0.25	35.80	1.12	0.55	0.38	0.43
626.29	0.08	11.24	1.10	0.12	0.26	0.26
626.60	0.14	14.84	0.99	0.00	0.27	0.27
627.00	0.06	8.37	0.66	0.17	0.24	0.24
627.30	0.14	29.98	2.19	0.00	0.29	0.29
627.52	0.20	18.35	0.54	0.00	0.29	0.29
627.52	0.22	22.42	0.67	0.11	0.31	0.31
627.81	0.18	82.90	1.00	0.33	0.57	0.55
628.09	0.17	37.06	1.24	0.69	0.49	0.52
628.09	0.14	35.12	0.85	0.06	0.36	0.36

Site 463 Major Element Data (cont.)

Depth (m)	Ba/Al	Ca/Al	Fe/Al	K/Al	Mg/Al	Mg/Al
628.38	0.24	56.10	1.35	0.42	0.53	0.58
628.38	0.21	58.25	0.85	0.00	0.48	0.48
628.60	0.14	55.92	4.76	0.02	0.32	0.31
632.63	0.08	22.84	3.00	0.38	0.27	0.28
633.52	0.20	12.68	1.55	0.41	0.26	0.26
634.14	0.10	23.34	1.27	0.00	0.28	0.28
635.05	0.07	13.71	4.31	0.31	0.25	0.25
635.60	0.10	13.92	2.68	0.39	0.25	0.25
636.53	0.11	27.27	2.31	0.14	0.25	0.26
636.53	0.12	28.78	4.02	0.00	0.28	0.28
651.88	0.08	19.05	0.95	0.09	0.36	0.36
652.81	0.09	30.89	1.05	0.09	0.46	0.45
653.58	0.10	50.23	1.28	0.05	0.48	0.48
661.17	0.09	45.81	1.17	0.10	0.49	0.47
661.74	0.11	45.29	1.17	0.17	0.49	0.47

Site 463 Major Element Data (cont.)

Depth (m)	Mn/Al	Na/Al	P/Al	Ti/Al
585.00	0.03	0.21	0.03	0.08
585.00	0.04	0.32	0.02	0.10
585.38	0.05	0.30	0.02	0.10
585.79	0.21	0.52	0.11	0.19
586.22	0.10	0.49	0.06	0.15
586.50	0.06	0.40	0.03	0.12
586.90	0.16	0.62	0.04	0.18
587.29	0.04	0.26	0.02	0.09
587.71	0.05	0.30	0.06	0.12
594.67	0.06	0.31	0.02	0.09
604.10	0.40	0.83	0.17	0.26
604.50	0.10	0.14	0.03	0.08
604.50	0.18	0.30	0.04	0.13
604.99	0.06	0.31	0.07	0.13
605.22	0.21	0.35	0.05	0.17
605.40	0.29	0.46	0.03	0.19
605.69	0.07	0.23	0.06	0.11
605.84	0.03	0.19	0.03	0.09
606.00	0.30	0.54	0.11	0.17
606.39	0.05	0.24	0.02	0.12
606.69	0.05	0.15	0.04	0.08
607.10	0.15	0.30	0.08	0.15
607.03	0.16	0.43	0.17	0.11
607.28	0.13	0.22	0.08	0.09
607.49	0.00	0.17	0.01	0.09
607.61	0.33	0.42	0.27	0.13
607.89	0.15	0.20	0.12	0.11
608.62	0.30	0.44	0.10	0.09
608.91	0.26	0.39	0.07	0.09
609.20	0.21	0.27	0.04	0.13
609.48	0.02	0.18	0.02	0.09
609.79	0.06	0.17	0.10	0.10
610.01	0.11	0.18	0.03	0.12
610.30	0.05	0.20	0.03	0.10
610.30	0.05	0.22	0.06	0.10
610.58	0.03	0.25	0.01	0.10
613.51	0.01	0.17	0.00	0.09
613.91	0.09	0.28	0.10	0.14
614.23	0.16	0.31	0.07	0.14
614.62	0.04	0.26	0.11	0.14
614.88	0.02	0.16	0.00	0.14
615.03	0.03	0.28	0.00	0.19
615.31	0.05	0.19	0.01	0.11

Site 463 Major Element Data (cont.)

Depth (m)	Mn/Al	Na/Al	P/Al	Ti/Al
615.59	0.02	0.26	0.03	0.15
615.89	0.09	0.24	0.03	0.12
615.89	0.01	0.24	0.01	0.12
616.21	0.03	0.18	0.04	0.14
616.46	0.05	0.19	0.02	0.12
616.60	0.02	0.30	0.04	0.06
616.92	0.01	0.24	0.07	0.11
617.29	0.02	0.19	0.02	0.12
617.60	0.00	0.24	0.02	0.13
617.88	0.01	0.21	0.00	0.12
618.02	0.00	0.20	0.02	0.13
618.02	0.00	0.22	0.03	0.13
618.28	0.02	0.24	0.01	0.13
618.60	0.13	0.27	0.04	0.09
618.90	0.00	0.21	0.02	0.15
619.20	0.01	0.21	0.01	0.14
619.70	0.01	0.18	0.01	0.16
619.70	0.01	0.21	0.02	0.15
620.20	0.22	0.22	0.04	0.14
620.70	0.11	0.26	0.02	0.11
621.20	0.44	0.22	0.04	0.12
621.70	0.02	0.21	0.01	0.12
622.20	0.01	0.22	0.01	0.12
622.50	0.00	0.24	0.04	0.13
622.95	0.00	0.24	0.01	0.11
623.01	0.09	0.20	0.02	0.10
623.28	0.03	0.24	0.00	0.09
623.59	0.01	0.22	0.07	0.13
623.88	0.01	0.17	0.00	0.12
623.88	0.00	0.18	0.02	0.14
624.21	0.09	0.26	0.04	0.12
624.80	0.06	0.34	0.04	0.11
625.10	0.00	0.27	0.01	0.10
625.40	0.13	0.27	0.03	0.13
625.71	0.18	0.33	0.05	0.13
626.00	0.27	0.52	0.06	0.14
626.29	0.07	0.25	0.01	0.10
626.60	0.07	0.28	0.04	0.12
627.00	0.04	0.34	0.02	0.10
627.30	0.18	0.46	0.03	0.12
627.52	0.06	0.21	0.01	0.10
627.52	0.09	0.24	0.01	0.13
627.81	0.35	0.26	0.11	0.15
628.09	0.14	0.84	0.06	0.15
628.09	0.13	0.25	0.06	0.12

Site 463 Major Element Data (cont.)

Depth (m)	Mn/Al	Na/Al	P/Al	Ti/Al
628.38	0.20	0.50	0.05	0.15
628.38	0.19	0.24	0.08	0.13
628.60	0.30	0.60	0.03	0.12
632.63	0.15	0.39	0.00	0.13
633.52	0.08	0.21	0.06	0.15
634.14	0.08	0.29	0.05	0.12
635.05	0.17	0.57	0.03	0.10
635.60	0.09	0.30	0.02	0.14
636.53	0.12	0.34	0.03	0.09
636.53	0.18	0.59	0.00	0.11
651.88	0.06	0.25	0.05	0.13
652.81	0.07	0.25	0.06	0.11
653.58	0.08	0.26	0.00	0.13
661.17	0.07	0.24	0.00	0.12
661.74	0.05	0.27	0.04	0.15

Site 463 Major Element Figures

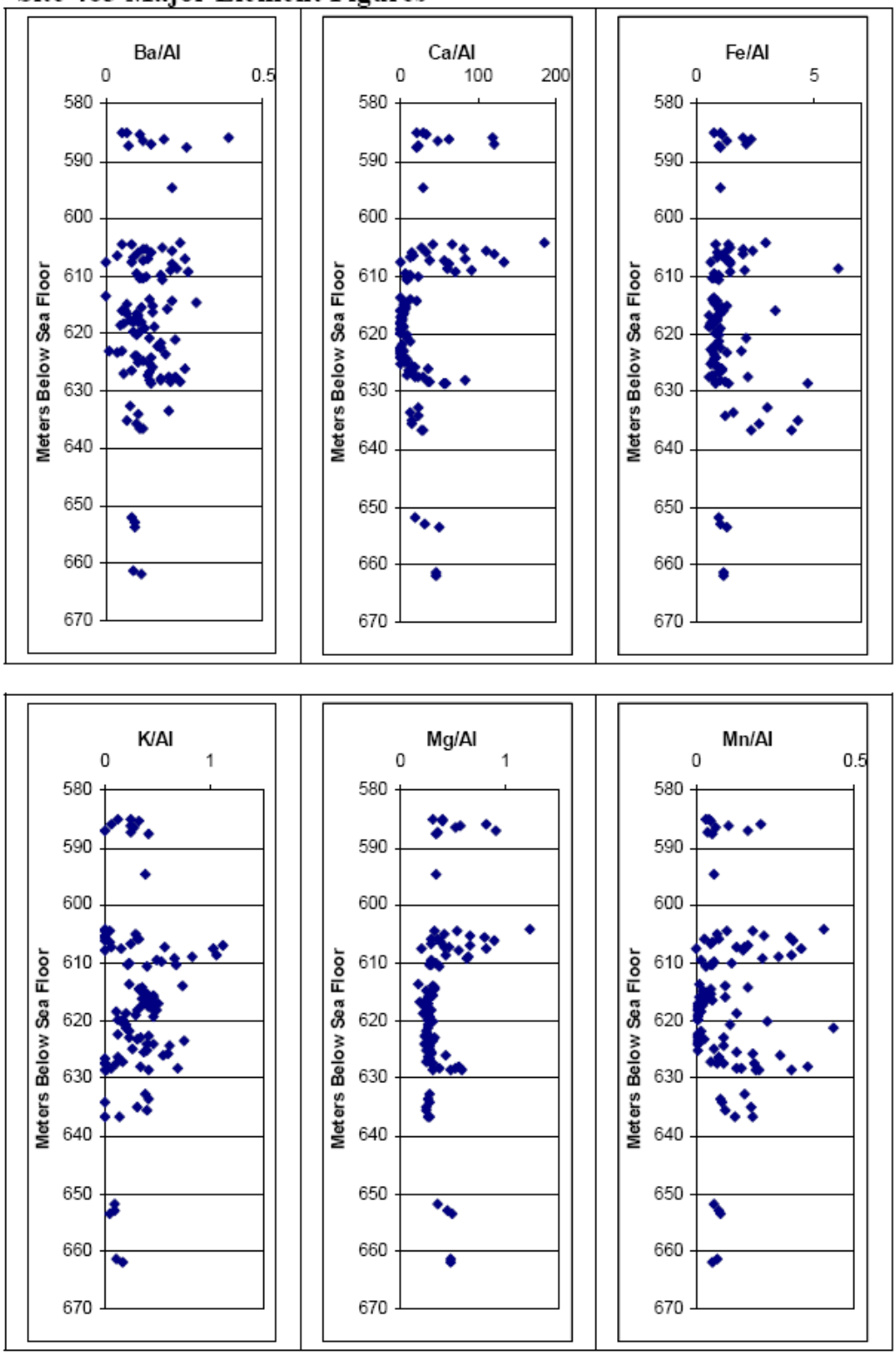

Site 463 Major Element Figures